

**Figure A-5-10.** Initial H basalt hydraulic conductivity field.

### A-5.2.2 Aquifer Simulation Domain and Discretization

Selection of the aquifer model grid was guided by the need to predict aquifer water quality resulting from historical injection of INTEC contaminants, influx of water and contaminants from the vadose zone, and the three-dimensional aquifer thickness. The aquifer model domain extends from approximately 2.5 km north of the INTEC to the southern INL boundary in the north to south direction, and approximately 5.5 km east of the INTEC to slightly east of the RWMC in the east to west direction. The model was discretized using 400 x 400 m grid blocks in the horizontal, as illustrated in Figure A-5-1. Local horizontal refinement corresponding to the discretization level applied in the vadose zone model is within the footprint of the INTEC (100 x 100 m grid block size) with a 200 x 200 m transition grid surrounding the vadose zone footprint. This local refinement was only performed in the top five layers of the aquifer model. Variable vertical discretization following the HI interbed was applied.

The model's top surface corresponded to a planar fit through the observed water table elevation, and the model's bottom surface was created from the thickness estimates discussed in Section A-4.1. Correspondingly, the total aquifer model thickness varied between 32 m and 379 m. The vertical discretization included five uniform 2 m layers directly beneath the water table, which were increased in thickness to the midpoint between the water table and the HI interbed surface. At this point the vertical discretization gradually decreased until 2 m thickness was reached within the HI interbed. The thickness gradually increased again until the aquifer bottom was reached. The decreasing layer thickness near the water table and around the HI interbed places more computation nodes where they are needed (i.e., high-gradient areas). In total, 27 model layers were

used and the minimum grid block thickness was 2 m. The aquifer model vertical discretization is illustrated in Figure A-5-12. The simulated HI interbed is depicted in red and basalt is depicted in white.

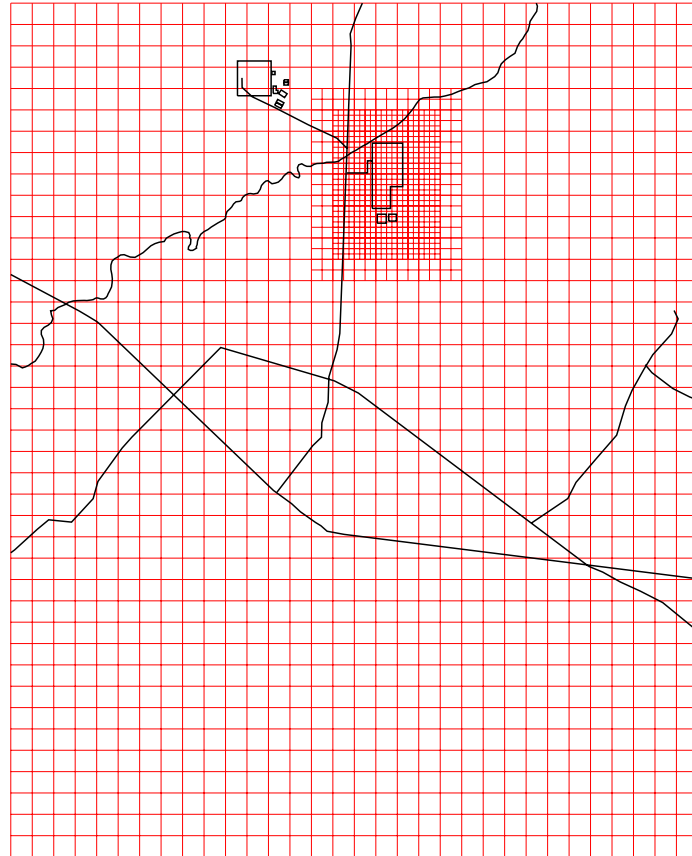


**Figure A-5-11.** Aquifer model domain and horizontal discretization.

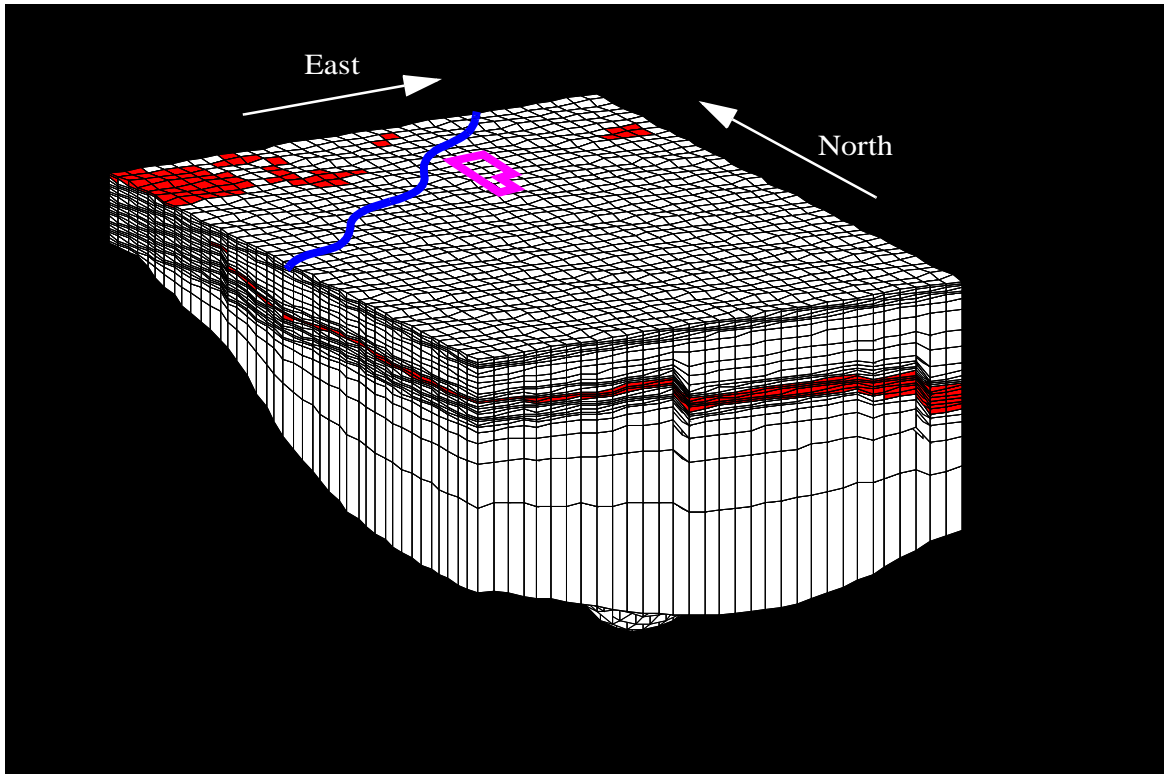


**Figure A-5-12.** Aquifer model vertical discretization with 30x vertical exaggeration.

### A-5.2.3 Aquifer Boundary Conditions and Water Sources

The Snake River Plain Aquifer underlies INTEC and is located approximately 460 ft bgs. Water generally flows through the Snake River Plain Aquifer under unconfined conditions, but may be confined in local areas. It is mainly recharged from underflow originating from regional basins adjacent to the INL Site and from regional groundwater flow. Additional recharge can be attributed to intermittent streams that terminate on the INL Site and to precipitation. In this model, the following assumptions were made:

- The underflow contributions are not transient and the aquifer behaves as though confined.
- Variation in discharge and pumping rates in the service and potable water wells will be neglected. With the exception of CPP-03, the pumping rates will be simulated as steady state. The variability in injection rate for CPP-03 will be accounted for.
- Water levels from summer 2004 are representative of the natural gradient and will form the basis of model calibration to observed heads.
- Underflow contributions are accounted for by using steady-state Dirichlet boundary conditions. This allows matching water levels (2004 heads) throughout the simulation domain but does not constrain the magnitude of the flux entering through those boundaries. The flux will be constrained through the transport velocity. Transport velocity will be constrained by adjusting the permeability and porosity distribution to obtain matches to key contaminant arrival histories downgradient of their sources.

Under these assumptions, flow through the vadose zone and flow within the aquifer can be simulated separately. Transient water and contaminant flux leaving through the lower vadose zone model boundary are first computed using the vadose zone model. These fluxes then are used as recharge sources applied to the

upper boundary condition of the aquifer model. Precipitation, and recharge from the former percolation ponds and Big Lost River occurring within the vadose zone footprint are not directly simulated in the aquifer model but are accounted for in the flux from the vadose zone model used as the upper aquifer model boundary condition.

Water sources and sinks directly accounted for in the aquifer model include (1) infiltration from the vadose zone, (2) recharge from the Big Lost River reaches extending outside of the vadose zone footprint, (3) infiltration from precipitation, (4) reinjection of CPP-3 disposal well water, (5) pumping from CPP-1 and CPP-2 service water production wells, (6) pumping from the CPP-4 and CPP-5 potable water sources, (7) pumping from the RTC production well, (8) injection into the RTC disposal well and ponds, and (9) production in the CFA-1 and CFA-2 water supply wells. Infiltration from the vadose zone water and infiltration from the Big Lost River were applied to the upper layer of aquifer grid blocks as specified flux. The CPP-3, CPP-5, CPP-4, CPP-2, CPP-1, RTC production, and RTC disposal wells were simulated as injection/production wells in the TETRAD software with well screen intervals defined in the corresponding model grid blocks. The amount of water injected in the RTC disposal well included the injection well water and RTC disposal pond water. This was done to simplify model parameterization, while including the TRA water sources. As discussed in Sections A-5.3.1, Big Lost River fluxes were transient values (See Section A-5.3.1 and Table A-5-1). The aquifer model water sources are summarized in Table A-5-9.

#### A-5.2.4 Aquifer Initial Conditions

The simulation initial conditions were achieved using the natural recharge sources of 1 cm/year infiltration from precipitation, the long term average Big Lost River infiltration rate (1.9 m/year per meter), and the steady-state Dirichlet lateral boundary conditions. The model was run for 1,000 years prior to the transport simulation start time. As with the vadose zone model, the 1,000 year initial condition time period was determined by monitoring the maximum grid block pressure change between simulation time steps and extending the initial condition time period until the pressure change is approximately zero. The aquifer model achieved steady-state conditions long before 1,000 years, but running a longer initialization period did not increase the computational burden because time steps are allowed to increase after a near steady-state is achieved.

**Table A-5-9** Aquifer model water sources and amounts.

Water Source	Application Amount	Notes
Recharge from vadose zone	Spatially and temporally variable (0.01 m/year to approximately 70 m/year)	Transient drainage from the vadose zone model is the aquifer model upper boundary condition.
Big Lost River infiltration	Temporally variable (0. to 3.2 m <sup>3</sup> /day per m of river length)	Infiltration is only applied outside the vadose zone footprint.
CPP-3 injection	Temporally variable (0 to 7,000 m <sup>3</sup> /day)	Injection rate was determined from service waste disposal records.
CPP-1 pumping	2,785 (m <sup>3</sup> /day)	Service water production estimated from INTEC water balance (DOE-ID 2003b).
CPP-2 pumping	2,785 (m <sup>3</sup> /day)	Service water production estimated from INTEC water balance (DOE-ID 2003b).
CPP-4 pumping	68 (m <sup>3</sup> /day)	Potable water production estimated from INTEC water balance (DOE-ID 2003b).
CPP-5 pumping	68 (m <sup>3</sup> /day)	Potable water production estimated from INTEC water balance (DOE-ID 2003b).

Water Source	Application Amount	Notes
TRA-4 pumping	5,968.95 (m <sup>3</sup> /day)	Potable water production estimated from Five-Year Review Report for the Test Reactor Area (DOE-ID 2005a).
TRA-DISPOSAL cold waste pond injection	2,017 (m <sup>3</sup> /day)	Potable water production estimated from Five-Year Review Report for the Test Reactor Area (DOE-ID 2005a).
CFA-1 pumping	358 (m <sup>3</sup> /day)	Obtained from CFA operation records.
CFA-2 pumping	770 (m <sup>3</sup> /day)	Obtained from CFA operation records.

### A-5.3 Simulation Code

The TETRAD multipurpose simulator (Vinsome and Shook 1993), Version 12.7, was chosen to simulate water and contaminant migration through the vadose zone and aquifer. This code was chosen because it is robust, multiphase, multicomponent, and three-dimensional and can simulate dual porosity systems. TETRAD was originally developed as an enhanced oil recovery simulator for the petroleum industry. It has been successfully applied to simulate groundwater flow and transport at the INL Site for Waste Area Groups 1, 3, and 7. TETRAD has undergone limited verification and validation (Shook 1995) to demonstrate proficiency of the TETRAD simulator for use in modeling environmental fate and transport processes.

To solve the governing equations for variably saturated flow, TETRAD requires parameterization of saturation versus capillary pressure and saturation versus permeability for each lithologic material. The van Genuchten (1980) equations were used to describe the constitutive relationships for the alluvium and interbed (sediment). TETRAD uses two-phase van Genuchten constitutive equations, as adapted by Parker et al. (1987) with slight modifications to the normalized saturation terms. The van Genuchten constitutive relations are

$$\bar{S}_w = \frac{S_w - S_{wr}}{1 - S_{wr}}; \quad \bar{S}_a = \frac{S_a}{1 - S_{wr}}; \quad \bar{S}_o = \frac{S_o}{1 - S_{wr}} \quad (1)$$

$$\bar{S}_L = \bar{S}_o + \bar{S}_w \quad (2)$$

$$P_{c\ ow} = \frac{\sigma_{ow} \rho_{fw} g}{\sigma_{aw} \alpha} [(\bar{S}_w)^{1/\gamma} - 1]^{1/\beta} \Leftrightarrow \bar{S}_w = \left[ 1 + \left( \frac{\alpha P_{c\ ow} \sigma_{aw}}{\rho_{fw} g \sigma_{ow}} \right)^\beta \right]^{-\gamma} \quad (3)$$

$$P_{c\ ao} = \frac{\sigma_{ao} \rho_{fw} g}{\sigma_{aw} \alpha} [(1 - \bar{S}_a)^{1/\gamma} - 1]^{1/\beta} \Leftrightarrow \bar{S}_a = 1 - \left[ 1 + \left( \frac{\alpha P_{c\ ao} \sigma_{aw}}{\rho_{fw} g \sigma_{ao}} \right)^\beta \right]^{-\gamma} \quad (4)$$

$$P_{c\ aw} = \frac{\rho_{fw} g}{\alpha} [(1 - \bar{S}_a)^{1/\gamma} - 1]^{1/\beta} \Leftrightarrow \bar{S}_a = 1 - \left[ 1 + \left( \frac{\alpha P_{c\ aw}}{\rho_{fw} g} \right)^\beta \right]^{-\gamma} \quad (5)$$

$$k_{rw} = (\bar{S}_w)^{1/2} [1 - [1 - (\bar{S}_w)^{1/\gamma}]^\gamma]^2 \quad (6)$$

$$k_{ro} = (\bar{S}_o - \bar{S}_{or})^{1/2} [[1 - (\bar{S}_w)^{1/\gamma}]^\gamma - [1 - (\bar{S}_L)^{1/\gamma}]^\gamma]^2 \quad (7)$$

$$k_{ra} = (\bar{S}_a)^{1/2} [1 - (\bar{S}_L)^{1/\gamma}]^{2\gamma} \quad (8)$$

where

$S_w$  = water saturation

$S_o$  = oil saturation

$S_a$  = air saturation

$S_{wr}$  = residual water saturation

$S_{or}$  = residual oil saturation

$\alpha$  = curve fitting parameter, related to inverse air entry potential ( $m^{-1}$ , van Genuchten Alpha)

$\beta$  = curve fitting parameter, affects nonlinearity of characteristic curve (van Genuchten n)

$\gamma = 1 - 1/\beta$

$\sigma_{aw}$  = air-water interfacial tension (N/m)

$\sigma_{ow}$  = oil-water interfacial tension (N/m)

$\sigma_{ao}$  = air-oil interfacial tension (N/m)

$\rho_{fw}$  = fresh water density ( $kg/m^3$ )

$g$  = gravitational acceleration ( $m/s^2$ ).

Determining constitutive relationships for fractured media continues to be an active research area. A Brooks-Corey (1966) analytical formulation was used to describe the constitutive relationships for the fractured basalt, which was treated as an equivalent porous media. The general Brooks-Corey formulas implemented in TETRAD are

$$P_{c\ aw} = A_{aw}(1 - S_w)^{B_{aw}} \quad (9)$$

$$k_{ri} = A_i((S_i - S_{ir})/(1 - S_{ir}))^{B_i} \quad (10)$$

where

$P_{c\ aw}$  = capillary pressure between air and water (kPa)

$k_{ri}$  = relative permeability of any phase  $i$

$S_i$  and  $S_{ir}$  = saturation and residual saturation of any phase  $i$

$A_{aw}$  (kPa),  $B_{aw}$ ,  $A_i$ , and  $B_i$  = fitting parameters for the Brooks-Corey functions.

## A-6 SIMULATION CODE

The TETRAD multipurpose simulator (Vinsome and Shook, 1993), Version 12.7 ms was chosen to simulate water and contaminant migration through the vadose zone and aquifer. This code was chosen because it is robust, multiphase, multicomponent, and three-dimensional and can simulate dual porosity systems. TETRAD was originally developed as an enhanced oil recovery simulator for the petroleum industry. It has been successfully applied to simulate groundwater flow and transport at the INL Site for Waste Area Groups 1, 3, and 7. TETRAD has undergone limited verification and validation (Shook 1995) to demonstrate proficiency of the TETRAD simulator for use in modeling environmental fate and transport processes.

The general conservation equation solved by the TETRAD simulator for accumulation, flux, decay or degradation, and sources for any component  $i$  can be written as

$$\frac{\partial W_i}{\partial t} + \vec{\nabla} \cdot \vec{N}_i - R_i + q_i = 0 \quad (\text{A-6-1})$$

where

$\frac{\partial W_i}{\partial t}$  = is the accumulation term that consists of net changes in the concentration of the component  $i$  in any phase, including the adsorbed phase

$\vec{\nabla} \cdot \vec{N}_i$  = is the flux of component  $i$

$R_i$  = the change in concentration arising from decay of component  $i$

$q_i$  represents sources or sinks of component  $i$ .

The accumulation term can be written as

$$W_i = \phi(S_w \rho_w w_i + S_g \rho_g y_i + S_o \rho_o x_i) + ((1 - \phi) \rho_s V_i) / M_i \quad (\text{A-6-2})$$

where

$\phi$  = the porosity

$S_j$  = the phase saturations ( $w$  aqueous,  $g$  gaseous,  $o$  oleic)

$\rho_j$  = the phase molar densities

$w_i, y_i,$  and  $x_i$  = the mole fractions of  $i$  in the aqueous, gaseous, and oleic phases, respectively

$\rho_s$  = the solid phase density

$V_i$  = the mole fraction of  $i$  adsorbed on the solid phase

$M_i$  = the molecular weight of  $i$ .

A generalized adsorption relationship is available in TETRAD that allows for adsorption onto the solid phase from any of the other three phases.

The flux term in Equation (A-6-3) is comprised of an advection and dispersion term for each phase given by

$$\vec{N}_j = [\rho_w \vec{u}_w w_i - \vec{D}_{iw} \cdot \vec{\nabla}(\rho_w w_i)] + [\rho_g \vec{u}_g y_i - \vec{D}_{ig} \cdot \vec{\nabla}(\rho_g y_i)] + [\rho_o \vec{u}_o x_i - \vec{D}_{io} \cdot \vec{\nabla}(\rho_o x_i)] \quad (\text{A-6-3})$$

In Equation (A-6-3) the  $\vec{n}_j$  are the phase advective fluxes, given by the multiphase version of Darcy's law:

$$\vec{n}_j = \frac{kk_{rj}}{\mu_j} (\vec{\nabla} P_j - \rho_j \vec{g}) \quad (\text{A-6-4})$$

where

$k$  = the intrinsic permeability

$k_{rj}$  = the relative phase permeability

$\mu_j$  = the phase viscosity

$P_j$  = the phase pressure

$\vec{g}$  = gravitational constant in vector form.

$\vec{D}_{ij}$  = the phase-dependant dispersion tensor comprised of molecular diffusion modified by porosity, phase saturation, tortuosity, and mechanical dispersion consisting of phase dispersivities modified by directional components of advective phase fluxes (Bear 1972).

The reaction term in Equation (A-6-1) accounts for decay or degradation of component  $i$  and is written as:

$$R_i = -A_{i\zeta}[m_j + V_i(1 - \phi)\rho_r] + A_{\omega i}[m_\omega + V_\omega(1 - \phi)\rho_r]; \zeta \neq \omega \quad (\text{A-6-5})$$

where  $m_i$  is the total aqueous mass of  $i$ . The first term on the right hand side of Equation (A-6-5) accounts for  $i$  decaying with a rate constant  $A_{i\zeta}$  into component  $\zeta$ , whereas the second term on the right-hand side is the formation of  $i$  from destruction of component  $\omega$  with a rate constant  $A_{\omega i}$ . The final term on the right-hand side in Equation (A-6-1) is the source/sink term,  $q_i$ . This term accounts for the addition or extraction of component  $i$  through wells or boundary conditions.

To solve the governing equations for variably saturated flow, TETRAD requires parameterization of saturation versus capillary pressure and saturation versus permeability for each lithologic material. The van Genuchten (1980) equations were used to describe the constitutive relationships for the alluvium and interbed (sediment). TETRAD uses two-phase van Genuchten constitutive equations, as adapted by Parker et al. (1987) with slight modifications to the normalized saturation terms. The van Genuchten constitutive relations are

$$\bar{S}_w = \frac{S_w - S_{wr}}{1 - S_{wr}}; \quad \bar{S}_a = \frac{S_a}{1 - S_{wr}}; \quad \bar{S}_o = \frac{S_o}{1 - S_{wr}} \quad (\text{A-6-6})$$

$$\bar{S}_L = \bar{S}_o + \bar{S}_w \quad (\text{A-6-7})$$

$$P_{c\ ow} = \frac{\sigma_{ow} \rho_{fw} g}{\sigma_{aw} \alpha} [(\bar{S}_w)^{1/\gamma} - 1]^{1/\beta} \Leftrightarrow \bar{S}_w = \left[ 1 + \left( \frac{\alpha P_{c\ ow} \sigma_{aw}}{\rho_{fw} g \sigma_{ow}} \right)^\beta \right]^{-\gamma} \quad (\text{A-6-8})$$

$$P_{c\ ao} = \frac{\sigma_{ao} \rho_{fw} g}{\sigma_{aw} \alpha} [(1 - \bar{S}_a)^{1/\gamma} - 1]^{1/\beta} \Leftrightarrow \bar{S}_a = 1 - \left[ 1 + \left( \frac{\alpha P_{c\ ao} \sigma_{aw}}{\rho_{fw} g \sigma_{ao}} \right)^\beta \right]^{-\gamma} \quad (\text{A-6-9})$$

$$P_{c\ aw} = \frac{\rho_{fw} g}{\alpha} [(1 - \bar{S}_a)^{1/\gamma} - 1]^{1/\beta} \Leftrightarrow \bar{S}_a = 1 - \left[ 1 + \left( \frac{\alpha P_{c\ aw}}{\rho_{fw} g} \right)^\beta \right]^{-\gamma} \quad (\text{A-6-10})$$

$$k_{rw} = (\bar{S}_w)^{1/2} [1 - [1 - (\bar{S}_w)^{1/\gamma}]^\gamma]^2 \quad (\text{A-6-11})$$

$$k_{ro} = (\bar{S}_o - \bar{S}_{or})^{1/2} [[1 - (\bar{S}_w)^{1/\gamma}]^\gamma - [1 - (\bar{S}_L)^{1/\gamma}]^\gamma]^2 \quad (\text{A-6-12})$$

$$k_{ra} = (\bar{S}_a)^{1/2} [1 - (\bar{S}_L)^{1/\gamma}]^{2\gamma} \quad (\text{A-6-13})$$

where

$S_w$  = water saturation

$S_o$  = oil saturation

$S_a$  = air saturation

$S_{wr}$  = residual water saturation

$S_{or}$  = residual oil saturation

$\alpha$  = curve fitting parameter, related to inverse air entry potential ( $\text{m}^{-1}$ , van Genuchten Alpha)

$\beta$  = curve fitting parameter, affects nonlinearity of characteristic curve (van Genuchten n)

$\gamma = 1 - 1/\beta$

$\sigma_{aw}$  = air-water interfacial tension (N/m)

$\sigma_{ow}$  = oil-water interfacial tension (N/m)

$\sigma_{ao}$  = air-oil interfacial tension (N/m)

$\rho_{fw}$  = fresh water density ( $\text{kg}/\text{m}^3$ )

$g$  = gravitational acceleration ( $\text{m}/\text{s}^2$ ).

Determining constitutive relationships for fractured media continues to be an active research area. A Brooks-Corey (1966) analytical formulation was used to describe the constitutive relationships for the fractured basalt, which was treated as an equivalent porous media. The general Brooks-Corey formulas implemented in TETRAD are

$$P_{c\ aw} = A_{aw}(1 - S_w)^{B_{aw}} \quad (\text{A-6-14})$$

$$k_{ri} = A_i((S_i - S_{ir})/(1 - S_{ir}))^{B_i} \quad (\text{A-6-15})$$

where

$P_{c\ aw}$  = capillary pressure between air and water (kPa)

$k_{ri}$  = relative permeability of any phase  $i$

$S_i$  and  $S_{ir}$  = saturation and residual saturation of any phase  $i$

$A_{aw}$  (kPa),  $B_{aw}$ ,  $A_i$ , and  $B_i$  = fitting parameters for the Brooks-Corey functions.

The residual saturation was 0.01. Numeric values for the  $A_{aw}$  (kPa),  $B_{aw}$ ,  $A_i$ , and  $B_i$  curve-fitting parameters were 32kPa, 1.5, 1, and 2, respectively.

## A-6.1 Modifications to Version 12.7 Resulting in Version 12.7ms

Modifications to improve the computation efficiency for environmental modeling applications with the TETRAD, Version 12.7, simulator were described in Shook et al. (2003). The modified code resulting from this effort is called TETRAD, Version 12.7ms. Modifications were performed as part of an in-house laboratory-directed research and development project and consisted of allowing component-specific convergence criteria to be specified. This allowed tighter convergence criteria on those components representing contaminants and looser criteria for those components representing pure water, air, and a required nonaqueous phase liquid. Given the much larger mass of water and air present in the simulations, allowing appropriate convergence criteria for each component was a logical change.

Two additional changes were implemented in the TETRAD simulator during the transition from Version 12.7 to Version 12.7ms: (1) an implementation of a Millington formulation for calculating tortuosity during the simulation, based on total porosity and gaseous phase saturation; and (2) modifications to limit repetitive time-step output for problems with frequent surface or internal boundary condition changes (e.g., emulating barometric pressure fluctuations or positive pressures imposed downhole during drilling of wells). These two changes only affected input and output from the TETRAD simulator and did not affect the solution method used internally in the simulator.

## A-6.2 Quality Assurance

The TETRAD 12.7ms simulator is a proprietary code and its use constitutes an off-the-shelf application by modeling staff from the INL Site. Quality assurance and quality control for these types of simulations consist of ensuring that results are reproducible. This requires archiving a version of the simulator, the model inputs, the model outputs, and the processing codes used to create the inputs and outputs. An extensive searchable electronic archive is maintained by the OU 3-14 project for this purpose.

## A-7 VADOSE ZONE MODEL CALIBRATION

In this section, the adjustment of model parameters necessary to match simulated water levels and contaminant arrival histories to observed vadose zone data is presented. This calibration step is required because many of the model parameters tend to be scale-dependent. For example, the permeability measured in an interbed core sample may not adequately represent the interbed permeability represented by the numerical grid block volume. Further, it is not feasible for a large-scale numerical model, based on averaged hydrologic and transport properties and discrete grid sizes, to exactly represent each field observation of moisture content, perched water level, or solute concentration. Instead, the best overall match between simulated and observed water and solute movement becomes the target goal. Results presented here represent the best match between simulated and measured values achieved during the parameter adjustment or calibration process. The degree of agreement between the model and calibration data was quantitatively assessed through the use of a comparative statistical indicator (i.e., the root mean square error) and qualitatively assessed by graphically comparing simulated and observed data. The model calibration was performed manually, as opposed to being achieved through an automated or more rigorous parameter estimation process. As a result, it is neither unique, nor mathematically optimal.

The primary objective of the vadose zone flow calibration was to match the distribution of perched water. Specific aspects of the perched water distribution were the focus of calibration, including the (1) absence of perched water in some wells, (2) long-term water levels available in other wells, and (3) transient behavior of perched water resulting from recent perturbations in recharge rates. Recent perturbations include the current hydrologic drought, which began in 1997, and the relocation of the percolation ponds in 2002. Both of these changes have altered the recharge rate enough to result in the decline of perched water levels in some locations.

The primary objective of the vadose zone transport calibration was to match the timing and concentration of contaminant arrival in the perched water bodies and aquifer resulting from releases in the tank farm. Four contaminants were identified as having reasonably accurate source terms. These were Tc-99, Sr-90, H-3, and I-129. Although discussed in this section, nitrate was not used in calibration because arrivals in perched water did not coincide with the known nitrate sources. The highest emphasis was on matching the Tc-99 and Sr-90 concentration histories because their sources in the tank farm were large relative to the service waste releases. The Sr-90 calibration is presented separately in Appendix J, along with the geochemical model development. Less emphasis was placed on matching the H-3 and I-129 because of the difficulty in differentiating the arrival of H-3 and I-129 in the deep perched water from tank farm sources as opposed to the distribution originating during the injection well failure.

Concentration of the calibration targets and of all COCs are very small (dilute) and, because they are dissolved constituents in water, they do not affect transport velocity. However, the hydraulic and transport parameters cannot be obtained independently because, in unsaturated flow, the permeability and porosity influence both water pressure and transport velocity. As a result, the vadose zone model is calibrated in two iterative stages. In the first stage, the constitutive hydraulic model parameters are adjusted to match the observed water levels in the perched zones. In the second stage, transport parameters (porosity and dispersivity) are adjusted to obtain a match between simulated and observed contaminant arrival at monitoring locations. Changes in perched water levels resulting from the second step are reevaluated in an iterative fashion.

The model calibration process was performed in the following steps, beginning with the spatial distribution of lithology interpolated onto the grid in Section A-5, and the associated high/low-permeability flags for each grid block:

- 1). Assign constitutive parameters to the high/low-permeability groups. At the end of this step, the complete description of the six material types (2-alluvium, 2-basalt, and 2-interbed) was available.
- 2). Assign and adjust constitutive parameters ( $\alpha$  and  $n$ ), porosity and dispersivity to each material type. Initial parameterization of the model used the measured data discussed in Section A-3.2 and

the range of values permitted in the calibration process was constrained by the range of observed values.

- 3). Run the model to obtain the distribution of perched water and the arrival history for calibration targets.
- 4). Compare predicted perched water levels and contaminant arrival histories to observed data.
- 5). Adjust the lithologic database used to define permeability groups and use kriging to assign the permeability groups to model grid.
- 6). Go back to Step 1, reassigning the constitutive parameters to the changed lithology blocks.

At the end of several iterations, the parameters that provided the best visual agreement and minimized the difference between simulated and measured data were obtained. This calibration process is fairly standard with the exception of adjusting the lithology in Step 5. Adjusting the lithological description was an added step made necessary by the available material description in many well logs. In many wells, the material description was vague and did not differentiate between high- and low-permeability sediment or between high- and low-permeability basalt. In the initial assignment of material types, the material types were always assumed to be high permeability if the general description was “basalt” or “sediment” in the well logs. This default results in overestimating the areal extent of high permeability and prevents the formation of perched water in some locations. The high permeability identified in well logs at locations of known perched water was switched to low permeability and the geostatistics of the overall lithology were reestimated and the field reinterpreted using kriging (i.e., as described in Appendix C). Likewise, a few locations identified as low permeability in the well logs were changed to high permeability, if perched water was not observed in the field data but was predicted by the simulation.

Only a subset of the data presented in Section A-3 was used in the model calibration because the complete data set was too voluminous or would not provide useful information for model calibration. The specific observational data used in this calibration process are presented in Section A-7.1 along with a description of any data manipulation needed prior to model calibration. Final vadose zone model calibration results are presented in Sections A-7.2 and A-7.3 even though the calibration of flow and transport was achieved simultaneously. In these latter two sections, the match between simulated and observed values was evaluated qualitatively and quantitatively. Qualitative assessment of perched water simulations included time series plots of predicted and observed values versus time and vertical plots of simulated saturation versus depth. Qualitative assessment of contaminant arrival is similar, with predicted and observed values presented as a function of time. The root mean square (RMS) statistic was chosen to quantitatively evaluate the match between the field data and simulation results. The RMS statistic illustrates the average relative error between two data sets. The RMS is defined as

$$RMS = \sqrt{\frac{\sum_{i=1}^k (s_i - f_i)^2}{k}} \quad (A-7-1)$$

where

$f_i$  = field data point

$s_i$  = simulation data point

$k$  = number of comparison points.

The RMS was not calculated if the observed or simulated well screen locations did not have perched water present, and the average RMS presented in Section A-7.2 does not include these cases. The RMS was calculated separately for each well over the monitoring period.

The log of the simulated and observed perched water concentrations was taken before calculating the RMS error for the transport model calibration. This was done to reduce the bias of the error statistic towards wells with the highest concentrations. Perched water contaminant concentrations vary over many orders of magnitude in the vadose zone and using the log of the concentration provides a better estimation of the model's agreement with all the data. The RMS error was not calculated if either the simulated or observed concentration was zero, and the average RMS error presented in Section A-7.3 does not include these data.

## **A-7.1 Specific Data Used In Vadose Zone Model Calibration**

Calibration data were taken from the OU 3-13 RI/BRA (DOE-ID 1997), the OU 3-13 Group 4 MWTS report (DOE-ID 2003a), and ongoing remedial investigations at INTEC and ICDF. The specific vadose zone calibration data included (1) observed transient responses in perched water levels following the relocation of the percolation ponds and resulting from changes in Big Lost River fluxes and (2) perched water concentrations. The perched water level data used in the model calibration are discussed in Section 7.1.1, and the concentration data and the perched water chemistry data are presented in Section A-7.1.2.

### **A-7.1.1 Water Level Data**

Perched water levels in the 1992 through 2004 time period were used for calibration. Sources for these data include measurements taken manually and measurements obtained through automated field instrumentation. The raw water level data contained various irregularities and were reviewed and corrected as needed. Some of the automated water level data contained nearly 50,000 data points per well which was reduced before they could be efficiently used in model calibration. Often, both manual and automated water level measurements were available for the same well location and the data sets were combined before reducing the data. The techniques used to reduce the water level data are discussed below.

- **Manual Water Level Data**

The manual water level data were reviewed to locate any "suspect" data points (i.e., anomalously high or low elevations relative to the surrounding data). At locations where measurements were "suspect," the original field logbooks/field notes were reviewed and corrections were made. This included (1) correcting for transcription errors from the logbook to the project spreadsheet, (2) correcting surface casing stick-up values used to calculate depth to water, and (3) removing data points that were unrealistically different from measurements made the month prior/following. Since all measurements were made using the depth to water below measuring point, the stick-up value of the surface casing where the measuring point is located was subtracted from the field-measured value. These stick-up values came from WAG 3, Group 4, field measurements and from the ICDF well completion diagrams. Finally, the depth to water from land surface was subtracted from the brass cap elevation at each location to determine a water level elevation which was then converted to meters for the model. These data were flagged within their respective files to indicate that the source for the measurement was manual.

Dates for manual water level measurements reflect the general day on which water level measurements were taken and may not have been the exact date of data collection. The discrepancy in exact date arises because the recorded date corresponded to the start of a sampling campaign, which may have taken several days.

- **Automated Water Level Data**

Several of the wells contain one of four different automated pressure transducers: Solinst Leveloggers, Insitu Minitrols, In-situ Hermit dataloggers, and Sentinel dataloggers. In these wells, water levels were either recorded as head above the monitoring unit, depth to water from a known elevation, or an actual water level elevation, depending on the instrument. All data were converted to depth below a measurement location.

Files containing head measurements as depth to water were first checked to ensure that the data conversions were correctly applied. These measurements were compared to the manually recorded data taken during the same time period to confirm that the automated measurements were correct. Where discrepancies existed, logbooks describing the transducer installation and/or manual water level measurements were reviewed and the discrepancies were corrected. If data did not accurately represent water levels at that location over time, they were removed from the data set. Examples of these data points include automated measurements taken during water sampling events and erroneous automated measurements occasionally recorded by the instrument. The Hermit transducers were programmed to record water levels below a given elevation and did not require conversions. The Sentinel data contain the oldest automated data collected in this study. These recorders report water level elevation. Logbooks describing their installation have not been located and manual water level measurements have not been found for this time period. These data were flagged within their respective files to indicate that the source for the measurement was automated and the type of instrument that took the reading.

- **Water Level Data Reduction**

Prior to data reduction, the number of measured data points in most wells containing automated measuring instrumentation ranged from 234 (Well PW-3) to 42,611 (Well CPP-37-4). Using data collected every 30 minutes for model calibration is not efficient and adds little additional information to the slowly changing seasonal trends. To improve calibration efficiency, most of the automated water level data sets were reduced to a few hundred data points. The data were averaged over a number of observations while preserving seasonal variations and the influence of changing recharge rates. The data reduction algorithm averaged the data points over a selected time-window range. Water levels within a given time window were averaged and the averaged value was assigned to the center of the time increment. The mean and variance statistics of the raw and reduced data were calculated and compared to ensure that the data character had not significantly changed during the data reduction.

### **A-7.1.2 Water Chemistry Data**

Perched water chemistry and COC concentrations were collected from the INL Environmental Data Warehouse (EDW), the INL's Hydrologic Data Repository (HDR), and the MWTS report (DOE-ID 2003a). For the purposes of calibration, focus was on tritium, Sr-90, I-129, and Tc-99. In general, chemistry data are sparse, many INTEC perched water wells have never been sampled for these data, and only a few recent measurements are available in most wells. In a few wells, some data are available beginning in the early 1960s and extending through 2004.

As with the water level data, concentration data contained various irregularities and required review and correction. Data quality indicators are associated with chemistry data indicating nondetected values, estimated values (rather than measured), and rejected samples (U and/or UJ, J, and R). For calibration and plotting purposes, U and UJ flagged data indicate nondetect and were recorded as zero. In these data, samples were flagged nondetect if the radionuclide analytical results were not statistically positive at the 95% confidence level. Although the choice of confidence level is somewhat arbitrary, in practice 90%, 95%, and 99% levels are often used in science and engineering to denote the data has acceptable error, with 95% being the most commonly used value. The J-flagged data indicated that the sample concentration was a recorded estimate in the EDW/HDR data base. These values were retained. R-flagged data indicated that the sample was rejected and the data points were removed from the calibration data set. Flags were included in the model input file to record relevant information associated with the sample result.

## **A-7.2 Vadose Zone Flow Calibration Results**

Observations of perched water elevations indicate that northern INTEC wells respond to variations in Big Lost River flow, and that southern INTEC wells responded to the removal of the percolation ponds. In between those two regions, the discharge rates prior to taking remedial action were quite similar to the rates after remedial action was taken. The relatively small change was reflected in the lack of transient perched

water level response in the central INTEC region. In the final calibration results presented here, the predicted high saturation elevations are generally in agreement with this observed behavior. On the average, the simulated decline in perched water elevations resulting from the percolation pond relocation was less than observed. The model predicted that the positive pressure would become negative but that the saturations would remain high. The model did not predict that percolation pond water would spread horizontally to the contaminated perched water in northern INTEC. This will result in the model predicting higher interbed contaminant concentrations in northern INTEC perched water and aquifer than was predicted by the OU 3-13 model.

The vadose zone model predicted the existence of perched water bodies beneath the Big Lost River and the percolation ponds. The model predicted positive pressure to only occur beneath these areas. However, both the pre- and post-remedial action discharge rates were sufficient to result in nearly saturated conditions in the low permeability interbed material. The saturation in all low-permeability interbed areas within the INTEC fence line was very near saturation.

Hydraulic parameters used in the final calibrated model are presented in Table A-7-1. The constitutive relationships used for the fractured basalt were those used by Magnuson (1995) and are discussed in Section A-6. However, the residual saturation was increased to 0.01 and the  $B_i$  parameter in Equation 6-15 was increased to 2.0. These values did not significantly change water and solute transport results but greatly reduced simulation run times. The very small residual saturations in Table A-7-2 for the alluvium and low-permeability interbeds were adjusted up from the zero value reported in the MWTS report (DOE-ID 2003a) to prevent numerical problems. These values represent a best fit to the measured moisture versus matric potential data. The reported moisture characteristic data are not accurate at the dry extreme, but the simulated recharge does not allow soil to drain to these conditions. The calibrated high permeability interbed porosity was 0.60. This value is within the range of measured values of interbed porosity obtained from core samples documented in DOE-ID 2003a and is representative of the data measured from the highest permeability cores.

The predicted and observed saturations are spatially and temporally varying. To simplify presentation, we first illustrate the distribution of perched water following the relocation of the percolation ponds (2002) and during the peak flow year for the Big Lost River recorded at Lincoln Boulevard bridge gauge (1999) in Figure A-7-1. This figure shows that areas of positive pressure (saturation = 1, and represented by red) and areas that are near saturation (0.99, represented by blue) are aerially extensive. It also illustrates that high saturations occur in the low- and high-permeability interbeds near the Big Lost River and percolation ponds, in addition to occurring in the low-permeability interbeds between these two primary recharge areas. These high saturations result in ephemeral perched water forming at the well screens as observed in many of the INTEC perched water wells where only small amounts of water can be withdrawn from the well.

The distribution of water and association with specific media are further illustrated in the vertical well profiles given in Figures A-7-2 through A-7-5. In the low-permeability interbeds, the saturations are nearly one; in the high-permeability interbeds, the saturations approach 0.5; and, in the basalt regions, the saturations are much lower. The vertical moisture profiles presented in Figures A-7-2 through A-7-5 correspond to dates in the 2003-2004 time period where field data are available and include the locations of the well screen top and bottom (dashed blue horizontal lines) and the observed elevations of the perched water (red horizontal line). If the red horizontal line is at the plot bottom, the well was dry. The wells are ordered from the north to the south with wells north of CPP-3 presented in Figures A-7-2 and A-7-3 and wells south of CPP-3 presented in Figures A-7-4 and A-7-5. The calibration results for the northern upper shallow, northern lower shallow, northern deep, southern shallow, and southern deep perched water zones and discussions of observed and simulated perched water behavior are further discussed in Sections A-7.2.1 through A-7.2.5, respectively.

**Table A-7-1** Final calibrated hydraulic parameters.

Material Type	Horizontal Permeability	Horizontal Hydraulic Conductivity	Porosity	Permeability Anisotropy	Residual	van Genuchten Parameters	
	(mD)	(cm/sec)		(Horizontal to Vertical)	Saturation	Alpha (1/m)	n
High-permeability alluvium	34,570	2.79E-2	0.32	1 to 1	0.0002	100	1.40
Low-permeability alluvium	1	8.04E-7	0.39	1 to 1	0.0002	0.2	1.34
High-permeability interbed	4,107	3.30E-3	0.60	1 to 1	0.11	10.5	1.29
Low-permeability interbed	3	2.41E-6	0.49	1 to 1	0.0002	0.01	1.38
High-permeability basalt	42,310.	3.40E-2	0.03	10 to 1	0.01	a	a
Low-permeability basalt	5,230.	4.20E-3	0.03	10 to 1	0.01	a	a

a. The basalt did not use the van Genuchten constitutive relationship (see Section A-6.)

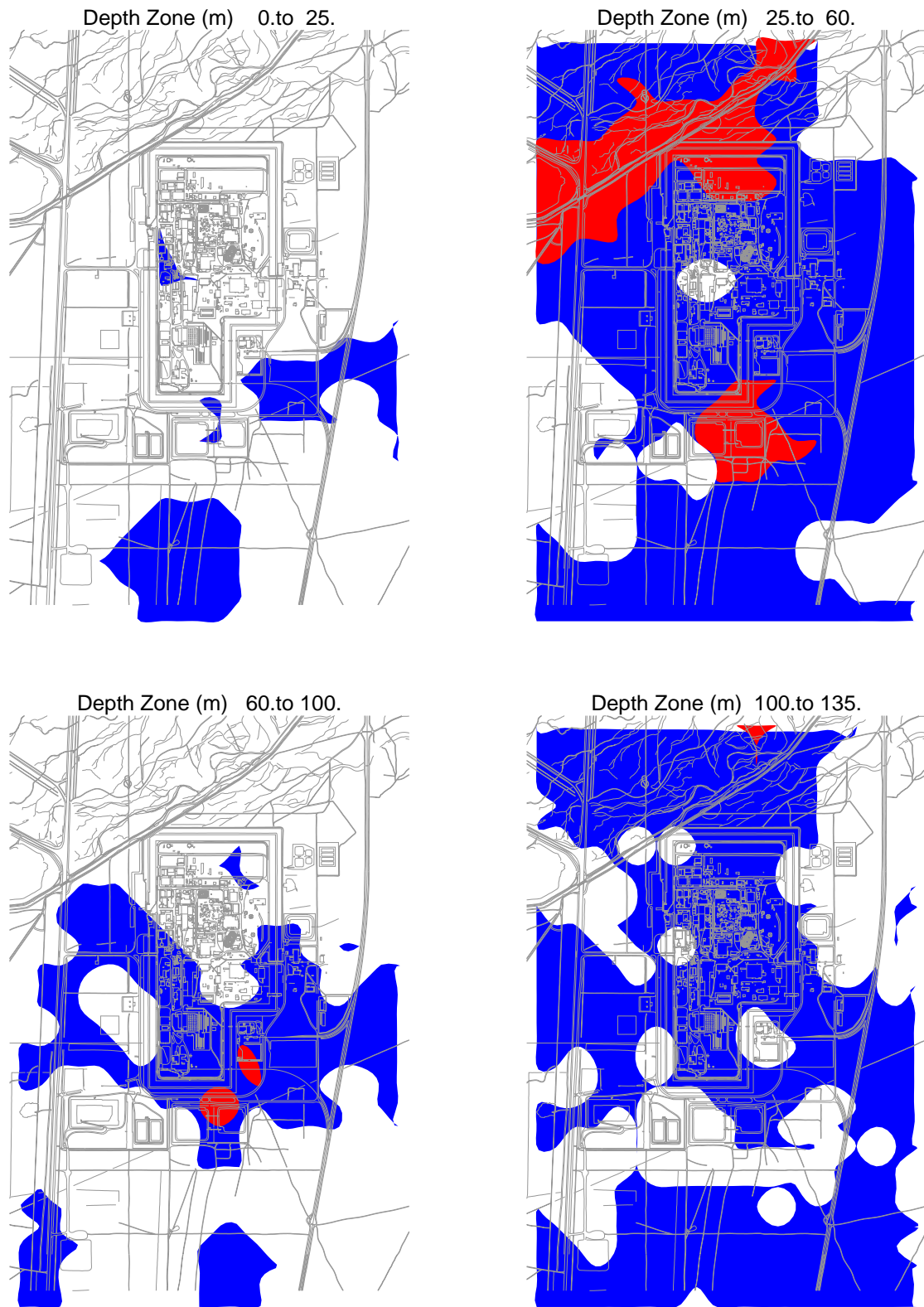


**Figure A-7-1.** Horizontal extent of simulated perched water at different depth intervals during the peak Big Lost River flow in 1999 (blue saturation = 0.99, red saturation = 1.0).

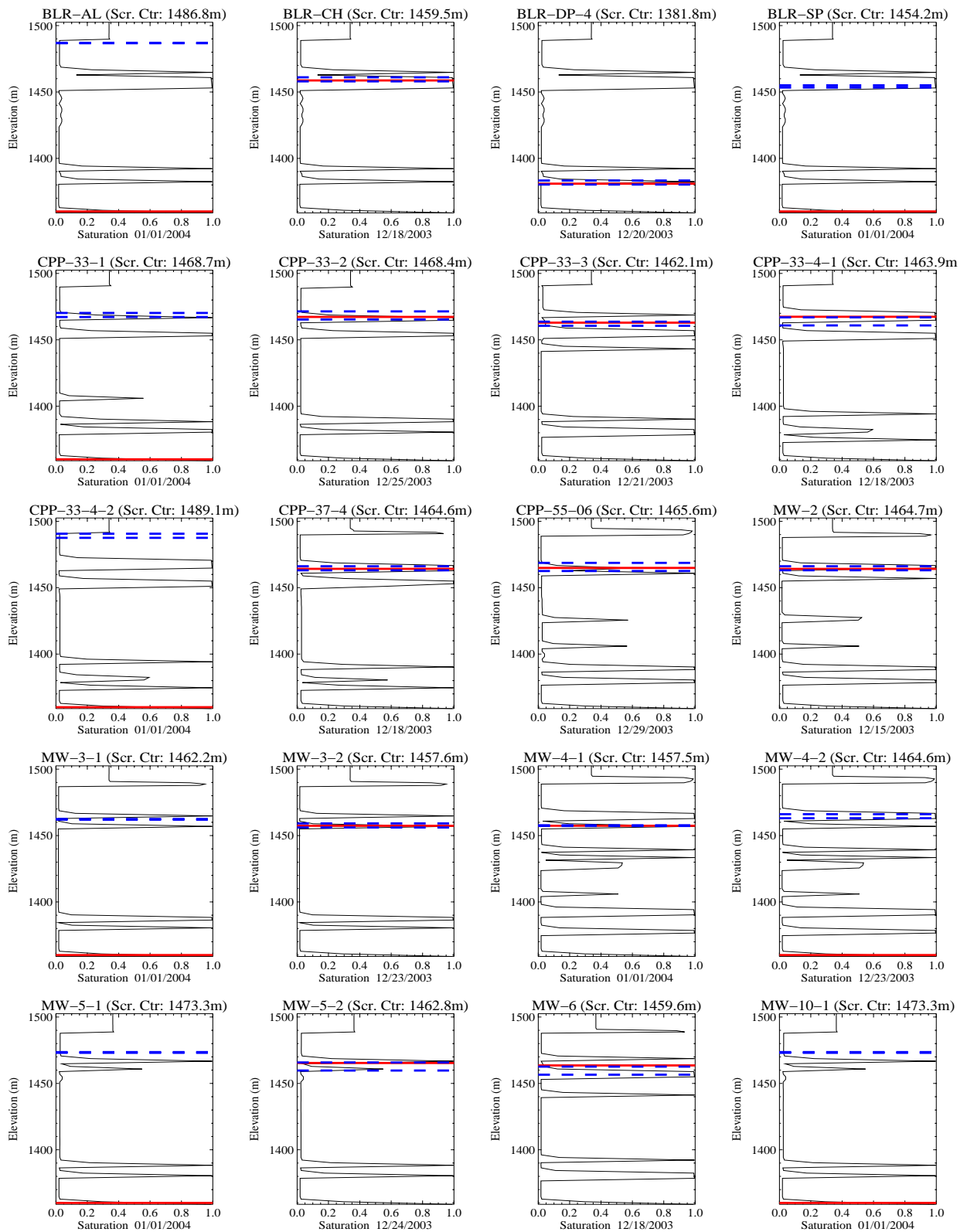


**Figure A-7-2.** Simulated saturation versus depth for northern perched water well locations after percolation pond relocation (dashed blue line = well screen top and bottom, red line = water elevation).

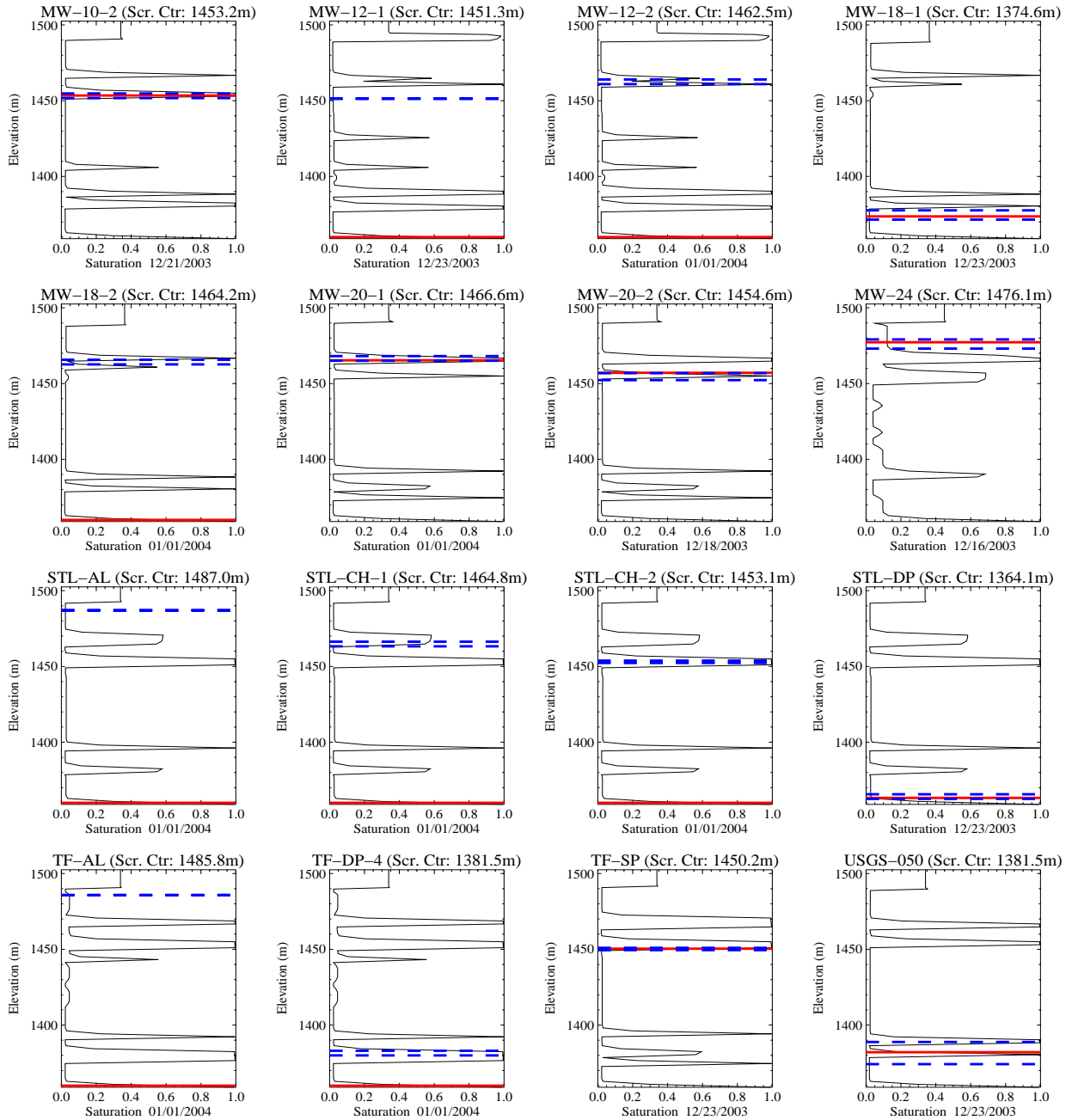


**Figure A-7-3.** Simulated saturation versus depth for northern perched water well locations after percolation pond relocation (continued) (dashed blue line = well screen top and bottom, red line = water). elevation).

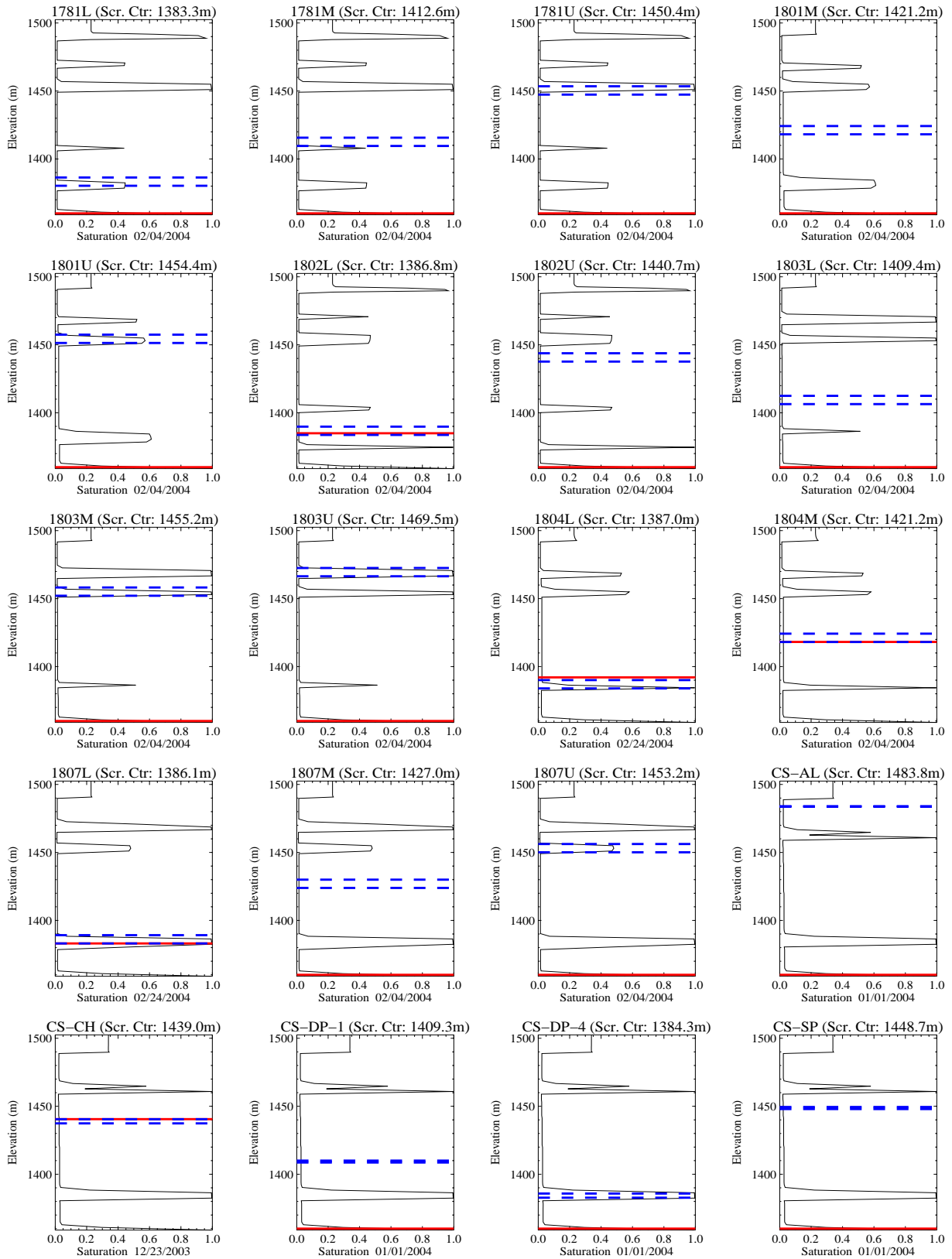


**Figure A-7-4.** Simulated saturation versus depth for southern perched water well locations after percolation pond relocation (dashed blue line = well screen top and bottom, red line = water elevation).

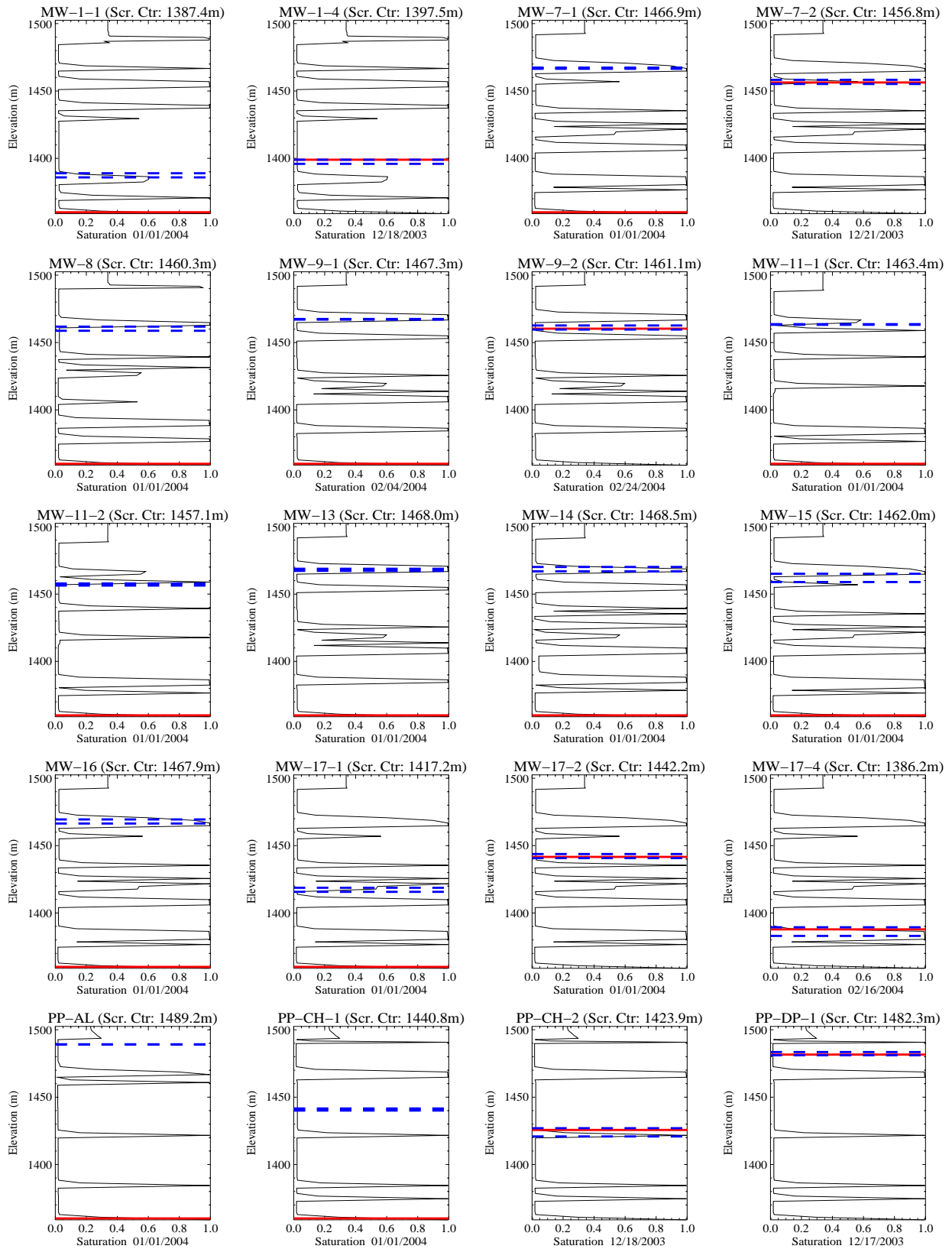


**Figure A-7-5.** Simulated saturation versus depth for southern perched water well locations after percolation pond relocation (dashed blue line = well screen top and bottom, red line = water elevation).

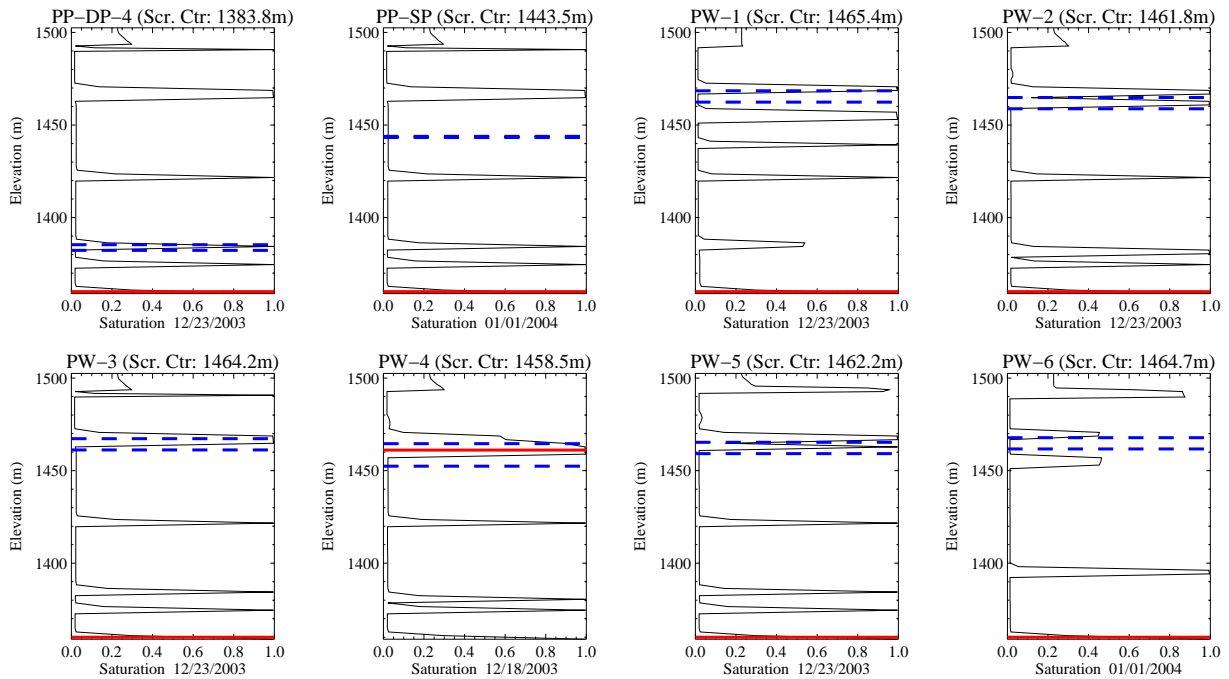


**Figure A-7-6.** Simulated saturation versus depth for southern perched water well locations after percolation pond relocation (dashed blue line = well screen top and bottom, red line = water elevation).

### A-7.2.1 Northern Upper Shallow Perched Water

The northern upper shallow perched water is associated with the 110-ft interbed. The recharge sources may include the Big Lost River, the sewage treatment lagoons, precipitation, irrigation, and facility releases from leaking pipes and steam vents. A recent geochemical study of perched water indicates the sewage lagoons probably had little influence on the northern shallow perched water (EDF-5758). The northern upper shallow perched water region was defined to include all well screens located north of the CPP-3 injection well and located higher than 4,780-ft elevation.

Most of the observed data from the northern upper shallow perched water wells reflect seasonal fluctuations corresponding to increased spring recharge from snowmelt, precipitation, flow in the Big Lost River, and anthropogenic sources. Some of the wells in this region have responded to the recent hydrologic drought that began in 2000. Wells responding to the drought include MW-4-2 and CPP-37-4, which exhibit a clear decline in perched water elevation since 2000. This can be more clearly seen in Figure A-3-3 of Section A-3.4. In contrast, water levels have been increasing in BLR-CH since 2003. The increase in the BLR-CH well is thought to be due to facility discharge, but the source is unknown. A match to this increase by the model would not be expected.

In general, the simulated high saturation elevations were in good agreement with observed data. Notable exceptions are wells MW-24 and CPP-55-06, where the elevation of predicted 0.95 saturation was lower than observed, and well MW-3-2, where elevation of the 0.95 saturation was predicted to occur at a higher elevation than observed. These observations suggest that the elevation of the interpolated interbeds in these areas is slightly different than the actual elevation. Observed data from CPP-33-1, MW-3-2, MW-2, MW-4-1, MW-4-2, MW-12-2, and MW-20-1 show that these wells experienced intermittent dry periods, which were not captured in the simulations. The intermittent dry periods could be inferred as absences in the otherwise continuous time series data. Wells BLR-AL, CPP-33-4-2, MW-5-1, MW-10-1, TF-AL and STL-AL did not have perched water present in either the simulations or observations.

Observed data reflect a transient response to quarterly variations in Big Lost River recharge. These quarterly variations were reflected in the model period spanning 1985-2004 (see Sections A-5.1.3). However, these observed temporal changes were not captured in the simulated northern upper shallow high saturation elevations except the BLR-CH well, which showed a slight increase in elevation during peak river flow. This suggests a lack of hydraulic connectivity between the Big Lost River water and the 110-ft interbed. In contrast, a transient response was predicted in most of the northern lower locations (see Section A-7.2.2). This is because the dip of the simulated 110-ft interbed beneath the river is away from the tank farm, but the dip of the 140-ft interbed is towards the tank farm. In all of the simulated responses, short-time-scale seasonal trends in observed data were not captured. The lack of seasonal response is a direct consequence of assuming precipitation is a steady-state process.

Time series plots of observed and simulated high saturation elevation for the northern perched water body are illustrated in Figures A-7-7 and A-7-8. The elevation of the model grid block nearest to the well screen in which a saturation above 0.95 was predicted was used to reflect the plotted value. The red lines correspond to this approximate elevation and the black crosses correspond to the observed elevation. Wells in which perched water was neither predicted or observed correspond to plots without data. Plots with only a red line indicate the model predicted the presence of perched water, but the observations indicated that the well is dry. Plots with only black crosses indicate perched water was measured but that perched water was not predicted to exist.

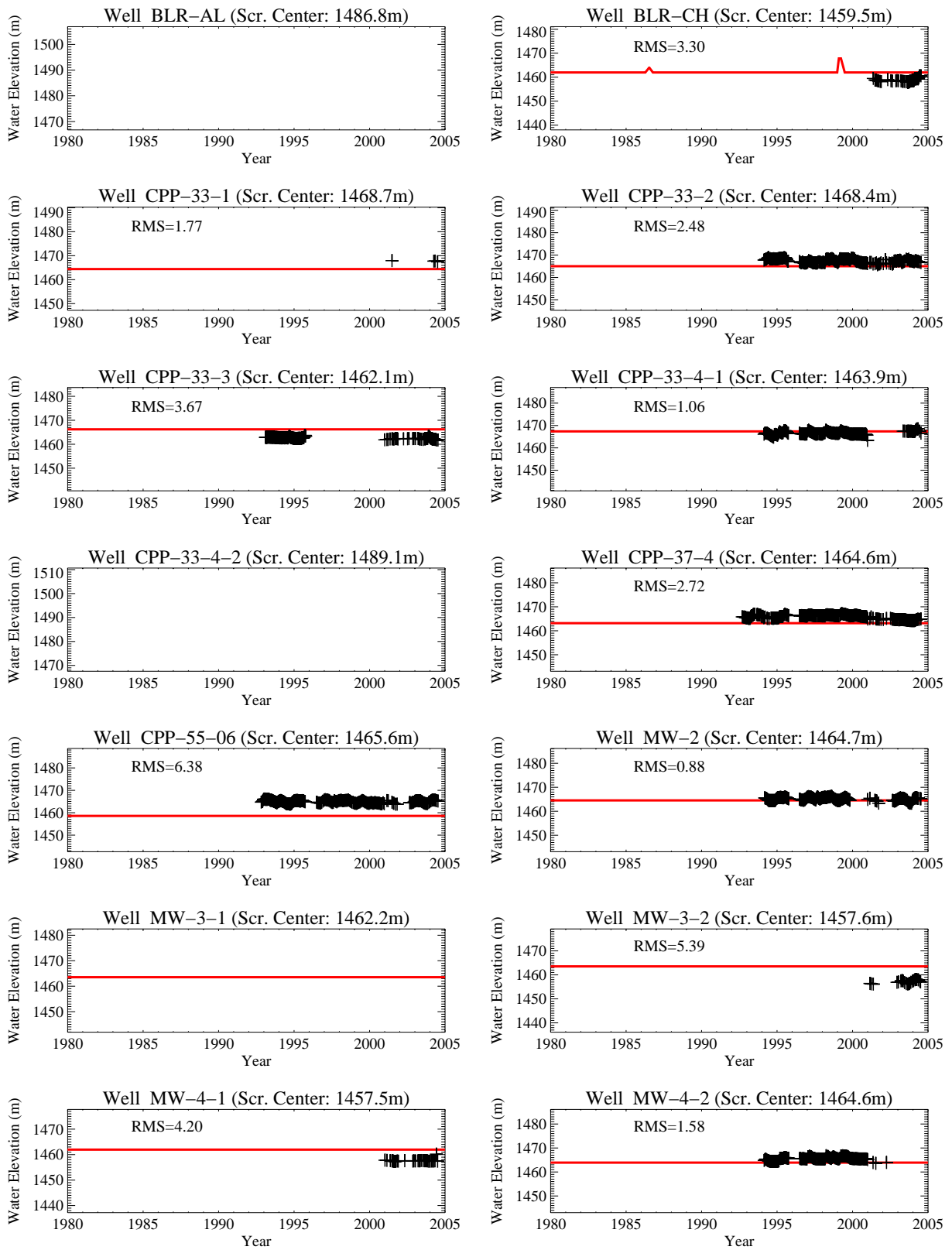


**Figure A-7-7.** Time series water elevation plots for the northern upper shallow perched water (red line = predicted elevation of 0.95 saturation, back crosses = measured data).

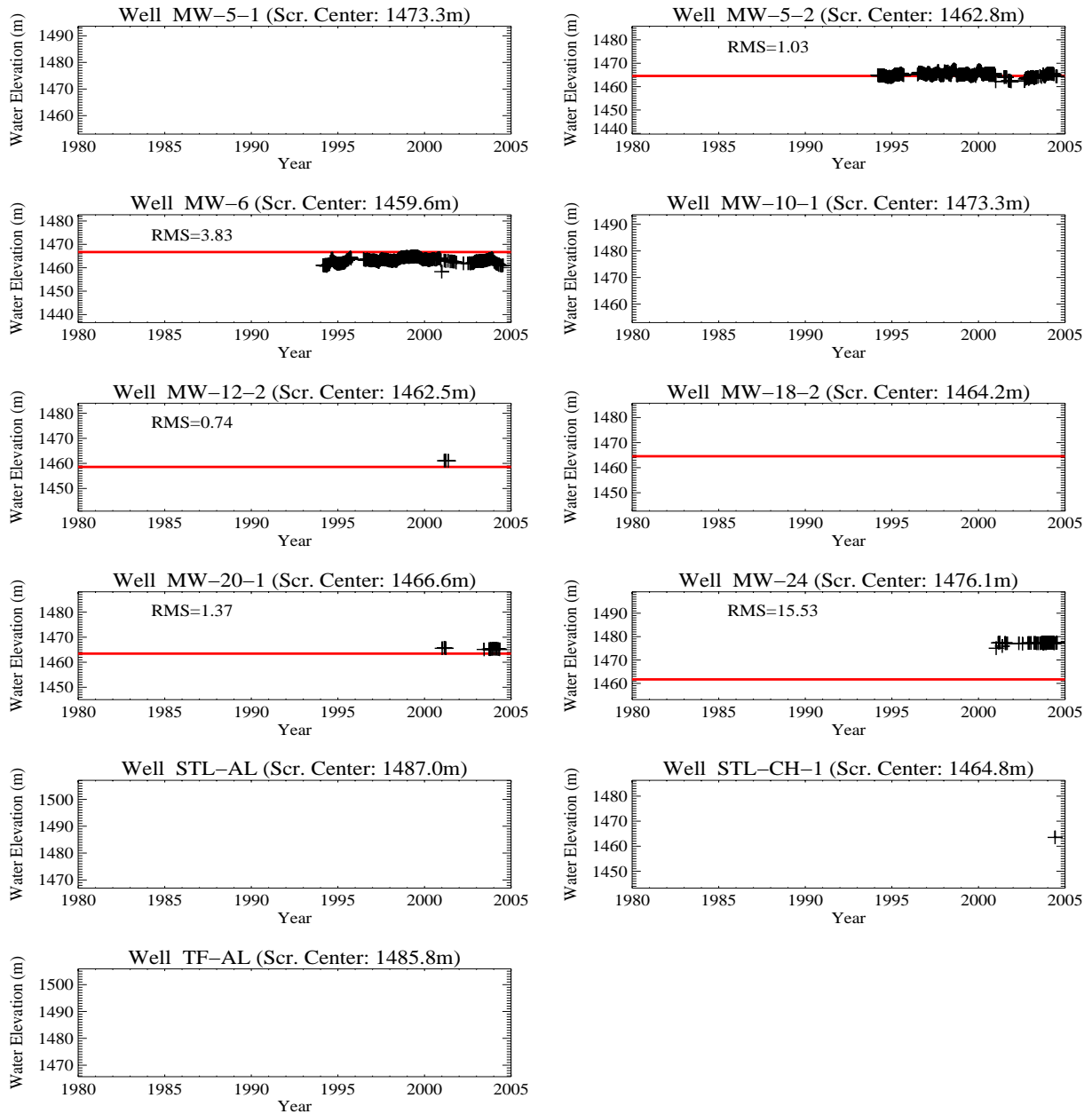


**Figure A-7-8.** Time series water elevation plots for the northern upper shallow perched water, continued. (red line = predicted elevation of 0.95 saturation, back crosses = measured data).

### A-7.2.2 Northern Lower Shallow Perched Water

The northern lower shallow perched water is associated with the 140-ft interbed, and the primary water sources are most likely the same as those for the northern upper shallow perched water. This region was defined to include all well screens located north of the CPP-3 injection well and located lower than 4,789-ft, but higher than 4,741-ft, elevation. Observational data are only available from the last couple of years in these

wells and, as a result, do not reflect the temporal variation in water levels that were observed in the northern upper shallow perched water.

In general, the simulated high saturation elevations were in good agreement with observations. Exceptions include well MW-12-1, in which the predicted water elevations were higher than observed, and Wells BLR-SP and STL-CH-2, which were predicted to have perched water present but did not have perched water observed. Additional anomalies include wells MW-10-2, MW-12-1, and TF-SP, which have historically been dry intermittently but were predicted to have perched water present throughout the simulated time period.

A transient response to the simulated Big Lost River fluctuations was predicted in all the northern shallow perched wells except MW-12, which suggests that the northern lower shallow perched water wells are recharged by the Big Lost River. This was not seen in the observed data, although several of the northern lower shallow perched water wells were constructed after the start of the 2001 hydrologic drought. These predicted responses suggest that the 140-ft interbed may be responsible for moving river water laterally. Time series plots of observed and simulated high saturation elevations for the northern perched water body are illustrated in Figure A-7-9.

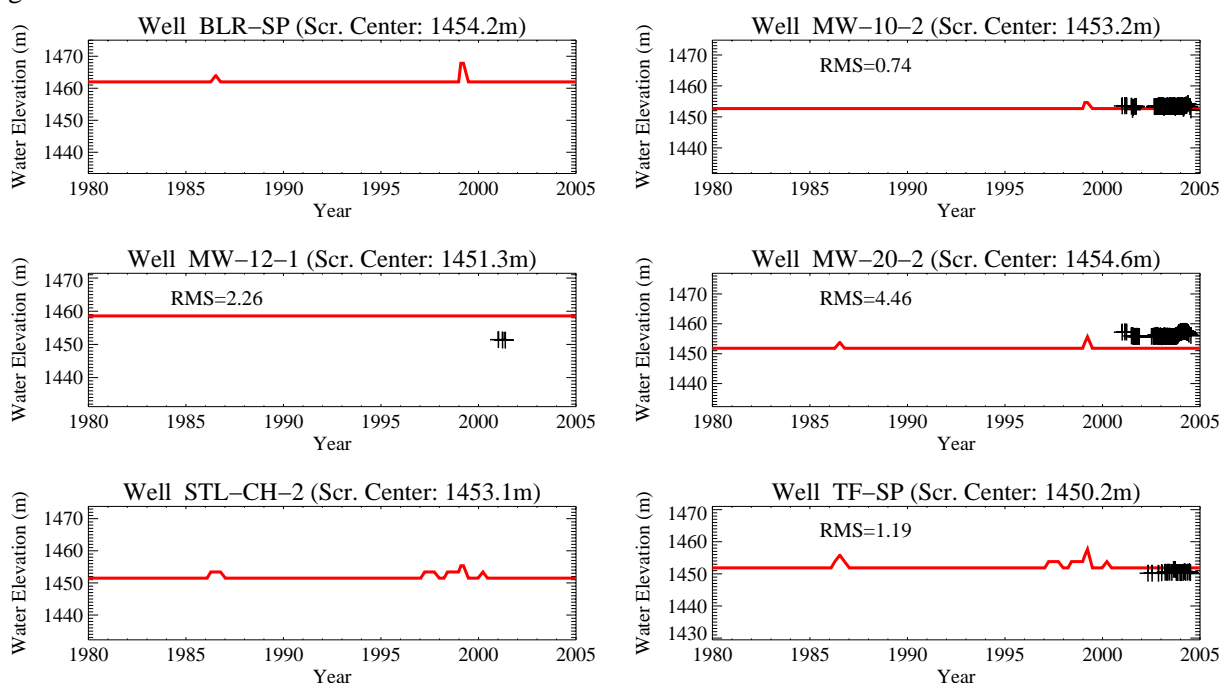


**Figure A-7-9.** Time series water elevation plots for the northern lower shallow perched water (red line = predicted elevation of 0.95 saturation, back crosses = measured data).

### A-7.2.3 Northern Deep Perched Water

Predictions discussed in this section correspond to well screens located lower than 4,741 ft in elevation and located north of the CPP-3 injection well. Perched water in this region is thought to be associated with the 380-ft interbed, although it has been encountered deeper than the 380-ft interbed at wells STL-CH, MW-18, and USGS-50. Deep perched water southwest of the tank farm has also been encountered in well MW-1 at approximately 320 ft and may be associated with low-permeability basalt at this depth. As with the northern shallow perched water zone, the northern deep perched water recharge sources may include the Big Lost River, the sewage treatment lagoons, precipitation, irrigation, and facility releases from leaking pipes and steam vents. However, the CPP-3 injection well and the USGS-50 well may have also contributed to the deep perched

water. The CPP-3 injection well collapsed during the late 1960s and was not repaired until 1970. During the repair period, USGS-50 was used as a temporary injection well.

The simulated and observed high saturation elevations generally had good agreement with the exception of well STL-DP and well TF-DP-4. The observed perched water at well STL-DP could not be matched with the model because this location is within basalt (high permeability and low porosity equivalent porous media representative of flow in fractures). Although low-permeability basalt exists in the vadose zone model, the hydraulic parameters do not significantly differ from the high-permeability basalt values and are not conducive to forming perched water. Globally reducing the low permeability enough to produce perched water in the basalt resulted in grossly overestimating the perched water extent in the basalt, and these parameters were not selected for the calibrated model. Other observations include

- Perched water elevations in wells BLR-DP and STL-DP have been declining in response to the recent hydrologic drought. The decline was not captured by the simulations although the longer term average was.
- Wells MW-18-1 and STL-DP have both been intermittently dry. This intermittent behavior was not captured in the simulations.
- The elevation of perched water predicted in well MW-18-1 was higher than the observed elevation.
- Well TF-DP-4 did not have observed perched water present, but the simulation predicted perched water was present.

Time series plots of observed and simulated high saturation elevations for the northern perched water body are illustrated in Figure A-7-10.

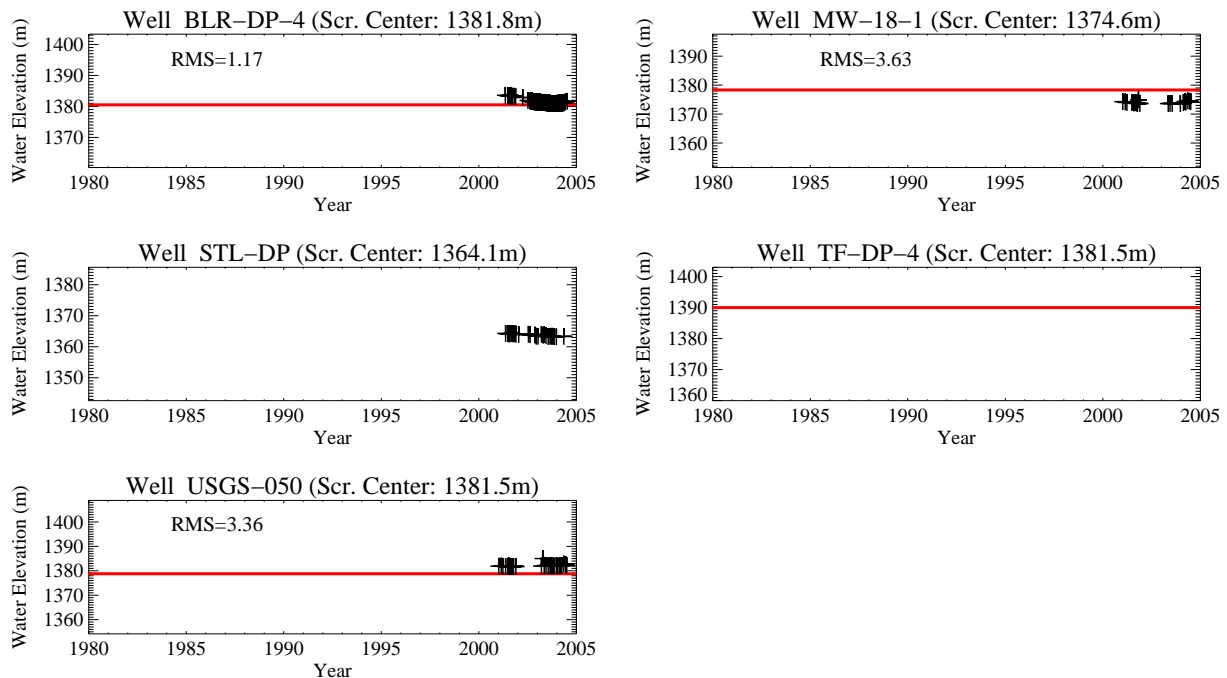


**Figure A-7-10.** Time series water elevation plots for the northern deep perched water (red line = predicted elevation of 0.95 saturation, back crosses = measured data).

#### **A-7.2.4 Southern Shallow Perched Water**

The southern shallow perched water region includes all well screens located south of the CPP-3 injection well and located higher than 4,741-ft elevation. As explained in Section A-3.4, there are two shallow perched water zones in this region. The first is near Building CPP-603 and is associated with the 140-ft interbed, and the second is a larger region located beneath the former percolation ponds and is associated with the 110- and 140-ft interbeds.

Time series plots of observed and simulated high saturation elevation for the northern perched water are illustrated in Figures A-7-11 and A-7-12. The transient decline in simulated perched water following the relocation of the percolation ponds was not as dramatic as the observed perched water decline. Wells PW-1, PW-2, PW-3, and PW-5, which are located near the former percolation ponds, went dry after percolation pond relocation on August 26, 2002. A decline in simulated water elevations was predicted in these wells, but they were predicted to remain nearly saturated through the end of the calibration period in 2005. However, the model did predict that positive pressures below the percolation ponds would quickly become negative after the percolation ponds were removed. The apparent discrepancy is, in part, due to the cutoff value chosen to represent saturation in the simulation results as opposed to using tensiometric data during the drainout period. The elevation of the model grid block nearest to the well screen in which a saturation above 0.95 was predicted was used to reflect the perched water elevation. If a higher threshold saturation was used, the wells would appear to drain faster. The 0.95 threshold value was chosen to be consistent with the results of the large-scale infiltration test and the resultant fractured basalt constitutive relationships used in this and other INL vadose zone models (Magnuson 1995).

Predicted high saturation elevations in wells PW-4 and PW-5 were lower than observed, while predicted elevations in wells MW-9-2, PP-DP-1, PW-2, and PW-3 were higher than observed. These results suggest that the simulated interbed elevation is slightly different than the actual interbed elevation in these areas. The predicted perched water decline in well PW-4 was very close to that observed. Wells MW-8, MW-9-2, MW-11-2, MW-13, MW-15, and PP-DP had intermittent dry periods which were not predicted. Wells 1781U, 1801U, 1807U, CS-AL, CS-SP, MW-7-1, MW-9-1, MW-11-1, MW-14, MW-16, and PW-6 did not have perched water present in the simulations or observations. The location of well PW-6 is approximately 1,000 ft west of the former percolation ponds. Intermittent perched water and contamination most likely originating from the former percolation ponds have been measured in this well. However, the vadose zone model did not predict water from the percolations ponds would travel this far west. This is because the simulated 110-ft interbed becomes discontinuous southeast of the INTEC facility.

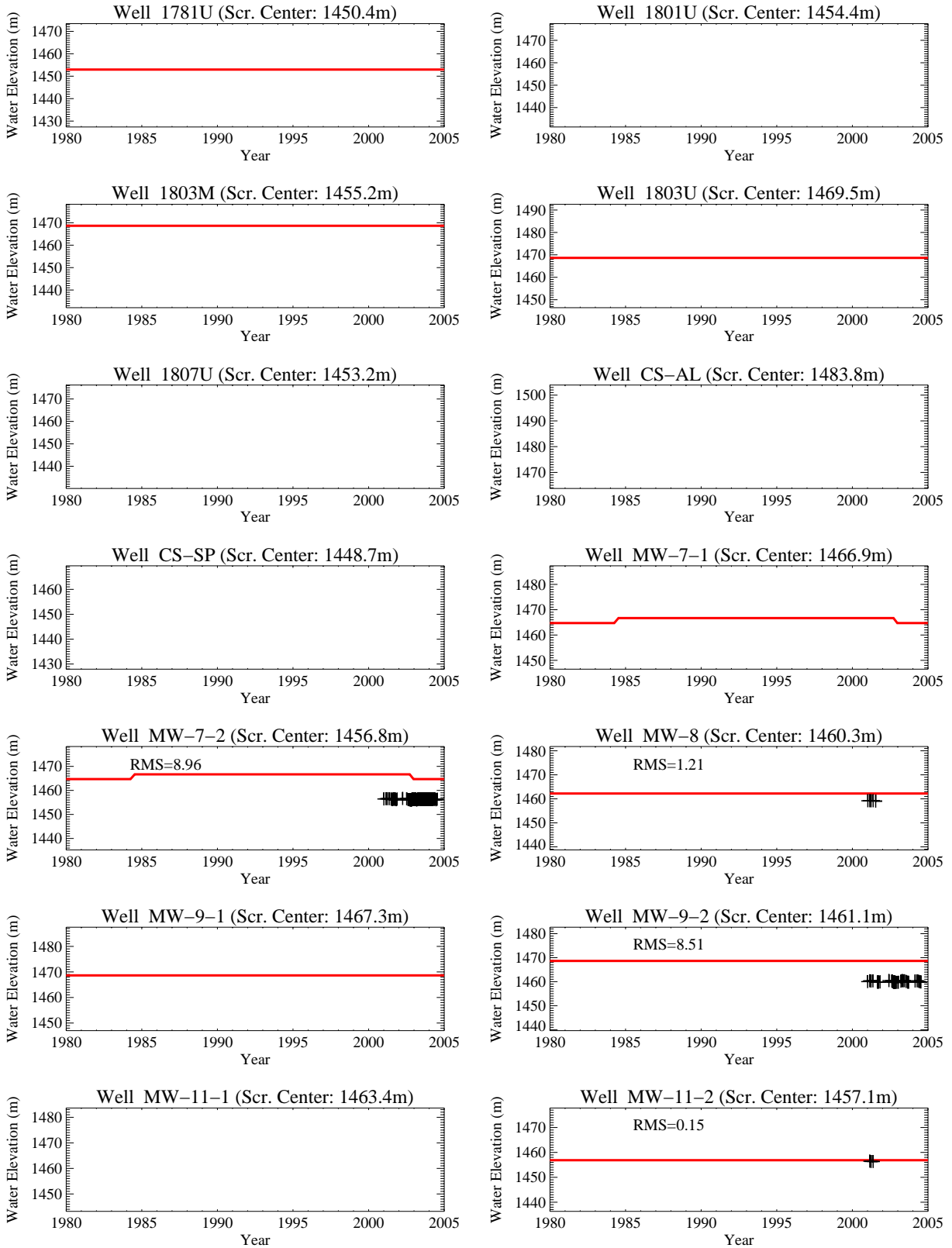


**Figure A-7-11.** Time series water elevation plots for the southern shallow perched water (red line = predicted elevation of 0.95 saturation, back crosses = measured data).

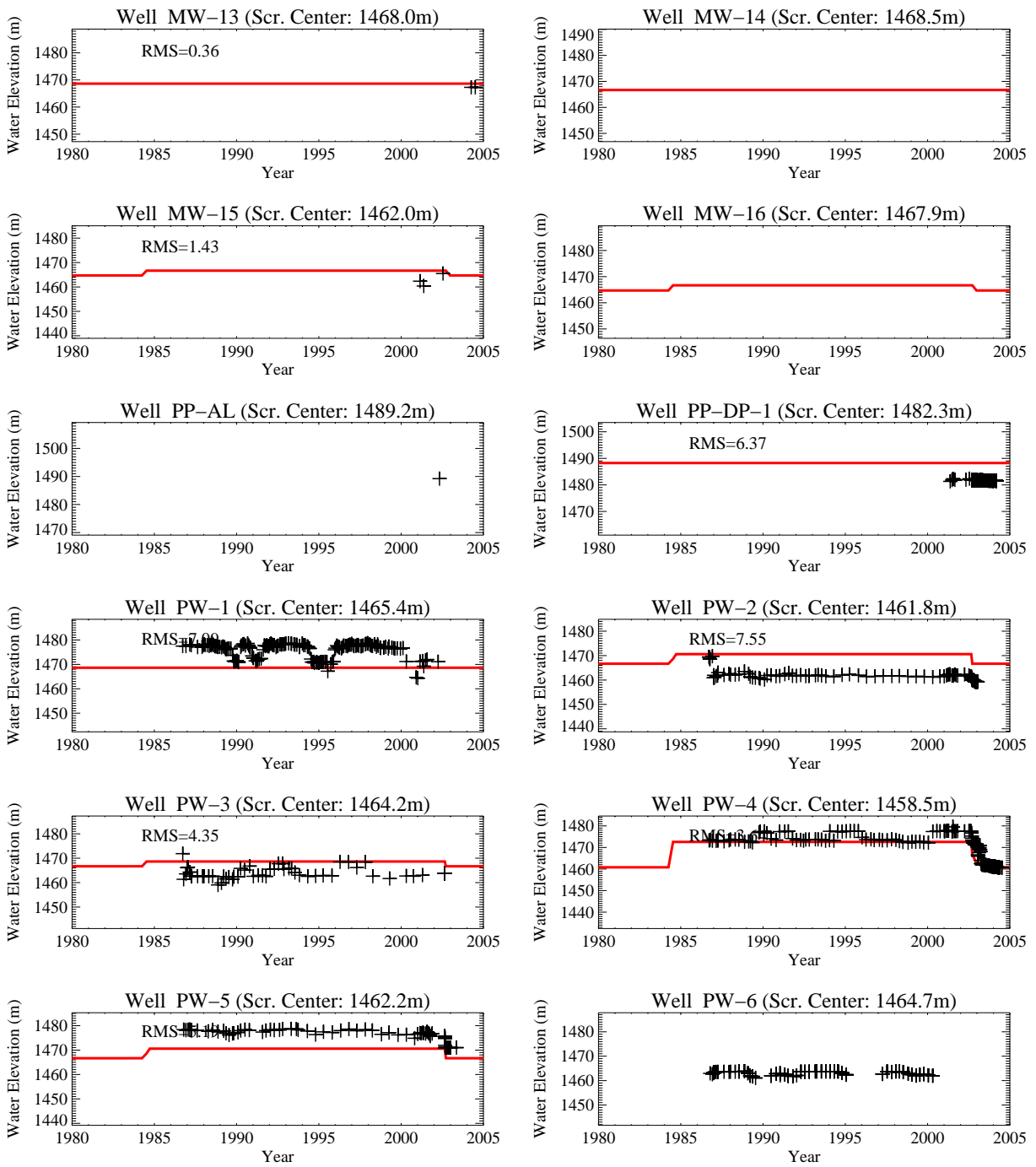


**Figure A-7-12.** Time series water elevation plots for the southern shallow perched water, continued (dashed blue line = well screen top and bottom, red line = predicted elevation of 0.95 saturation, black crosses = measured data).

### A-7.2.5 Southern Deep Perched Water

The southern deep perched water includes perched water encountered from 180 ft to 380 ft below land surface. It is primarily associated with the 380-ft interbed and appears to have been recharged by the former percolation ponds. This region includes all well screens located south of the CPP-3 injection well and lower than 4,741 ft elevation. Key observations include

- Perched water has never been observed in half of the southern deep perched water wells. These dry wells included 1781L, 1781M, 1801M, 1802U, 1803L, 1807M, MW-1-1, MW-17-1, PP-CH-1, and PP-SP. The simulated wells were also dry at these locations.
- There is an apparent discrepancy between actual and model interbed elevations in the area of wells 1804L and 1802L. Simulated high saturation elevations were lower in those wells than observed data.
- There were several wells in which perched water was observed but not predicted, again because of the conceptual model for flow in the fractured basalt. These wells with simulated completion intervals in basalt included 1804M, CS-DP-1, CS-CH, and MW-1-4.
- Wells 1802L, MW-17-2, MW-17-4, and PP-DP-4 had intermittent dry periods which were not predicted by the simulated perched water.
- Only well PP-DP-4, which is located near the former percolation ponds, went dry after the percolation pond relocation on August 26, 2002. A decline in simulated perched elevation was not predicted in this well, but a decline in simulated deep perched water was predicted in PP-CH-2 located approximately 40 m higher.

Time series plots illustrating these observations are given in Figures A-7-13 and A-7-14.

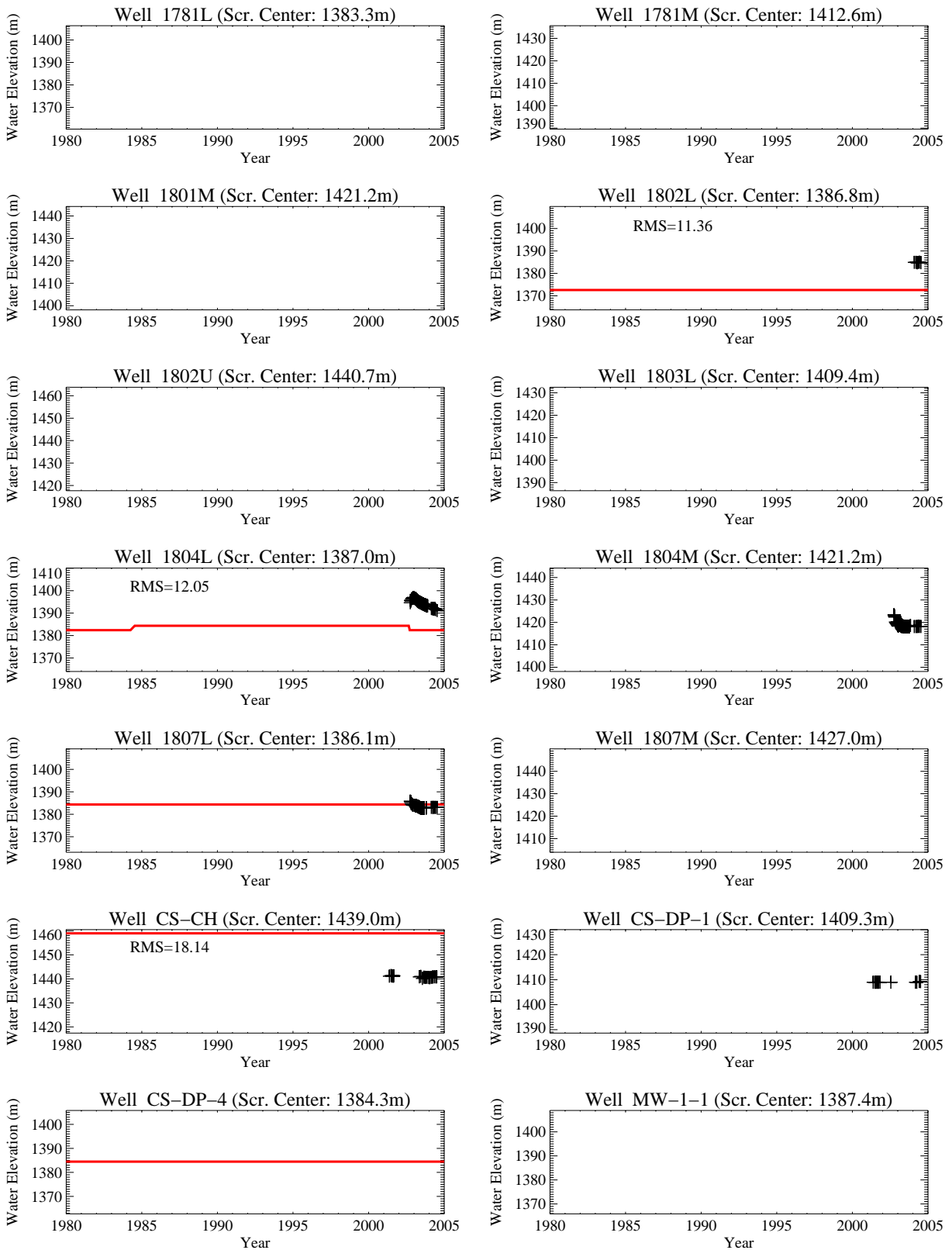


**Figure A-7-13.** Time series water elevation plots for the southern deep perched water (red line = predicted elevation, back crosses = measured data).

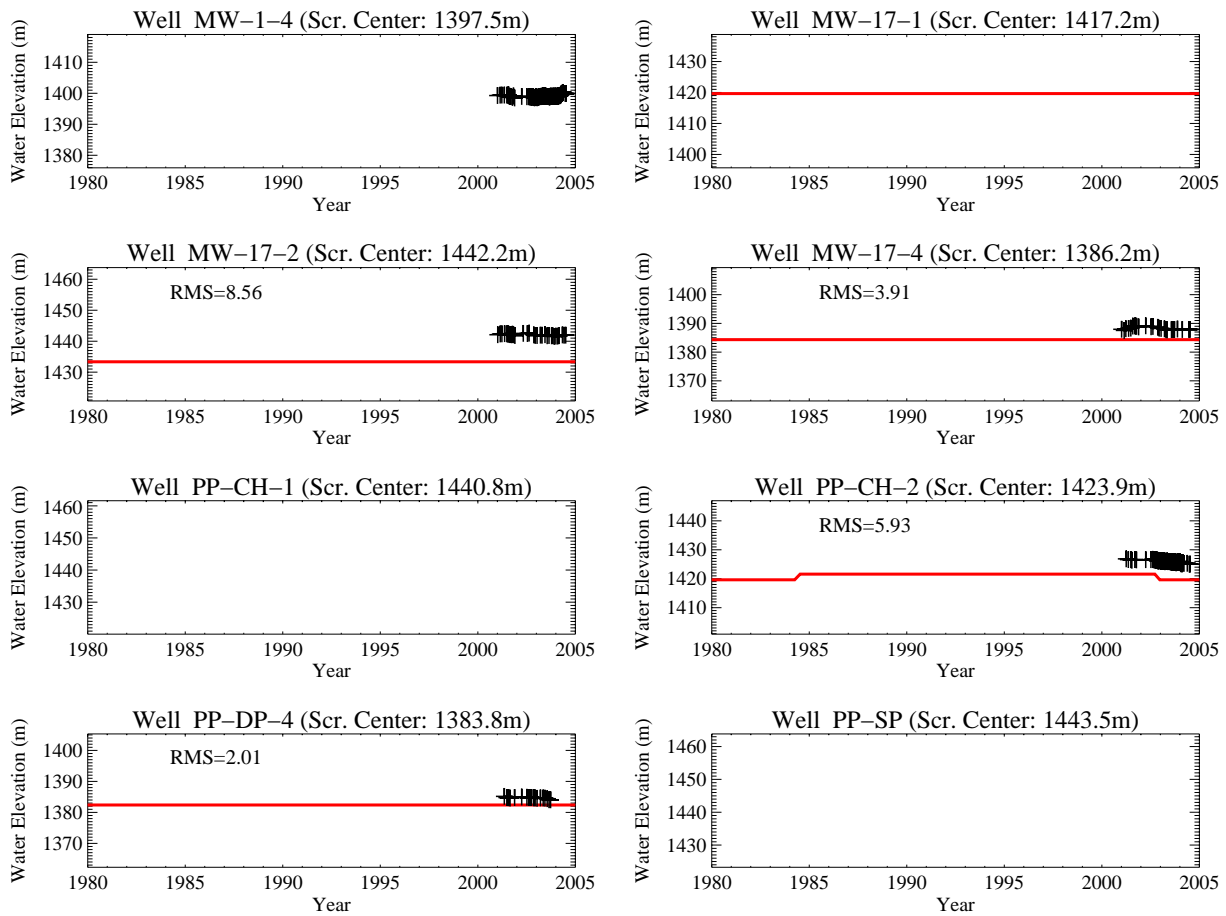


**Figure A-7-14.** Time series water elevation plots for the southern deep perched water, continued (red line = predicted elevation, back crosses = measured data).

### A-7.3 Vadose Zone Transport Calibration

Contaminants in the perched water beneath INTEC have resulted from various leaks and spills during liquid transfer operations in the vicinity of the tank farm and from the disposal of service waste in the vadose zone during the CPP-3 injection well failure. The service waste was the source of most of the tritium, I-129, and nitrate released to the subsurface. The tank farm releases were the source for most of the Sr-90. Comparable amounts of Tc-99 originated from the service waste and from the tank farm releases. Confidence in the Tc-99 service source term is poor because it was never monitored in the service waste and was estimated from far downgradient aquifer concentration ratios (see Section A-9.2).

All of the known releases of H-3, I-129, Sr-90, Tc-99, and nitrate were used in the calibration process. Tank farm releases; the OU 3-13, Group 3, soil sites; and the CPP-3 injection well failure are the dominant source locations in the northern portion of INTEC. The dominant sources in southern INTEC include the discharges in the former percolation ponds, the CPP-02 abandoned french drain located near Building CPP-603, and the OU 3-13, Group 3, soil sites. Most of the perched water concentration data were collected during and after the OU 3-13 RI/BRA and only date back to the early 1990s. Tritium and Sr-90 were often the most analyzed radionuclides, while Tc-99 and I-129 were analyzed less often. Because of the sampling history, matching contaminant arrival in the deep perched water for contaminants originating in the tank farm is

difficult. Additionally, the USGS-50 well has been monitored since the late 1960s. However, the arrival signals from tank farm releases have been dominated by the releases to the vadose zone occurring during the CPP-03 injection well failure and during use of the well for service waste disposal. The arrival of tank farm contaminants having a large service waste component and small tank farm component are not visible in USGS-50, because the service waste signal is much larger. The USGS-50 concentration history may not accurately represent travel time through the vadose zone because perched water has been seen cascading down the well bore and attempts at fixing the leaky well bore have been only partially successful.

The calibration results for Tc-99, tritium, I-129, and nitrate are presented in Sections A-7.3.1 through A-7.3.3, respectively. The Sr-90 calibration is presented in Appendix J along with the geochemical model development. Predicted concentration histories in the northern upper shallow, northern lower shallow, northern deep, southern shallow, and southern deep perched water zones are discussed separately in each section. The transport calibration was achieved by adjusting the hydraulic parameters, source term placement, and dispersivity as discussed below:

- The source term placement adjustment was only performed if the release site straddled two model grid blocks. This was the case for Site CPP-31, which was almost evenly divided by two model grid blocks in the east-west direction; placing the CPP-31 source in the east grid block improved agreement in both the western and eastern direction.
- A longitudinal dispersivity of 1 m and transverse dispersivity of 0.1 m provided best agreement between observed and simulated values for all calibration contaminants.

A summary of the calibrated model's transport parameters is presented in Table A-7-2.

**Table A-7-2** Calibrated model transport parameters.

Contaminant	Alluvium $K_d$ (mL/g)	Interbed $K_d$ (mL/g)	Basalt $K_d$ (mL/g)	Longitudinal Dispersivity (m)	Transverse Dispersivity (m)
Tc-99	0.	0.	0.	1.	0.1
Sr-90	Variable as predicted by geochemical modeling for CPP-31, 0.25 for all others	22.	0.	1.	0.1
I-129	1.5	0.7	0.	1.	0.1
H-3	0.	0.	0.	1.	0.1
Nitrate	0.1	0.1	0.	1.	0.1

### A-7.3.1 Tc-99

The simulated sources of Tc-99 in the vadose zone listed in order of increasing magnitude are the OU 3-13, Group 4, soil sources (0.1 Ci); service waste ponds (1.13 Ci); CPP-3 injection well failure (1.05 Ci); and tank farm sources (3.56 Ci). Tc-99 is primarily produced as a fission product and does not have a naturally occurring background concentration. It is long-lived and is very mobile (zero  $K_d$ ). Tc-99 was not sampled for regularly, the peak concentrations were often missed, and the concentration history within specific wells is not definitive. Current Tc-99 concentrations in the aquifer beneath northern INTEC are above the MCL and are most likely higher than those resulting from CPP-3 injection well operation, although there are no aquifer monitoring data available during this time period. This suggests that Tc-99 originating from tank farm releases has migrated deep into the vadose zone and is currently contaminating the aquifer beneath INTEC.

Figure A-7-15 illustrates the total simulated rate of Tc-99 arriving in the aquifer over time. Four peak activity periods can be seen in Figure A-7-15. These are the result of the following: (1) the injection well failure during the late 1960s, (2) the service waste ponds during the early 1980s to the early 1990s, (3) the transient Big Lost River recharge during the late 1990s, and (4) the long-term average Big Lost River recharge following the recent hydrologic drought.

The Big Lost River has a large impact on Tc-99 transport. The hydrologic drought during the early 1990s resulted in reduced recharge and a decrease in Tc-99 flux rate. This drought ended in the late 1990s and the year 1999 was the peak flow year for the Big Lost River recorded at Lincoln Boulevard bridge gauge. A sharp increase in Tc-99 arrival occurred as result of the increased recharge and continued until the current hydrologic drought began in the year 2000. The long term average was used to define future Big Lost River flow. Peak transport of Tc-99 from surface sources was predicted to occur during the late 1990s. A second, smaller peak in flux is predicted to occur in the 2004-2010 time period (also see Figure A-7-16). The highest concentrations deep in the vadose zone are predicted to occur just south of the tank farm near the MW-18 monitoring well. The shallow vadose zone contamination located immediately north-west of the former percolation ponds is due to the CPP-22 OU 3-13 soil site (0.1 Ci), which was placed in the model in 1990.

The simulated Tc-99 concentrations in the perched water generally showed good agreement with the sparse observed data. The arithmetic average log RMS and standard deviation for all well locations was 1.14 and 0.6, respectively. The minimum log RMS was 0.19 and the maximum was 2.8. This error represents an average error of one order of magnitude.

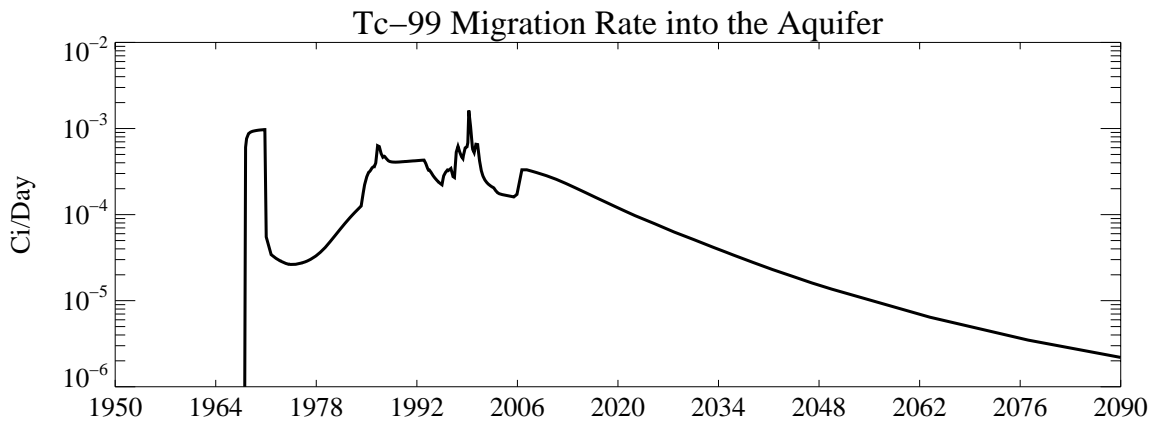


**Figure A-7-15.** Total flux of Tc-99 entering the aquifer (Ci/day).

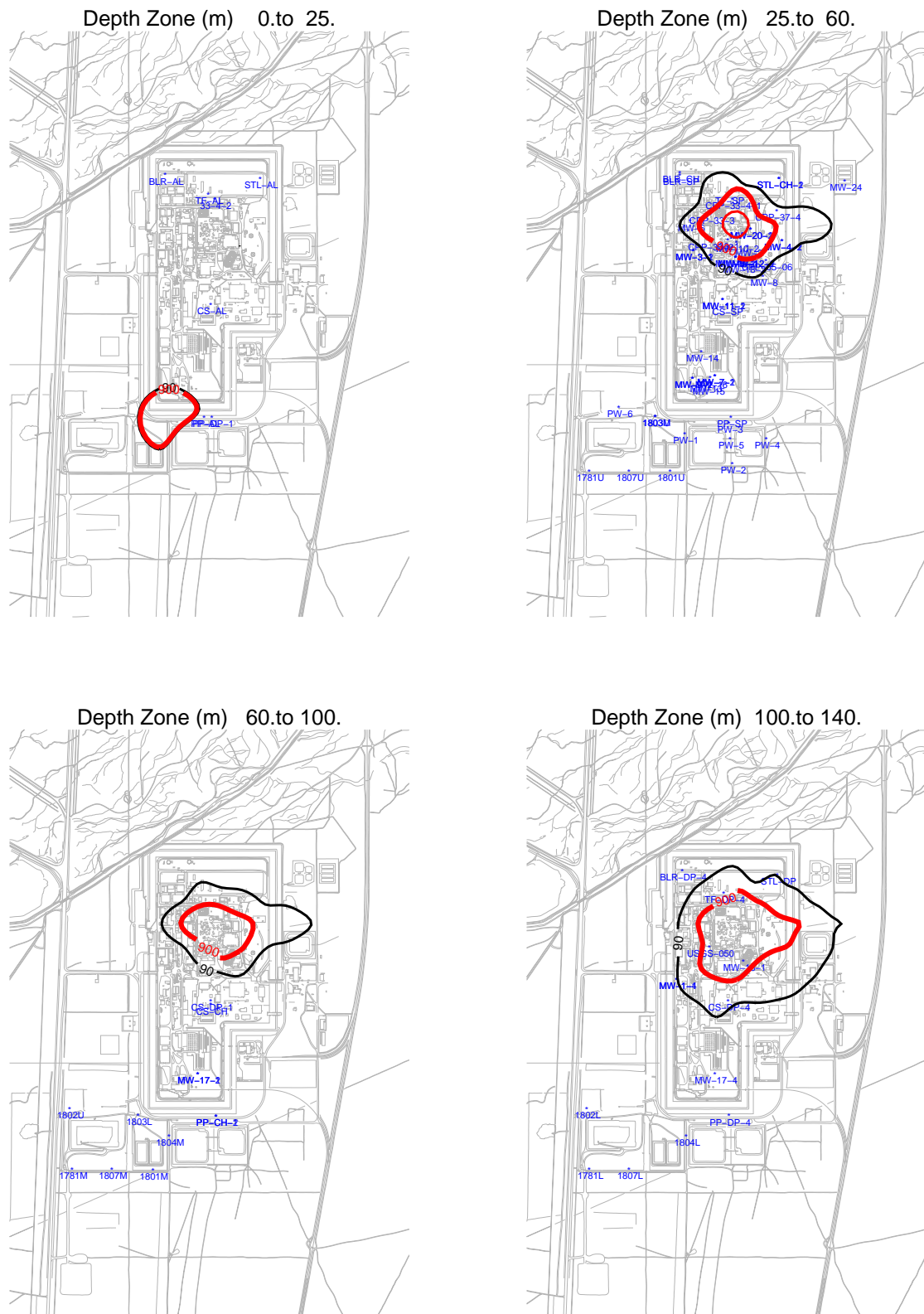


**Figure A-7-16.** Horizontal extent of simulated Tc-99 at different depth intervals in the vadose zone in 2004 (red isopleth is 900 pCi/L).

### **A-7.3.1.1 Northern Upper Shallow Perched Water Tc-99**

The northern upper shallow perched water is associated with the 110-ft interbed, and the contamination sources are the tank farm soil sources and OU 3-13, Group 3, soil sources. The highest observed Tc-99 concentrations were in well 33-1 at 690 pCi/L in 2004. High concentrations have also been measured in well MW-2 at 174 pCi/L in 1994 and 224 pCi/L in 2004. Concentrations in well MW-2 have been near 200 pCi/L since Tc-99 monitoring began in 1993 and continue to date. Well MW-5-2 has also had high observed Tc-99 concentrations, which have been near 100 pCi/L during the 1993-1995 time period but which have not been detected since 2001. The observations in the other northern upper shallow perched water wells have always been near or below 10 pCi/L. Tc-99 concentrations in the northern upper shallow perched water are not declining in all wells. They are persisting in well MW-2. The peak concentrations of Tc-99 in the northern shallow perched water most likely occurred early in the 1980s and the current concentrations are slowly tailing off.

Concentrations of Tc-99 were mostly overpredicted (Figure A-7-17). The higher simulated concentrations in the perched water wells surrounding the tank farm suggest that Tc-99 is not moving horizontally to the extent predicted by the model or the tank farm Tc-99 has already moved below the upper shallow perched water.

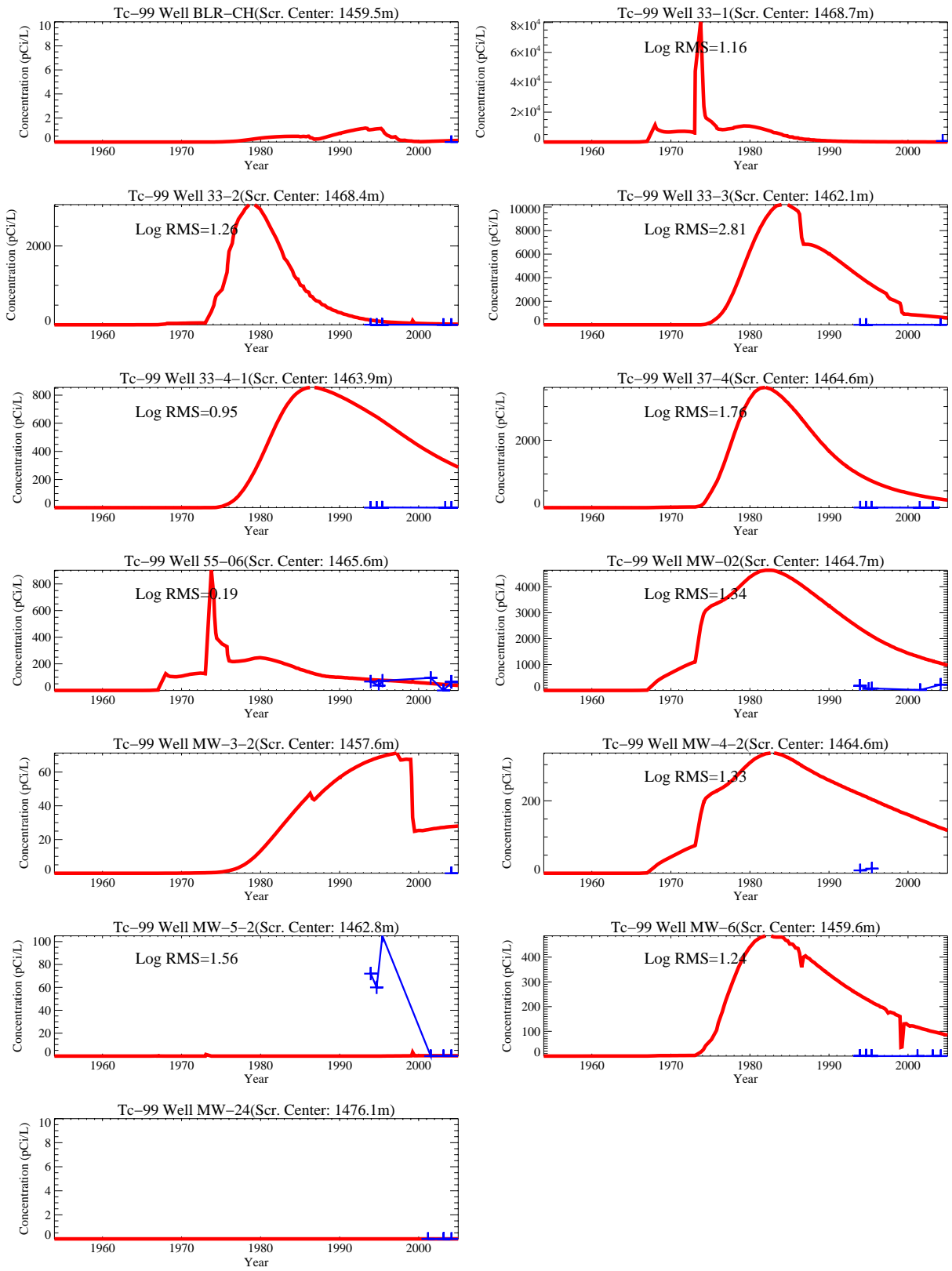


**Figure A-7-17.** Tc-99 concentrations in the northern upper shallow perched water (red line = simulated, blue crosses = observed, pCi/L).

### A-7.3.1.2 Northern Lower Shallow Perched Water Tc-99

The northern lower shallow perched water is associated with the 140-ft interbed and the contamination source is primarily associated with tank farm releases. The highest observed Tc-99 concentrations are in well MW-10-2 (592 pCi/L in 1994, and 451 pCi/L in 2004). Concentrations in well MW-20-2 have been variable throughout the sampled period and have ranged from zero to 49 pCi/L. Observed concentrations in the BLR-SP and TF-SP have been below detection. The low and relatively constant concentrations seen in the field data suggest peak arrival occurred prior to the first observations in 1994.

The simulated and observed concentration patterns are similar to those in the northern upper shallow perched water. The highest concentrations are beneath the tank farm and immediately south and east of the tank farm. The simulated concentrations overpredict the observed values (Figure A-7-18). The large abrupt changes in concentration predicted to occur in the northern lower shallow perched water are due to the quarterly step change in simulated Big Lost River recharge. The wells nearest to the Big Lost River reflect a larger response (i.e., wells TF-SP and TF-CH). The model predicts the 140-ft interbed to be more directly affected by the river than is the 110-ft interbed (see Section A-7.2.2). This is because the slope of the 110-ft interbed beneath the river is away from the tank farm, but the slope of the 140-ft interbed is towards the tank farm.

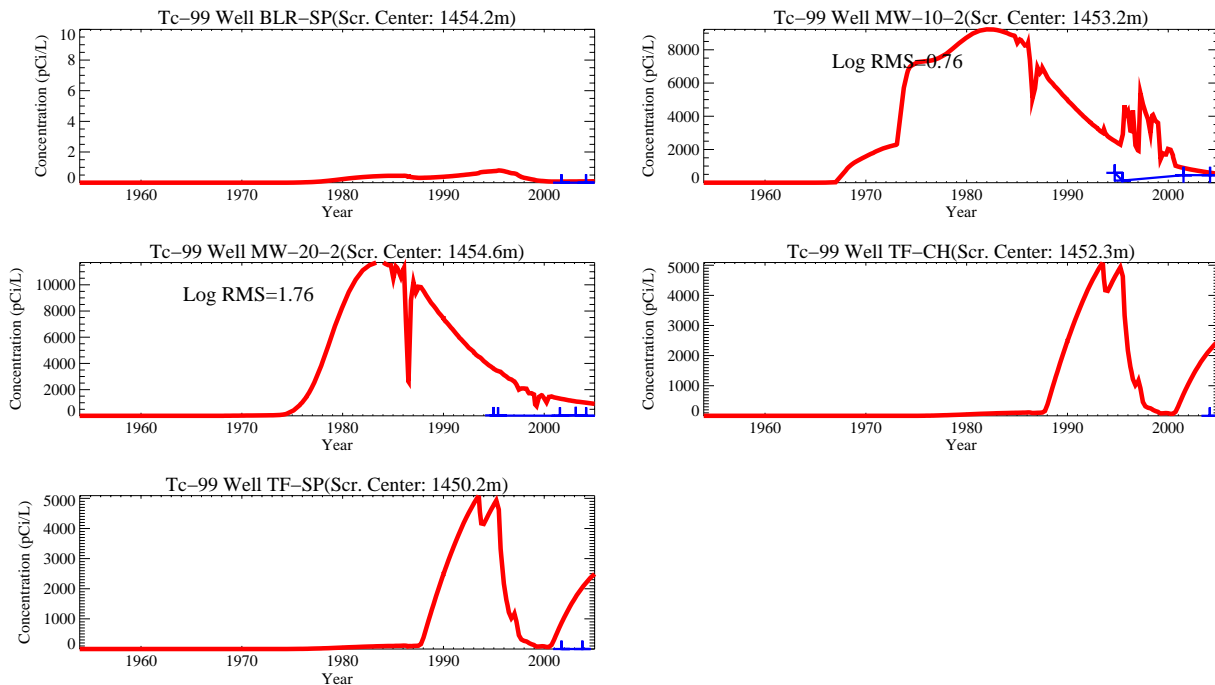


**Figure A-7-18.** Tc-99 concentration history in the northern lower shallow perched water (red line = simulated, blue crosses = observed, pCi/L).

### A-7.3.1.3 Northern Deep Perched Water Tc-99

The northern deep perched water is associated with the 380-ft interbed and possibly with a low-permeability basalt. The contamination sources include the tank farm releases and service waste discharged in the CPP-3 injection well. The CPP-3 well casing collapsed in 1968 and, during the period 1968 through 1970, the service waste entered the deep vadose zone. The well casing may have been compromised much earlier than 1968, resulting in earlier vadose zone contamination. The highest observed Tc-99 concentrations were in well MW-18-1 (736 pCi/L), where only one observation was recorded in 1995. The

background concentration of Tc-99 should be zero. Throughout the period recorded, concentrations in USGS-50 have been above background, and concentrations have been declining from a peak value of 77 pCi/L (1994) to 50.2 pCi/L (2001). Tc-99 concentrations in the BLR-DP well were below detection limits. The source of this Tc-99 is most likely from the failed injection well. In general, there is insufficient data to infer the arrival of Tc-99 originating from the tank farm sources in this region.

The simulated concentrations in MW-18-1 and well USGS-50 were several times higher than the observed values. The CPP-3 injection well casing began to fail in the early 1960s due to corrosion and was partially plugged by 1967. The well most likely discharged the service wastewater to the vadose zone during this time period (Buckham 1970). The model indicates that the vadose zone at the MW-18 and USGS-50 well locations appear to have been slightly impacted by the Tc-99 discharged to the CPP-3 well, but the later tank farm releases of Tc-99 had a much greater influence on water concentration. This is because tank farm Tc-99 sources were much larger than those discharged to the injection well during the simulated failure period. The tritium simulations showed the opposite, because the tank farm sources were much smaller than the injection well source.

The highest simulated deep perched water concentrations were under the eastern half of the tank farm and the high concentration area extended approximately 100 m southeast. The maximum simulated deep perched water concentration was approximately 3,000 pCi/L. The highest deep perched water concentrations were southeast of the tank farm near the MW-18 well and were not north of the tank farm near the ICPP-MON-A-230 well. Current aquifer concentrations in the ICPP-MON-A-230 and ICPP-2021 aquifer wells are above the Snake River Plain Aquifer maximum contaminant level and are as much as an order of magnitude higher than the simulated aquifer concentrations. The reason for this discrepancy is unknown but may be in part due to the CPP-1 and CPP-2 production well capture zone extending further south than that predicted by the aquifer model.

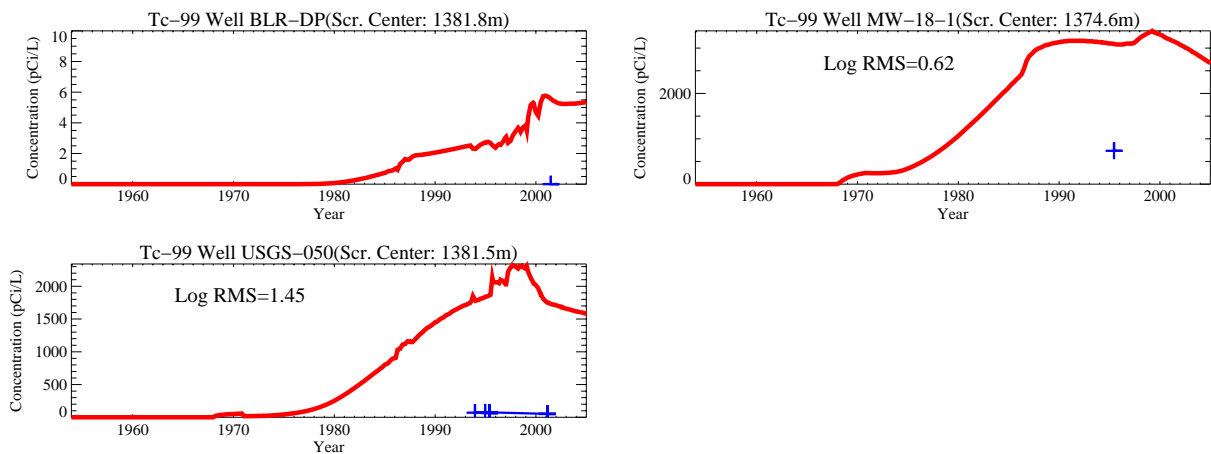


**Figure A-7-19.** Tc-99 concentration history in the northern deep perched water (red line = simulated, blue crosses = observed, pCi/L).

#### A-7.3.1.4 Southern Shallow Perched Water Tc-99

The southern shallow perched water is associated with the 110-ft and 140-ft interbeds. The primary source of Tc-99 should be the service waste discharged in the former percolation ponds. The percolation ponds operated from 1984-2002 and received low-level radioactive waste until the Liquid Effluent Treatment and Disposal (LET&D) facility became operational in 1993. Most of the data available in the southern shallow perched water was taken after year 2000, and concentrations are near zero.

The highest observed Tc-99 concentrations in the region occurred in well MW-15 (23.5 pCi/L in 1995). Tc-99 was sampled for in the shallow PW-series wells in 2001, and the measured concentrations were below detection. It is likely that Tc-99, discharged into the percolation ponds, had already moved below the shallow perched zone when the 2001 measurements were taken. The Tc-99 observed in well MW-15 is most likely from the percolation ponds.

Simulated concentrations in well MW-15 are similar in magnitude to the observed values (Figure A-7-20). The other wells have observed and simulated concentrations near zero, except well PW-1. The simulated increasing Tc-99 concentration seen in well PW-1 is from the OU 3-13 CPP-22 site located south of Building CPP-603. This site was placed in the model in 1990 and the source term for this site was very conservatively estimated. The model suggests that Tc-99 concentrations had been higher in the southern INTEC and were subsequently reduced after the LET&D facility became operational in 1993.

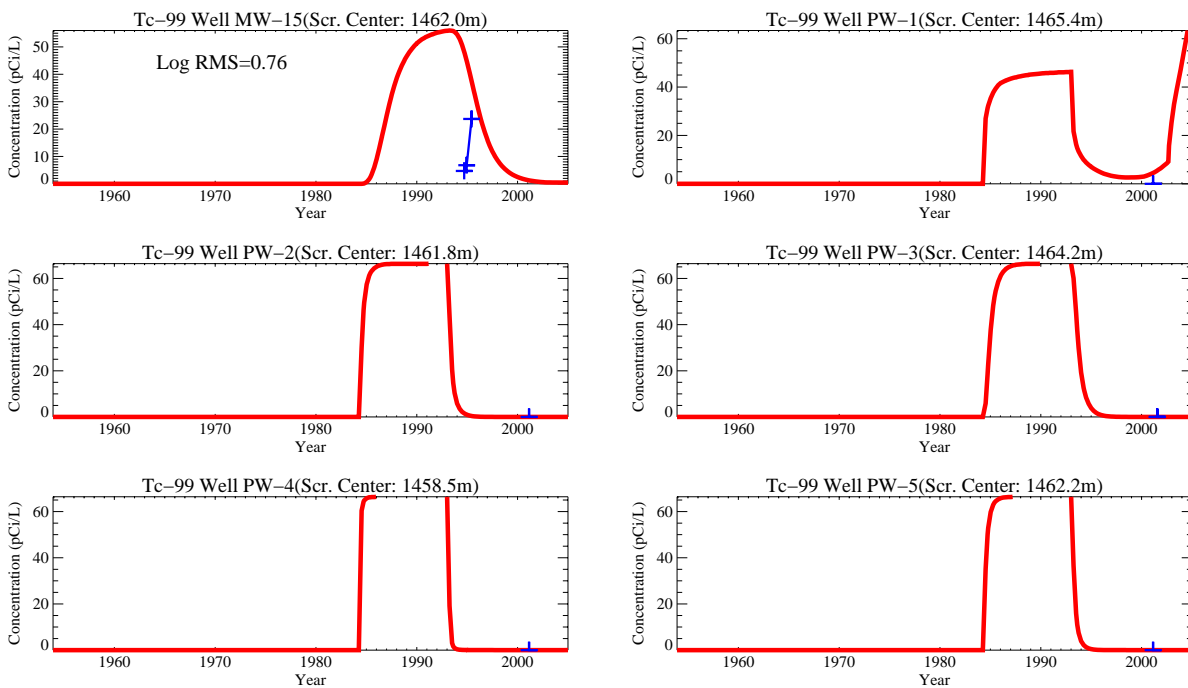


**Figure A-7-20.** Tc-99 concentration history in the southern shallow perched water (red line = simulated, blue crosses = observed, pCi/L).

### A-7.3.1.5 Southern Deep Perched Water Tc-99

The southern deep perched water is associated with the 380-ft interbed, but perched water has been encountered higher than 380 ft. As with the southern shallow perched water, the primary source of Tc-99 is the former percolation ponds, with some contribution from the southern Group 3 soil sites. Wells MW-1-4 and CS-CH lie near the northernmost extent of the southern well grouping area and they most likely reflect a combination of CPP-3 injection well failure and tank farm releases. The highest observed Tc-99 concentrations in the southern deep perched water were found in the CS-CH well (10.6 pCi/L in 2001). Tc-99 has also been detected in wells MW-17-2 (6.4 pCi/L in 1995), MW-17-4 (5.2 pCi/L in 1995), and well MW-1-4 (2.1 pCi/L in 1994).

The simulated well 1807L receives Tc-99 from the CPP-22 soil site and from the percolation ponds. The deep perched water concentrations in well M-17 were very close to the simulated concentrations. The

simulated and observed Tc-99 concentration histories in the southern deep perched water wells are illustrated in Figure A-7-21.

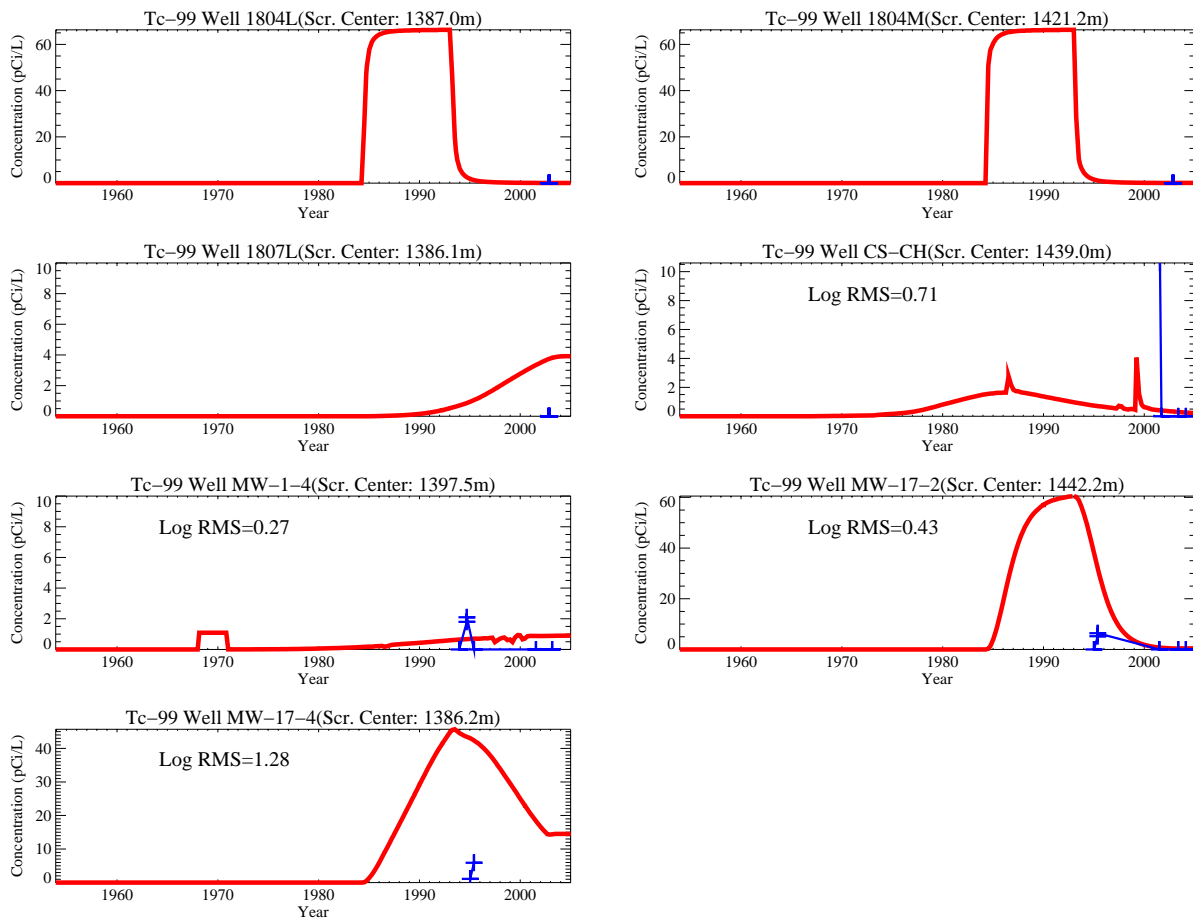


**Figure A-7-21.** Tc-99 concentration history in the southern deep perched water (red line = simulated, blue crosses = observed, pCi/L).

### A-7.3.2 Tritium

The simulated vadose zone sources of tritium listed in order of decreasing magnitude are the service waste ponds (999 Ci), CPP-3 injection well failure (708 Ci), CPP-02 abandoned french drain (378 Ci), and the tank farm sources (10 Ci). Tritium concentrations are a good calibration target in the southern portion of INTEC, because of the relatively high concentrations, and a much worse calibration target in the northern portion of INTEC. The background tritium concentration is approximately 100 pCi/L in the Snake River Plain Aquifer (Orr et al. 1991) and simulated concentrations presented in this section were adjusted upwards by that amount to account for it. The simulated tritium concentrations are higher than the background concentration in most of the vadose zone located south of the tank farm.

Tritium is not adsorbed to the porous media but is significantly attenuated via decay as it migrates through the vadose zone. The half-life of tritium is 12.3 years and the water travel through the INTEC vadose zone can be several times greater, depending on the recharge rate and the location.

The arithmetic average log RMS and standard deviation for all well locations was 0.97 and 0.59, respectively. The minimum log RMS was 0.17 and the maximum was 2.1. Figure A-7-22 illustrates the arrival

rate of tritium radioactivity in the aquifer. The peak corresponds to tritium injected in the deep vadose zone during the CPP-3 injection well failure. Tritium originating in the percolation ponds arrives in the early 1990s. The distribution of tritium predicted in the year 2004 is illustrated in Figure A-7-23. The high tritium concentrations located in the southern INTEC near well MW-17 is primarily from the CPP-02 site, which released approximately 378 Ci during the 1960s.

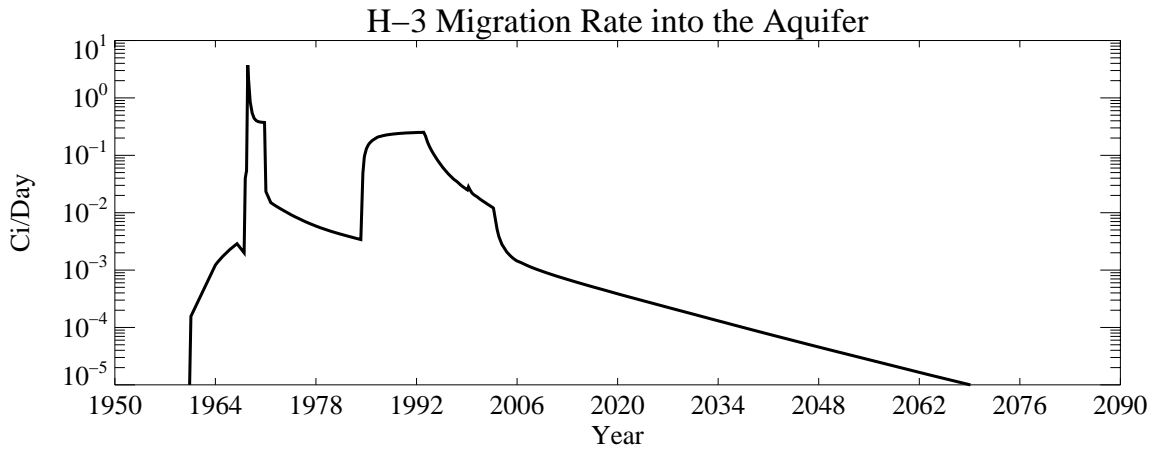


**Figure A-7-22.** Total flux of H-3 entering the aquifer (Ci/day).

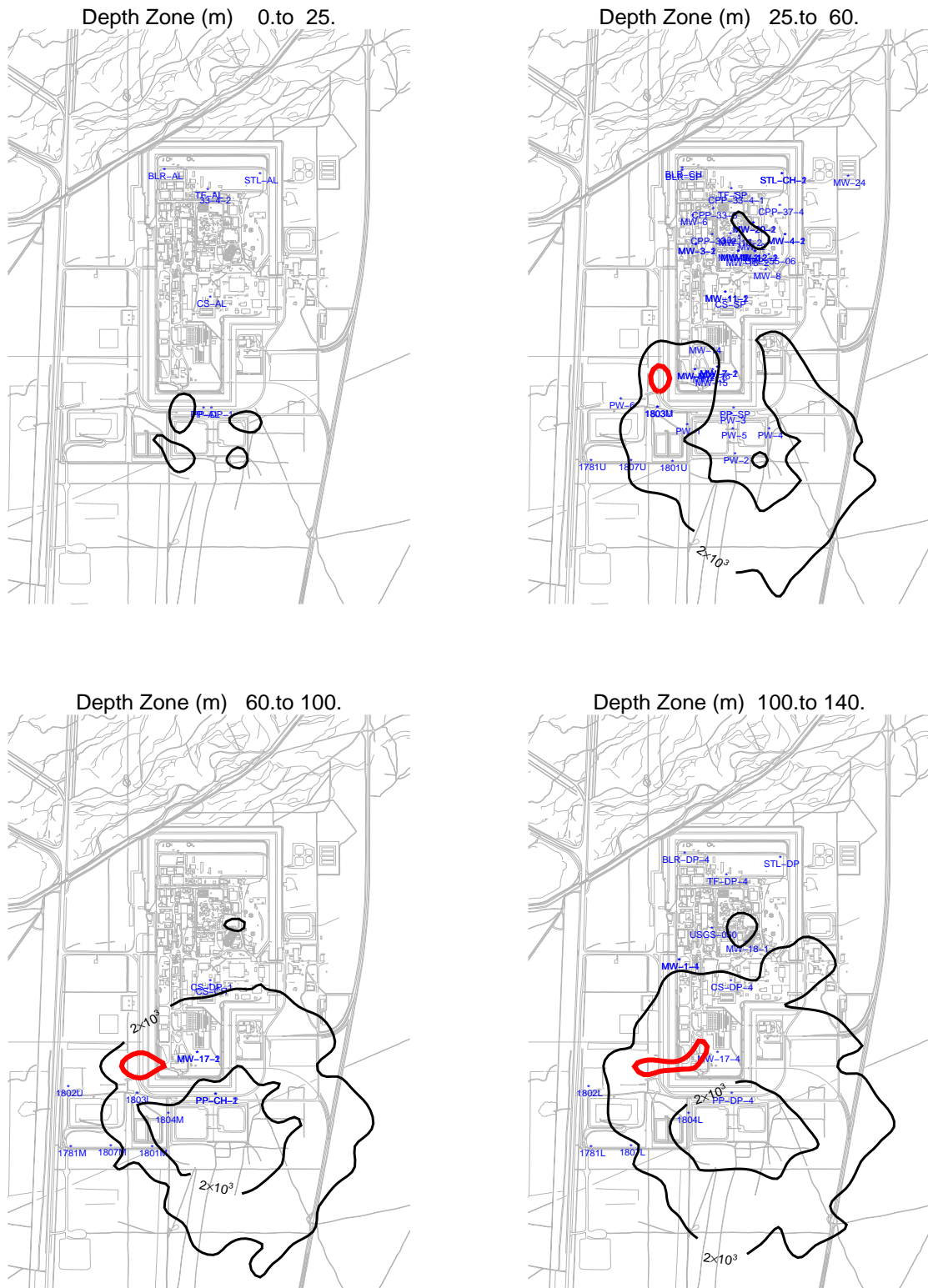


**Figure A-7-23.** Horizontal extent of simulated tritium at different depth intervals in 2004 (red isopleth is 20,000 pCi/L).

### **A-7.3.2.1 Northern Upper Shallow Perched Water Tritium**

The highest observed tritium concentrations in the northern upper shallow perched water were in well MW-5-2. Concentrations in well MW-5-2 were 15,300 pCi/L in 1995 but were 569 pCi/L in 2004. There is only one observed tritium concentration value available for well 33-1: 9,900 pCi/L in 2004. High tritium concentrations have also been measured in well MW-2. They were measured at 6,380 pCi/L and 7,350 pCi/L in 1995 and 2004, respectively. The observed tritium concentrations in the other northern upper shallow perched water wells have been near or below 1,000 pCi/L.

A well-represented concentration history for tritium is unavailable (Figure A-7-24). Sampling began in the 1990s, and the bulk of tritium likely passed through this region prior to that. The peak tritium concentrations in this region most likely occurred in the late 1970s, and current observations probably represent the relatively flat tail. Concentrations are continuing to decline more rapidly than Tc-99 (also conservative or nonretarding) because of the 12.3-year tritium half-life.

The predicted concentration magnitudes in wells CPP-33-1, CPP-33-3, and MW-2 agree with measured data. The model overpredicted tritium concentrations in the MW-4-2 and MW-6 wells. The model also agreed with nondetects (i.e., near the 100-pCi/L background concentrations) at the BLR-CH and MW-24 wells. Overall, the simulated and observed tritium concentrations were similar in the northern upper shallow perched water.

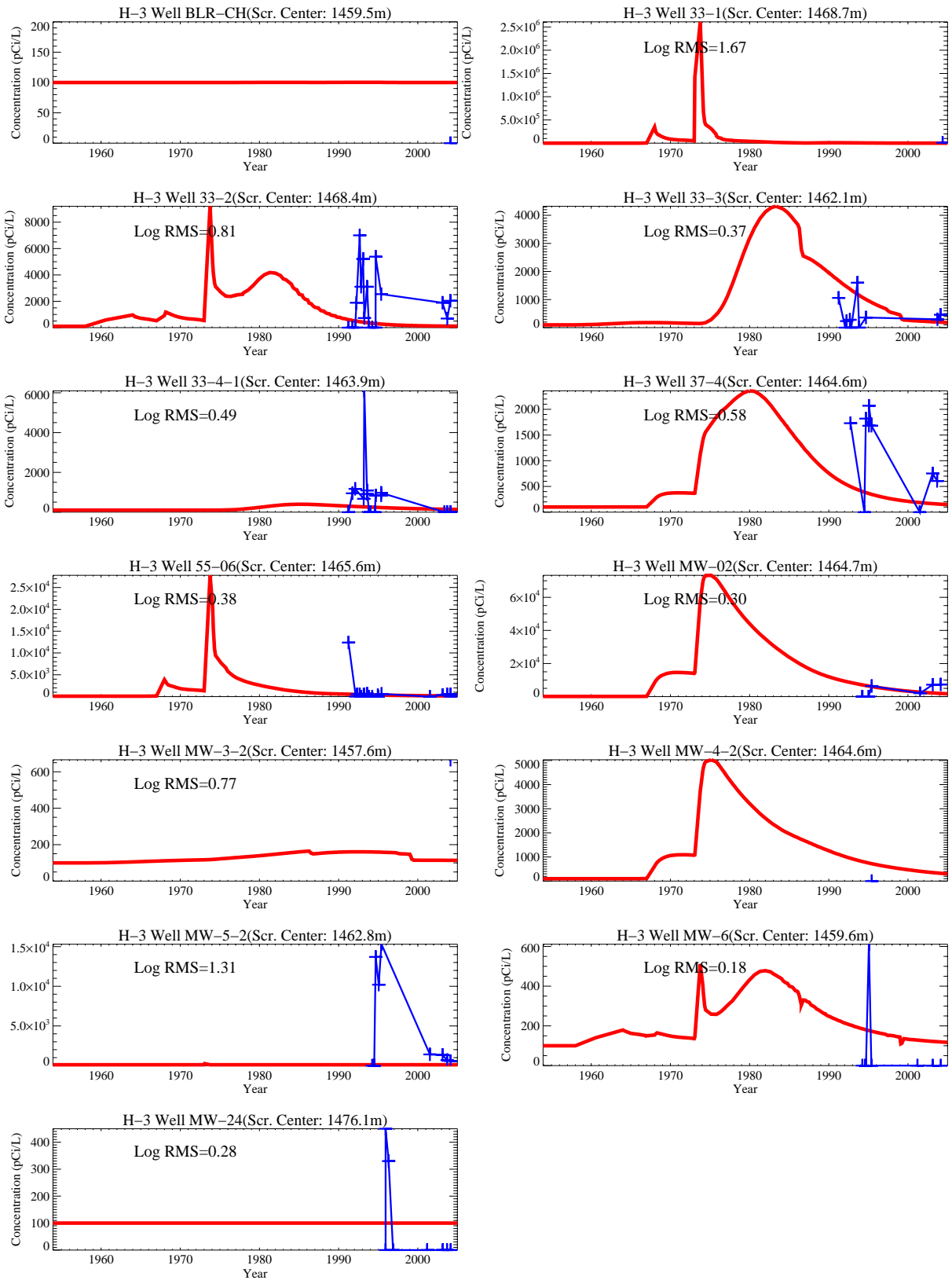


**Figure A-7-24.** Tritium concentration history in the northern upper shallow perched water (red line = simulated, blue crosses = observed, pCi/L).

### A-7.3.2.2 Northern Lower Shallow Perched Water Tritium

The northern lower shallow perched water is associated with the 140-ft interbed, and the contamination source is primarily the tank farm releases. The highest measured tritium concentrations in this region occurred in well MW-10-2, were 38,000 pCi/L in 1995, and have declined to 13,000 pCi/L in 2004. The observed tritium concentrations were also high in well MW-20-2. The highest measured value was 1,150 pCi/L in 1995, and the 2004 concentration was less than the detection limit. The tritium concentrations in wells TF-SP and BLR-SP were nondetect, indicating tritium released in the tank farm does not reach these wells. The actual tritium concentrations in these wells should be near the background concentration. The two wells with high observed tritium concentrations (MW-10-2 and MW-20-2) indicate tritium concentrations are declining more rapidly than only radioactive decay. This suggests that the perched water is being recharged. The peak tritium concentrations most likely occurred before monitoring began.

The simulated and observed concentration patterns are similar to those in the northern upper shallow perched water (Figure A-7-25). The model matched tritium concentrations in well MW-20-2 but underpredicted concentrations in well MW-10-2. The model correctly predicted that tritium should be near background in the BLR-SP well. The large abrupt changes in concentration are due to the quarterly step change in the simulated Big Lost River recharge. The wells nearest to the Big Lost River show the largest change (i.e., wells TF-SP and TF-CH). The model predicts the 140-ft interbed is affected by the river to a greater extent than is the 110-ft interbed (see Section A-7.2.2).

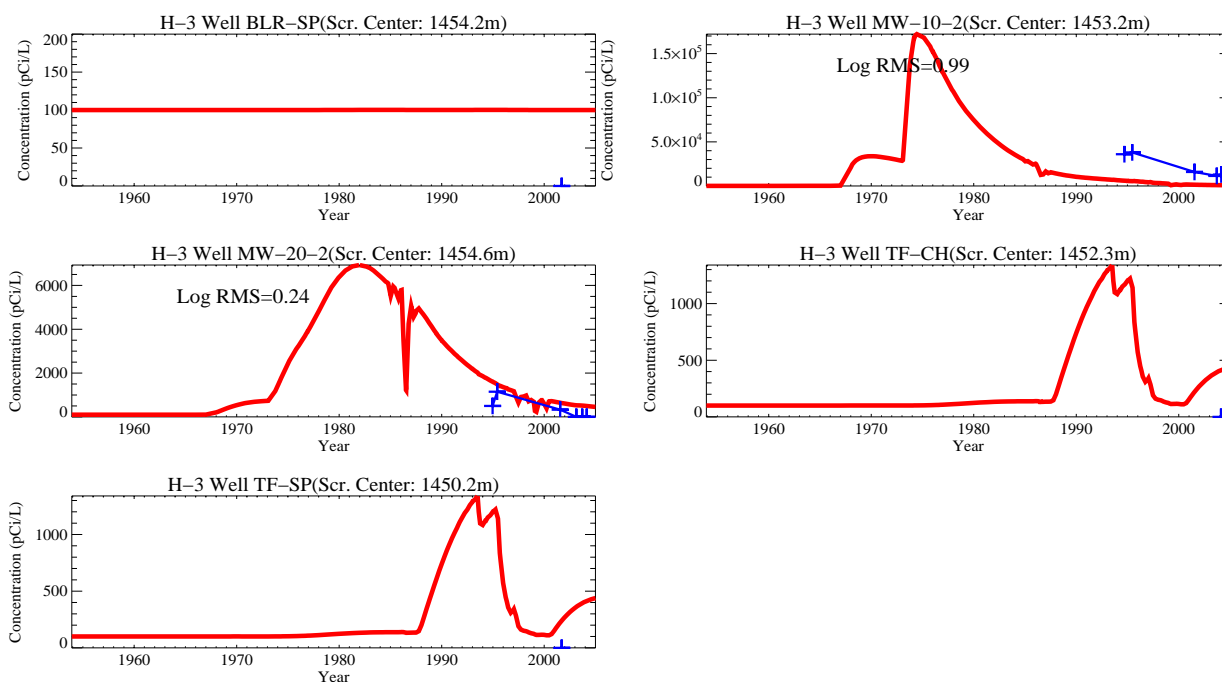


**Figure A-7-25.** Tritium concentration history in the northern upper shallow perched water (red line = simulated, blue crosses = observed, pCi/L).

### A-7.3.2.3 Northern Deep Perched Water Tritium

As with Sr-90, the highest observed tritium concentrations (4,180,000 pCi/L) are associated with the CPP-3 injection well. Peak concentrations in USGS-50 have been declining steadily since 1980. However, there is more variability in the tritium concentrations relative to those of Sr-90, which is a reflection of the greater variability in the tritium service waste source.

Tritium concentrations were measured in well MW-18 during 1995 and 2001 and were 73,000 pCi/L and 34,900 pCi/L, respectively. USGS-50 and MW-18 had similar concentrations in 1995 and 2001. The observed concentration in well BLR-DP was only measured in 2001 and was below detection.

The early arrival of the observed and simulated tritium seen at well USGS-50 is from the CPP-3 injection well failure during the late 1960s. The simulation also suggests the area near MW-18 was impacted by service waste during the CPP-3 injection well failure, although monitoring data are unavailable during this time period.

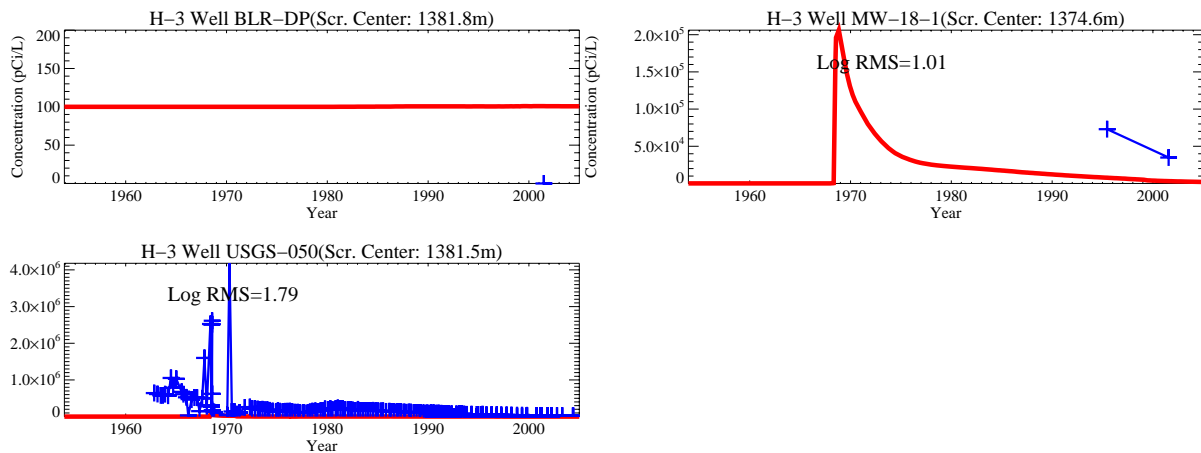


**Figure A-7-26.** Tritium concentration history in the northern deep perched water (red line = simulated, blue crosses = observed, pCi/L).

#### A-7.3.2.4 Southern Shallow Perched Water Tritium

The southern shallow perched water is associated with the 110-ft and 140-ft interbeds. The primary tritium contamination sources are the CPP-02 abandoned french drain and the former percolation ponds. The CPP-02 abandoned french drain operated from 1954 through 1966. The percolation ponds operated from 1984-2002 and received low-level radioactive waste until the LET&D facility became operational in 1993.

The highest observed tritium concentrations (100,000 pCi/L - 300,000 pCi/L) in this region were found in 1988 in the PW-series wells surrounding the former percolation ponds. After the LET&D facility was brought online in 1993, the tritium concentrations in the PW-series wells quickly declined to 100-1,000 pCi/L. The observed tritium concentration in well MW-15 was 3,630 pCi/L in 1995.

Most data collection in these wells began in the mid 1980s when the PW-series wells were installed. A definitive concentration history shows that the arrival of tritium in these wells is associated with the operation of the percolation pond (Figure A-7-27). Tritium discharge rates were much more variable than the discharge rates for Sr-90 in the service waste. The simulated discharges of tritium in the percolation pond were assumed to be constant throughout the discharge period, and, as a result, the model does not capture this variability (Figure A-7-27). High tritium concentrations observed in well PW-6 indicate the arrival of percolation pond water at that location, which was not predicted by the model.

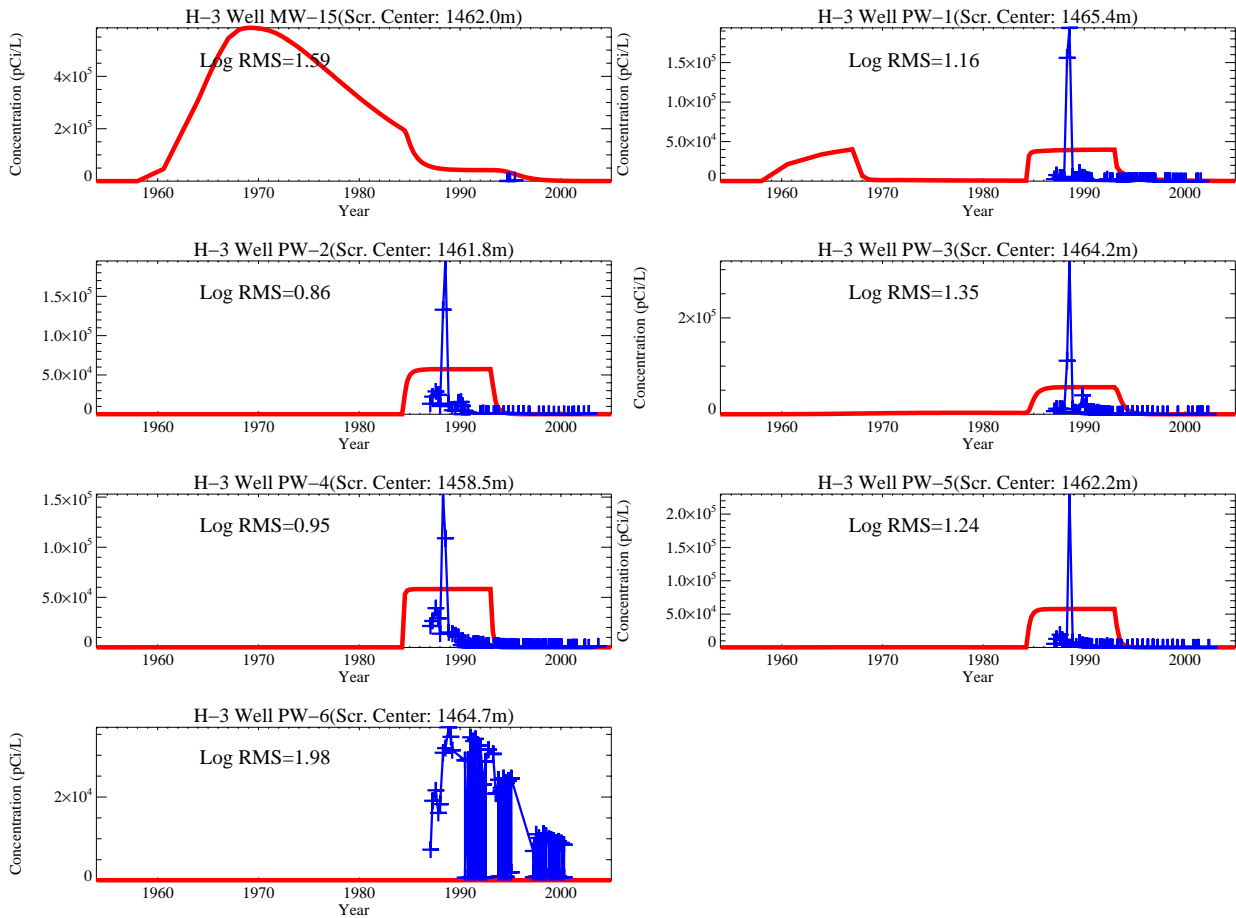


**Figure A-7-27.** Tritium concentration history in the southern shallow perched water (red line = simulated, blue crosses = observed, pCi/L).

### A-7.3.2.5 Southern Deep Perched Water Tritium

The southern deep perched water is associated with the 380-ft interbed, but perched water has been encountered higher than 380 ft. As with the southern shallow perched water, the tritium contamination sources are the CPP-02 abandoned french drain and the service waste disposed of in the former percolation ponds. Wells MW-1-4 and CS-CH lie near the northernmost extent of the southern well grouping area, and they most likely see contamination resulting from the CPP-3 injection well; OU 3-13, Group 3, soil sources; and the tank farm releases.

The highest observed tritium concentrations in this region were found in MW-17-2 at 40,400 pCi/L in 2001. High concentrations also occurred in MW-1-4 (24,700 pCi/L in 1995) and MW-17-4 (25,100 pCi/L in 1995). Elevated tritium concentrations have been observed for many years in monitoring wells surrounding the CPP-603 area and is attributed primarily to past discharges of contaminated CPP-603 basin water to the alluvium during the 1960s (Robertson et al. 1974). The large decline in observed levels of shallow tritium between 1963 and 1970 supports this conclusion (INEL 1995b). Since that time, the tritium (and Sr-90) released into the alluvium has been transported downward to the shallow and deep perched water zones. Sr-90 and tritium derived in the shallow vadose zone continue to be transported to greater depth by precipitation infiltration and clean water discharges, such as the 2005 discovery of an underground fire water line leak near the southeast corner of CPP-603. However, because tritium is not appreciably adsorbed to clays, tritium concentrations decline more rapidly than Sr-90. During four successive monitoring events, tritium

concentrations in southern perched monitoring well MW-17-2 have declined steadily from 40,400 pCi/L (2001) to 21,000 pCi/L (2005). This suggests that, aside from the residual secondary source in the contaminated alluvium, no other continuing tritium source is present in this area.

Tritium was below the 20,000 pCi/L federal drinking water standard but above the detection limit in wells 1804L at 8,200 pCi/L in 2002; well 1807L at 1,110 pCi/L in 2002, and CS-CH at 776 pCi/L in 2001. The simulated and observed tritium concentrations in the southern deep perched water wells are illustrated in Figure A-7-28.

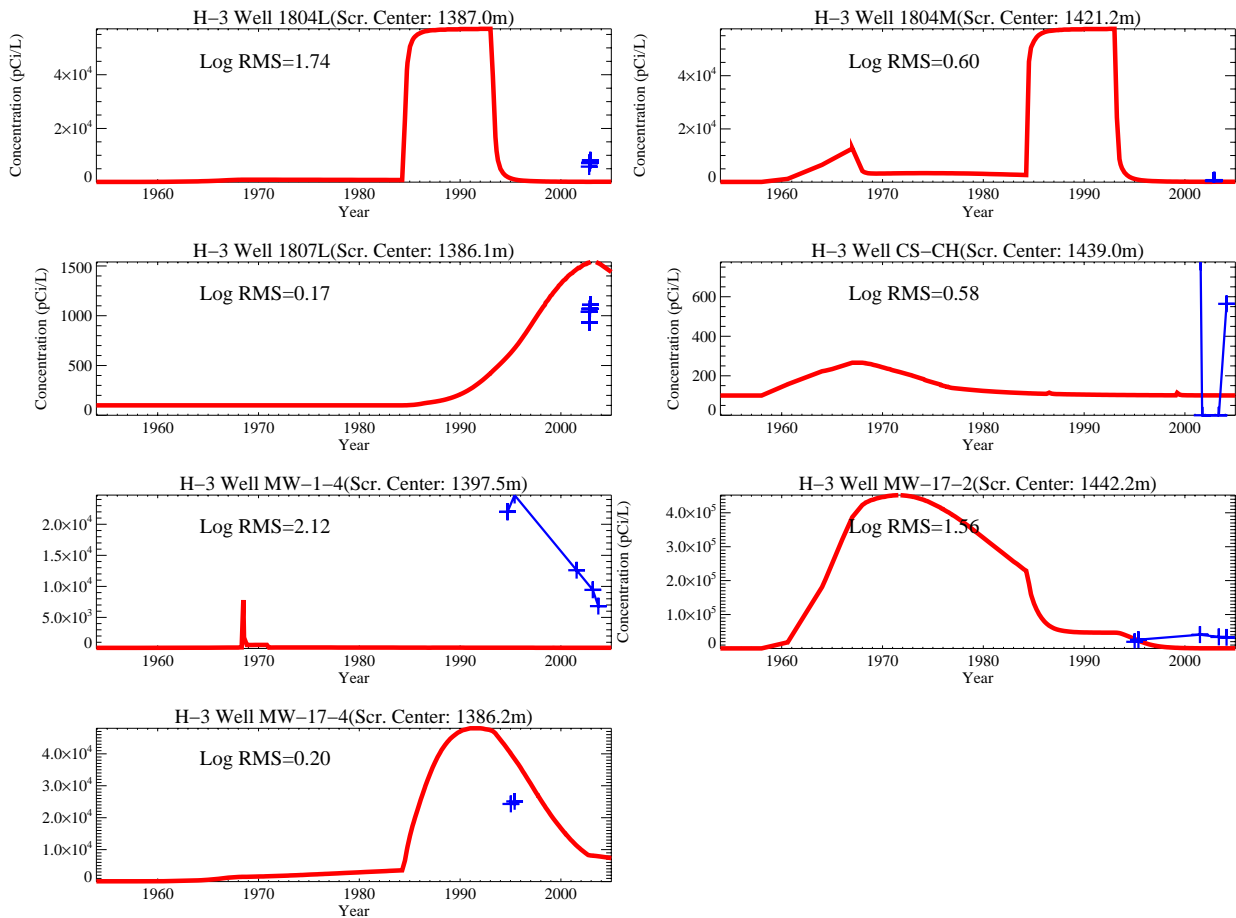


**Figure A-7-28.** Tritium concentration history in the southern deep perched water (red line = simulated, blue crosses = observed, pCi/L).

### A-7.3.3 I-129

The simulated sources of vadose zone I-129 listed in order of decreasing magnitude are the CPP-3 injection well failure (0.075 Ci), service waste ponds (0.082 Ci), and tank farm sources (0.002 Ci). The background I-129 concentration is approximately 0.05 pCi/L in the Snake River Plain Aquifer (Orr et al. 1991). The simulated concentrations were adjusted to account for the background concentrations by adding this amount to the simulated value. Like Tc-99, I-129 is long-lived and very mobile in the subsurface. On average, the I-129 detection limit is a much larger fraction of the observed concentration than other contaminants. This results in more nondetects where concentrations are lower than the detection limit, but not zero. All nondetects were compared to the model values as a zero measured concentration. This results in the model appearing to overpredict I-129 movement relative to the other radionuclides. The arithmetic average log

RMS and standard deviation for all well locations was 1.4 and 2.0, respectively. The minimum log RMS was 0.3 and the maximum was 8.2.

Like tritium, I-129 is volatile compared to Sr-90 and Tc-99 at the high temperatures encountered in the calcination process. The bulk of the I-129 that began in the fuel was contained in the first-cycle raffinate and sent to the tank farm. During the calcination process, very little of the volatile was contained within the calcine. The bulk (approximately 90%) of it was discharged to the atmosphere with the calciner off-gas. However, most of the I-129 that does get into the PEW evaporator volatilizes, is condensed with the dilute condensate stream, and was discharged to service waste. This is approximately 10% of the I-129 originally in the fuel. This accounts for the relatively large source magnitude in the percolation ponds and CPP-3 disposal well, compared to the tank farm sources. The simulated I-129 is widespread in the northern deep vadose zone and southern vadose zone because of the CPP-3 injection well failure and the former percolation ponds.

Figure A-7-29 illustrates the total flux of I-129 arriving in the aquifer over time. The highest peak corresponds to the CPP-3 injection well failure and occurred in the late 1960s. Arrival from the surface releases is predicted to have occurred in the early 1990s. Predicted concentrations in the vadose zone in 2004 are given at different depth intervals in Figure A-7-30. The I-129 concentrations illustrated in Figure A-7-30, which extend in the deep vadose zone from the northern to the southern INTEC, include sources from the tank farm in the north, failed CPP-3 injection well in the central INTEC, and percolation ponds in the south. The plotted data is pore water concentrations and includes unsaturated zones.

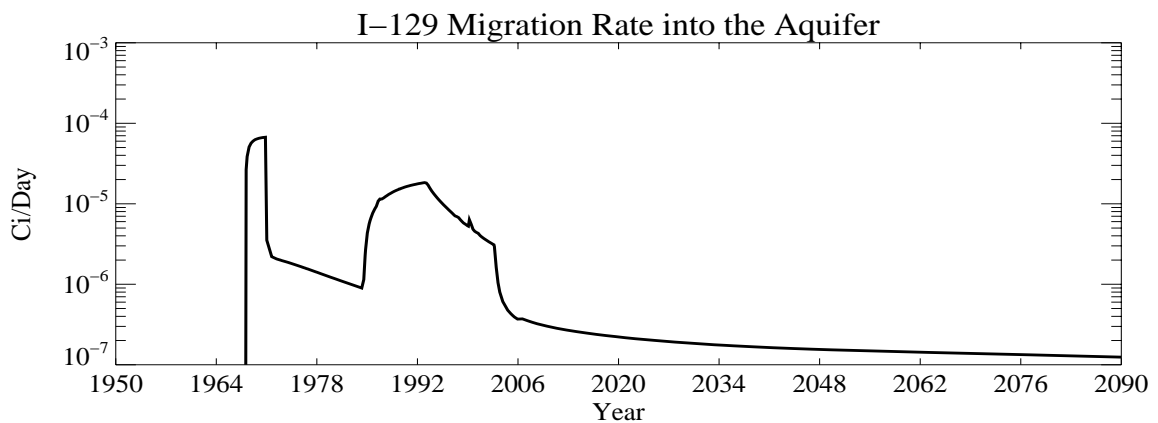


**Figure A-7-29.** Total flux of I-129 entering the aquifer (Ci/day).



**Figure A-7-30.** Horizontal extent of simulated I-129 at different depth intervals in 2004 (pCi/L).

### **A-7.3.3.1 Northern Upper Shallow Perched Water I-129**

The northern upper shallow perched water is associated with the 110-ft interbed and the primary source is from the tank farm releases. The observed I-129 concentrations in the northern shallow perched water have always been very low. The highest observed I-129 concentrations are in well MW-5-2 and were 0.18 and 0.71 pCi/L in 2001 and 2003, respectively. Isolated concentrations above 1 pCi/L were observed in wells CPP-33-1 and MW-24 during the early 1990s. Peak I-129 concentration most likely occurred in the early 1980s as illustrated in Figure A-7-31.

The recorded concentration-time data began after the peak arrival of I-129 in this region. The early measurements were probably performed using an analytical method with a corresponding high detection limit compared to in situ concentrations. The 13-pCi/L observation in MW-24 is relatively high and probably did not originate in the known tank farm releases.

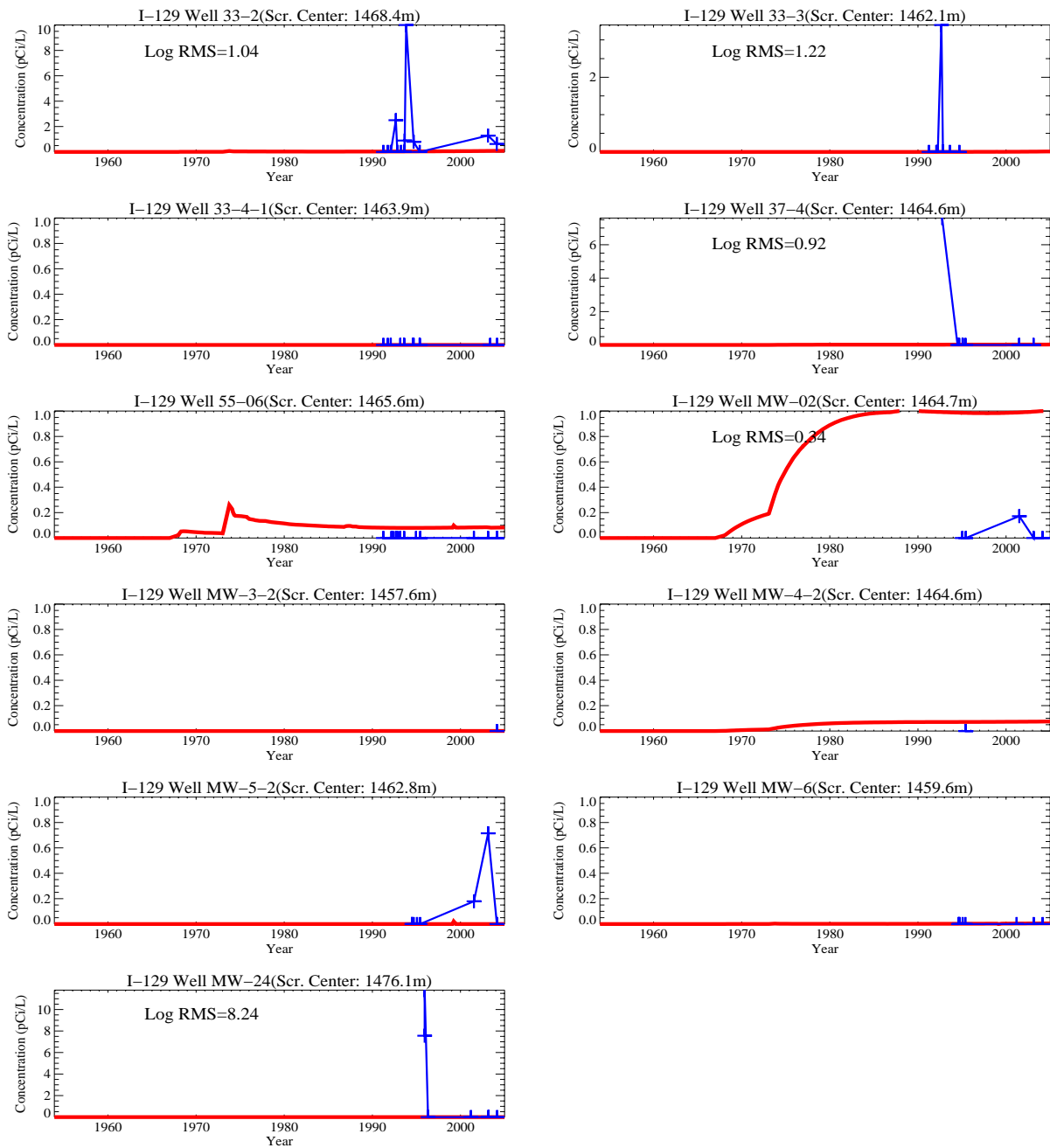


**Figure A-7-31.** I-129 concentration history in the northern upper shallow perched water (red line = simulated, blue crosses = observed, pCi/L).

### A-7.3.3.2 Northern Lower Shallow Perched Water I-129

The northern lower shallow perched water is associated with the 140-ft interbed and the contamination sources are primarily the tank farm releases. All of the data in this perched water were nondetect. The simulated concentration patterns are similar to those predicted for the northern upper shallow perched water, and the model overpredicts those values for one well, MW-10-2, as shown in Figure A-7-32.

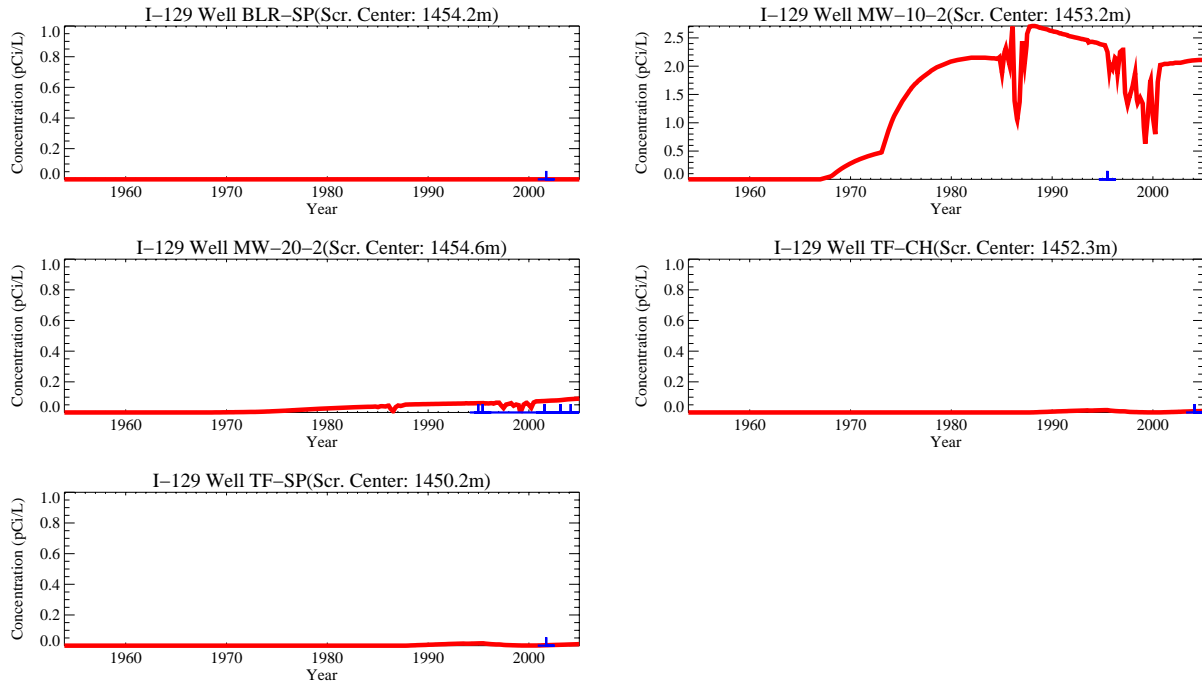


**Figure A-7-32.** I-129 concentration history in the northern lower shallow perched water (red line = simulated, blue crosses = observed, pCi/L).

### A-7.3.3.3 Northern Deep Perched Water I-129

The northern deep perched water is associated with the 380-ft interbed and possibly a low-permeability basalt. The contamination sources include the tank farm releases and the CPP-3 injection well during the 1968-1970 failure period. The well casing may have been compromised much earlier than 1968, which would have allowed earlier contamination of the vadose zone. The highest observed I-129 concentrations in the northern deep perched water were observed in well USGS-50. A 1.1-pCi/L concentration was measured in 1995 and 0.56 pCi/L was measured in 2004. The concentrations in well MW-18 and BLR-DP were below detection in 1995 and in 2001. The I-129 in well USGS-50 is most likely remnants of the CPP-3 injection well failure and I-129 discharge to the deep vadose zone.

Monitoring for I-129 was not performed frequently enough to reproduce the I-129 concentration history as illustrated in Figure A-7-33.

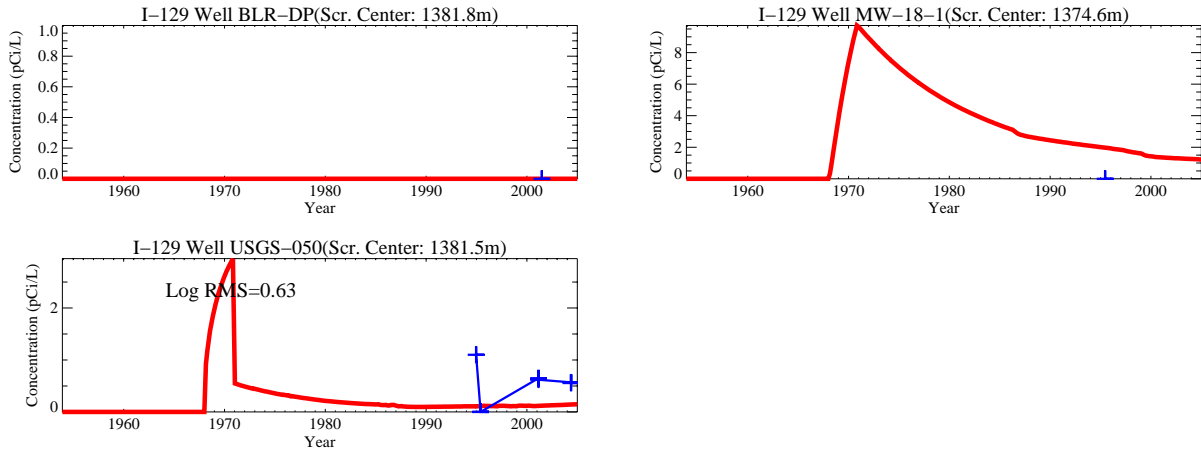


**Figure A-7-33.** I-129 concentration history in the northern deep perched water (red line = simulated, blue crosses = observed, pCi/L).

#### A-7.3.3.4 Southern Shallow Perched Water I-129

The southern shallow perched water is associated with the 110-ft and 140-ft interbeds. The primary contamination source is the former percolation ponds. The percolation ponds operated from 1984-2002, and the percolation ponds received significant amounts of low-level radioactive waste until the LET&D facility became operational in 1993. The PW-series wells were installed in the mid-1980s, but were not monitored for I-129 until the mid-1990s. This was after the LET&D facility became operational and I-129 concentration in the service waste water was near zero.

The highest observed I-129 concentrations in this region were found in the PW-series wells surrounding the former percolation ponds. Well PW-5 had the highest observed I-129 concentrations at 4.26 pCi/L in 1996. I-129 concentrations in the other PW series wells and well MW-15 were less than 1 pCi/L. All of the observed I-129 data in the southern shallow perched water postdates the LET&D facility (1993). It is likely that the service waste I-129 has already moved below the southern shallow perched water. The simulated and observed I-129 concentrations are illustrated in Figure A-7v34.

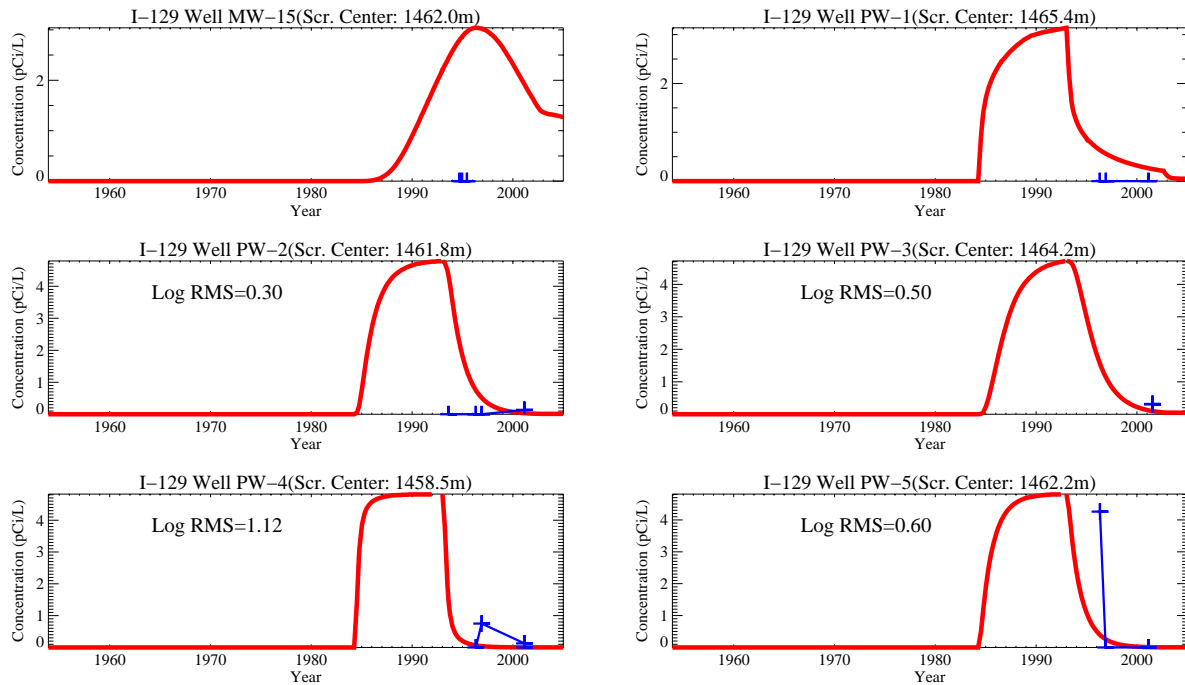


**Figure A-7-34.** I-129 concentration history in the southern shallow perched water (red line = simulated, blue crosses = observed, pCi/L).

### A-7.3.3.5 Southern Deep Perched Water I-129

The southern deep perched water is associated with the 380-ft interbed, but perched water has been encountered higher than 380-ft. As with the southern shallow perched water, the I-129 contamination source is the former percolation ponds. Wells MW-1-4 and CS-CH lie near the northernmost extent of the southern well grouping area and they most likely see I-129 resulting from the CPP-3 injection well; OU 3-13, Group 5, soil sources; and possibly the tank farm releases.

The highest observed I-129 concentrations in the southern deep perched water were found in well 1804M at 0.402 pCi/L in 2002. I-129 concentrations above the detection limit were also measured in wells 1804L at 0.368 in 2002, and 1807L at 0.355 pCi/L in 2002. The postyear 2000 slight increasing trend seen in the simulated concentration at well MW-17-4 is due to I-129 from the failed CPP-3 injection well slowly dispersing towards this well. Figure A-7-35 illustrates the simulated and measured I-129 concentrations in the southern deep perched water wells.

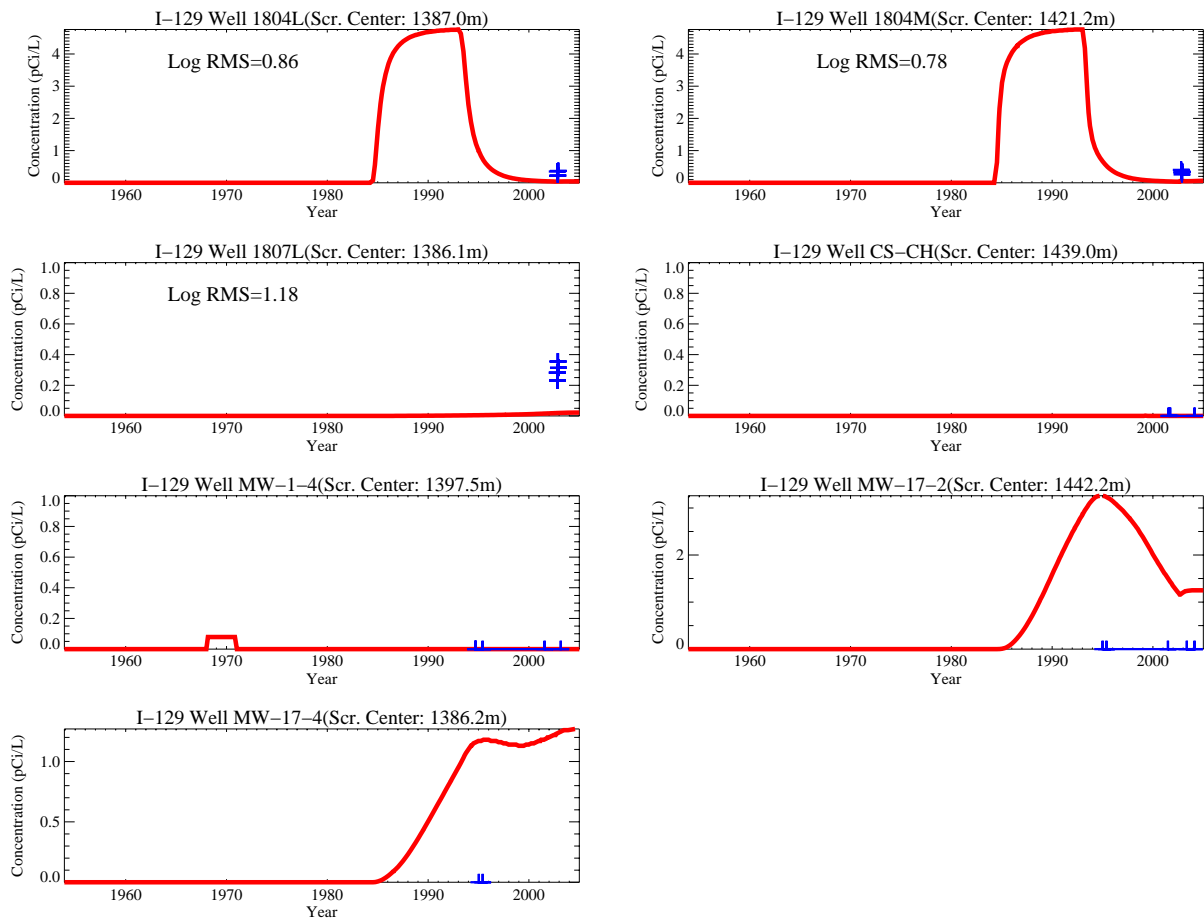


**Figure A-7-35.** I-129 concentration history in the southern deep perched water (red line = simulated, blue crosses = observed, pCi/L).

### A-7.3.4 Nitrate

The spent nuclear fuel was dissolved in either nitric or hydrofluoric acid during the uranium recovery process at INTEC, resulting in a large amount of nitrate in the liquid waste. The nitrate is very mobile in the subsurface and does not decay. The simulated sources of vadose zone nitrate listed in order of decreasing magnitude are the service waste ponds ( $1.3e + 6$  kg), CPP-3 injection well failure ( $2.2e + 5$  kg), and tank farm sources ( $2.1e + 4$  kg). The nitrate ( $\text{NO}_3^-$ ) ion is ubiquitous in most groundwaters, and the Snake River Plain Aquifer background concentration is approximately 1.5 mg/L as N (Orr et al. 1991). The perched water background nitrate concentration should be similar to those in the aquifer because very little nitrification occurs in the INL Site vadose zone and much of the water responsible for creating the perched water was taken from the aquifer. The simulated concentrations were adjusted to account for the background concentrations by adding this amount to the simulated value.

In many of the tank farm perched water wells, a classic concentration history was observed during the early 1990s. There are no known nitrate discharges accounted for during this time period. As a result, the model underpredicted nitrate concentrations in most of the perched water wells around the tank farm.

The service waste nitrate discharges were two orders of magnitude greater than the known tank farm sources and have resulted in widespread concentrations above background in the northern deep and southern

perched water. The arrival of nitrate at the aquifer interface is illustrated in Figure A-7-36. The early nitrate peak corresponds to the injection well failure, and the later peak is the arrival of percolation pond discharges. Figure A-7-37 illustrates nitrate concentrations at different depth intervals in the vadose zone. The arithmetic average log RMS and standard deviation for all well locations was 1.0 and 1.7, respectively. The minimum log RMS was 0.07 and the maximum was 1.7.

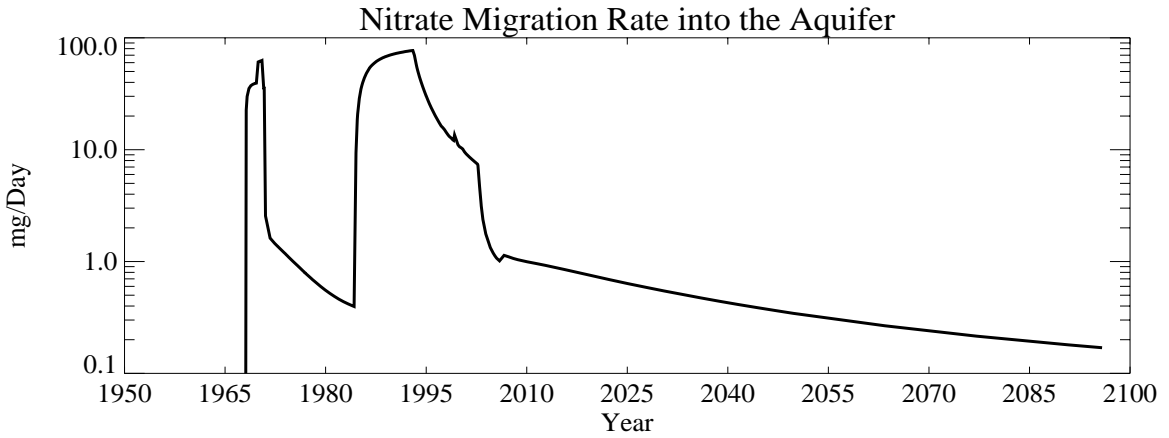


**Figure A-7-36.** Total flux of nitrate entering the aquifer (kg/day).

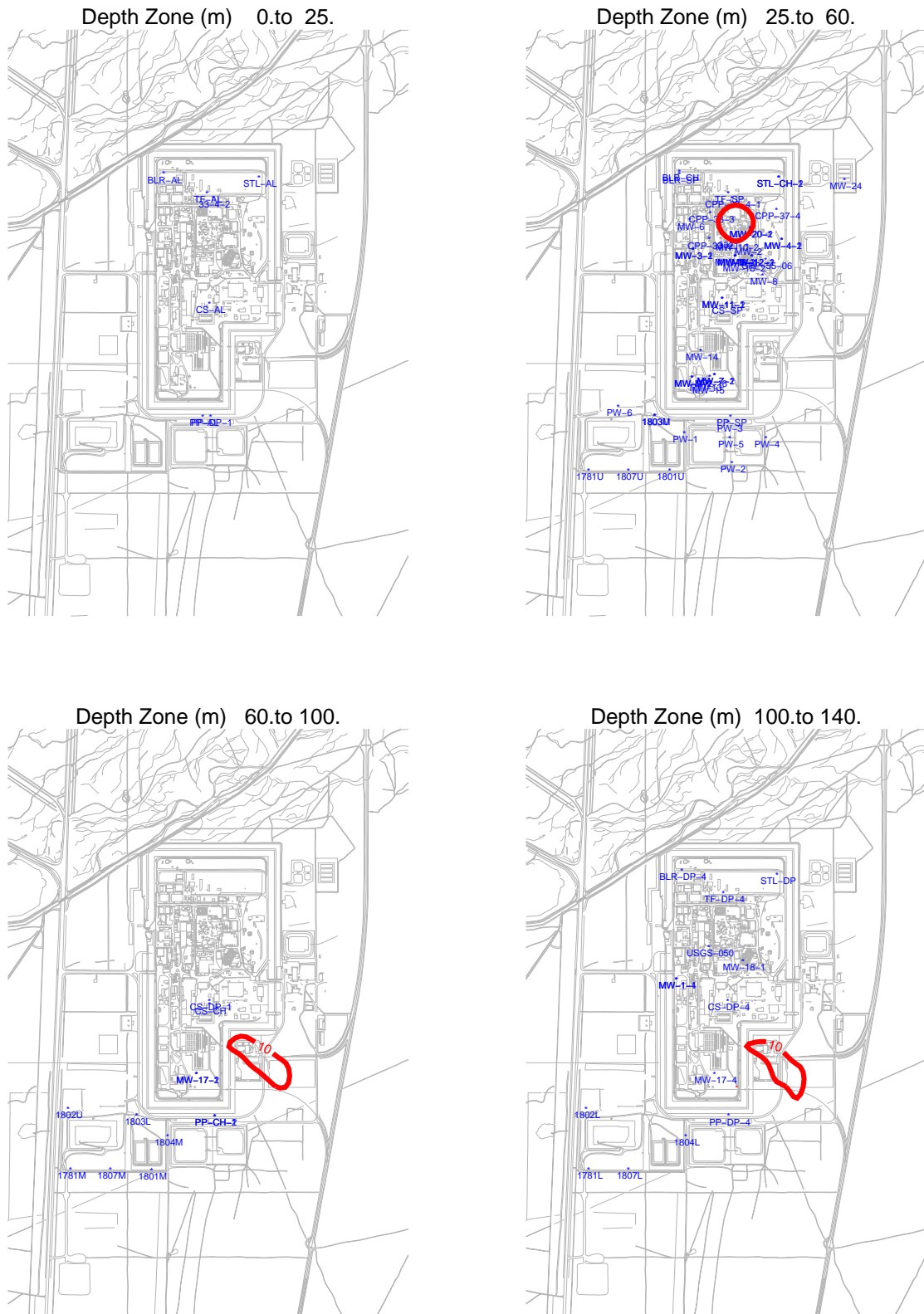


**Figure A-7-37.** Horizontal extent of simulated nitrate at different depth intervals in 2004 (mg/L as N).

#### **A-7.3.4.1 Northern Upper Shallow Perched Water Nitrate**

The northern upper shallow perched water is associated with the 110-ft interbed and the source of nitrate is primarily from the historical tank farm releases. The highest observed nitrate concentrations in this region have been observed in well MW-5-2. Concentrations in this well increased from 17.8 mg/L as N to 147 mg/L as N from 1991 to 1993 and then declined to 6.2 mg/L in 2001. The CPP-33-3, MW-6, and MW-2 wells also experienced a peak in nitrate during the early 1990s, but at a lower magnitude. Observed nitrate concentrations in well MW-24 are also high compared to background concentrations. However, the elevated concentrations from well MW-24 are most likely from the sewage treatment lagoon infiltration trench and not from the tank farm releases. Nitrate originating in the tank farm probably reached this region during the early 1980s. The source of the nitrate peaks observed in the early 1990s is unknown and was not matched with the model.

The CPP-31 site was the largest source of tank farm nitrate at  $1.92 \times 10^4$  kg. The CPP-79 site release occurred in 1986 but was orders of magnitude less than the CPP-31 release. The simulated Site CPP-31 nitrate can be seen arriving in the early 1980s, but there are no measured data until the early 1990s. The high observed nitrate in well MW-24 near the sewage treatment lagoon is most likely a result of sewage plant effluent. The model did not incorporate a sewage nitrate source and did not match the observed concentration at this location. The simulated and observed nitrate concentration in the northern upper shallow perched water wells is illustrated in Figure A-7-38.

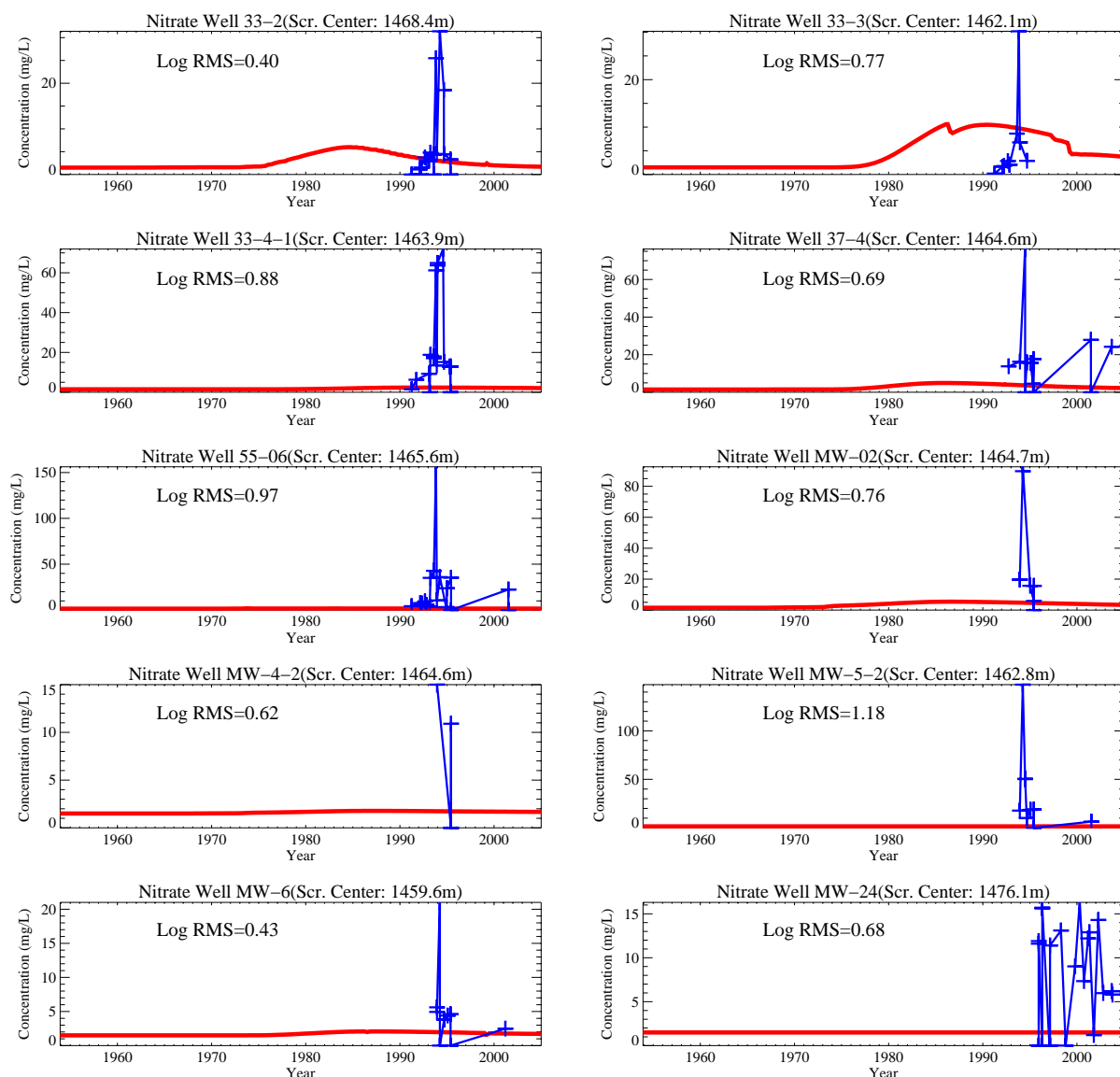


**Figure A-7-38.** Nitrate concentration history in the northern upper shallow perched water (red line = simulated, blue crosses = observed, mg/L as N).

#### A-7.3.4.2 Northern Lower Shallow Perched Water Nitrate

The northern lower shallow perched water is associated with the 140-ft interbed and the contamination source is primarily the tank farm releases. The simulated and observed concentration patterns are similar to those predicted in the northern upper shallow perched water. The observed concentrations in the two northern lower shallow perched water wells monitored for nitrate were above background. The highest concentrations were in well MW-10-2 at 27.4 mg/L as N in 1994. Well MW-20-2 had a maximum concentration of 12.4 mg/L as N in 1994. Concentrations in both wells were variable and ranged from the maximum value to zero and randomly ranged above and below the simulated concentrations. There are insufficient data in the two northern lower shallow perched water wells to determine concentration trends through time. The simulated and observed nitrate concentrations in this region are illustrated in Figure A-7-39.

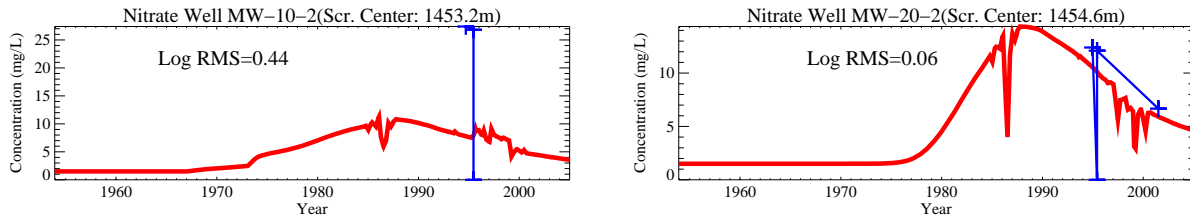


**Figure A-7-39.** Nitrate concentration history in the northern lower shallow perched water (red line = simulated, blue crosses = observed, mg/L as N).

#### A-7.3.4.3 Northern Deep Perched Water Nitrate

The northern deep perched water is associated with the 380-ft interbed and possibly with a low-permeability basalt. The nitrate sources include the tank farm releases and the CPP-3 injection well. The highest observed nitrate concentrations in the northern deep perched water were recorded in well USGS-50. The measured concentrations were 54.8 mg/L as N in 1993 and concentrations had declined to 36.5 mg/L as N in 2001 (Figure A-7-40). Nitrate was also above background concentrations in well MW-18 at 34.5 mg/L as N in 1995. The most recent nitrate concentrations recorded in wells USGS-50 and MW-18 could be either remnants of the CPP-3 injection well failure or from the tank farm releases. The simulated and observed nitrate concentrations in well BLR-DP are at background concentrations.

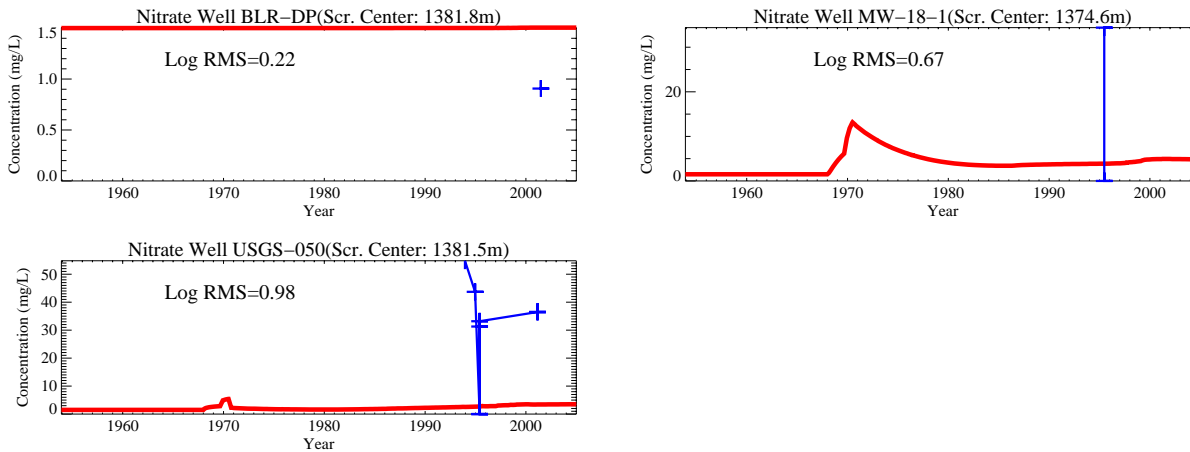


**Figure A-7-40.** Nitrate concentration history in the northern deep perched water (red line = simulated, blue crosses = observed, mg/L as N).

#### A-7.3.4.4 Southern Shallow Perched Water Nitrate

The southern shallow perched water is associated with the 110-ft and 140-ft interbeds. The primary nitrate contamination source is the service waste discharged to the former percolation ponds.

The highest observed nitrate concentrations were in well MW-15. The maximum observed value was 14.7 mg/L as N in 1995. Nitrate concentrations in the other southern shallow perched water wells were near the background concentration (1.5 mg/L as N) or nondetect. Like the I-129 observations, all of the data postdates 1993, the operational start of the LET&D facility. The nitrate originating in the percolation ponds has likely already moved below the southern shallow perched water.

The PW-series wells were installed in the mid-1980s but were not monitored for nitrate until after the LET&D facility became operational in 1993. The observed nitrate concentrations were near background in all the southern shallow perched water wells except well MW-15. The observed concentrations ranged above and below the simulated concentrations in well MW-15. The simulated and observed nitrate concentration in the southern shallow perched water wells is illustrated in Figure A-7-41.

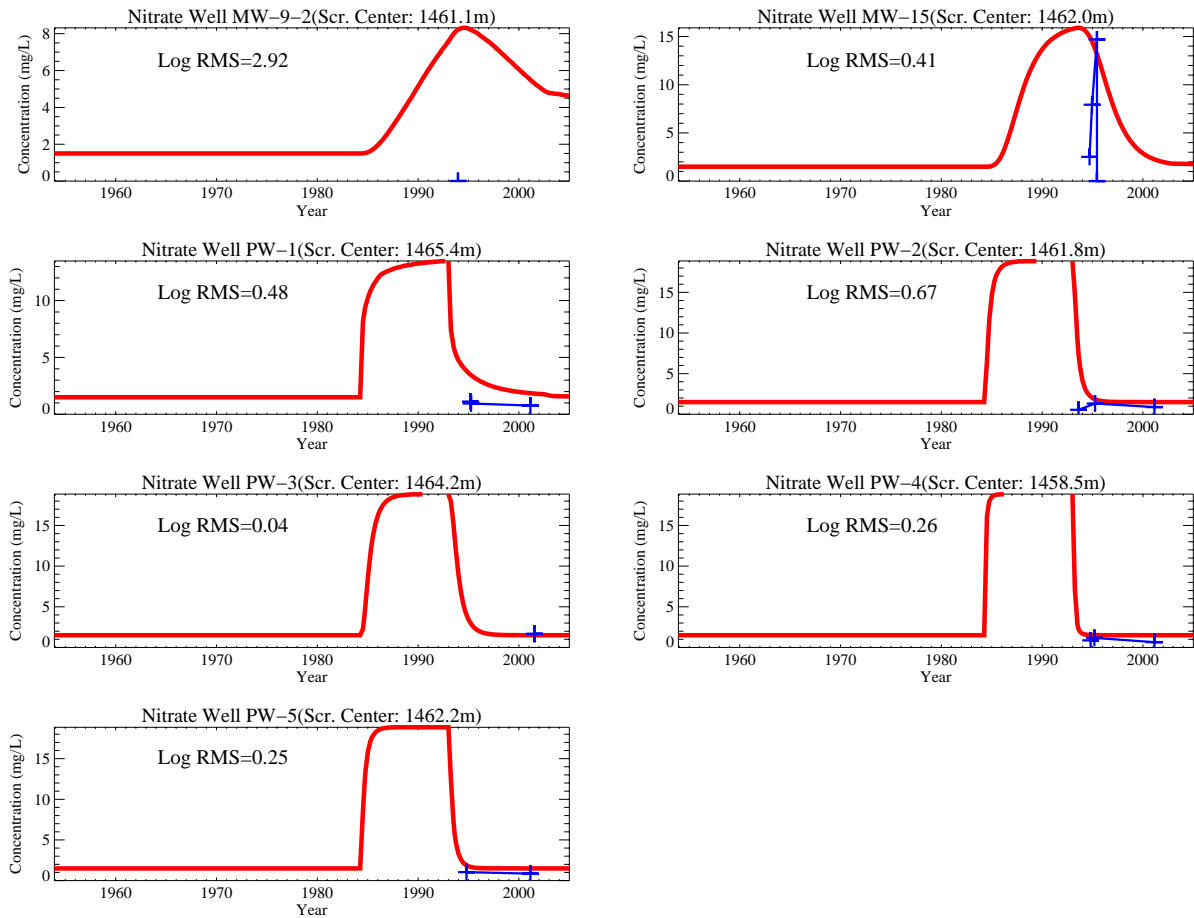


**Figure A-7-41.** Nitrate concentration history in the southern shallow perched water (red line = simulated, blue crosses = observed, mg/L as N).

#### A-7.3.4.5 Southern Deep Perched Water Nitrate

The southern deep perched water is associated with the 380-ft interbed, but perched water has been encountered higher than 380 ft. As with the southern shallow perched water, the nitrate contamination source is from the former percolation ponds. Wells MW-1-4 and CS-CH lie near the northernmost extent of the southern well grouping area, and they most likely see contamination resulting from the CPP-3 injection well and the tank farm releases.

The highest observed nitrate concentrations in the southern deep perched water were found in well MW-1-4 at 694 mg/L as N in 1993. Nitrate concentrations were much lower in the southern perched water wells surrounding the percolation pond. The only other southern deep perched water well with nitrate concentrations above the 10-mg/L federal drinking water standard was well MW-17-2 at 15.4 mg/L as N in 1995. However, nitrate was also measured in wells CS-CH at 8.14 mg/L as N in 2001, MW-17-4 at 4.6 mg/L as

N in 1994, 1804M at 0.99 mg/L as N in 2002, 1807L at 0.67 mg/L as N in 2002, and 1807L at 0.62 mg/L as N in 2002.

The model agrees with the magnitude of observed nitrate concentration except for well MW-1-4. The observed 1993 concentration of 694 mg/L may be an error because observations immediately before and after this date were approximately 70 mg/L. The simulated and observed nitrate concentrations in this region are illustrated in Figure A-7-42.

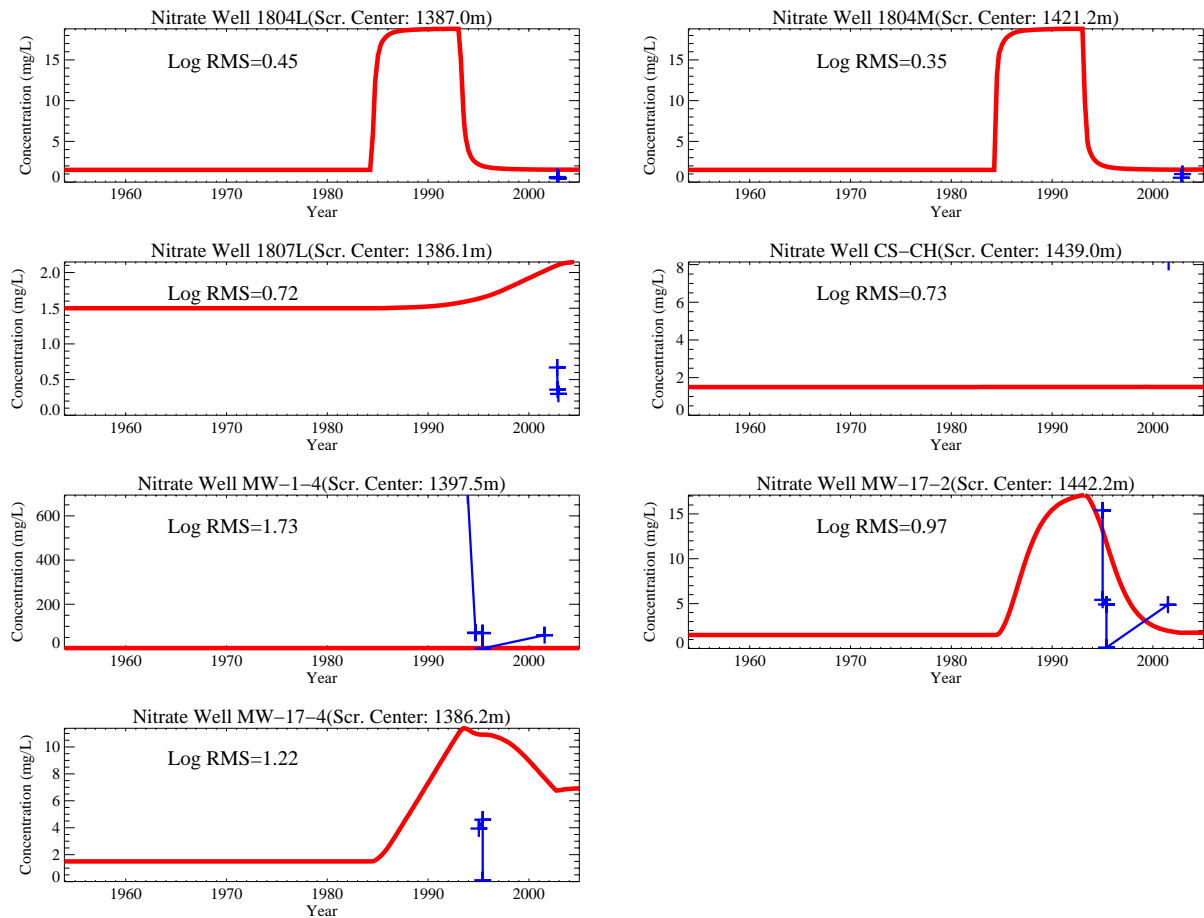


**Figure A-7-42.** Nitrate concentration history in the southern deep perched water (red line = simulated, blue crosses = observed, mg/L as N).

### A-7.3.5 Transport Calibration Conclusions

The primary objective of the vadose zone transport calibration was to match the timing and concentration of contaminants in the perched water bodies and aquifer resulting from the tank farm soil contamination. The transport calibration was achieved by adjustment of hydraulic parameters, source term placement, and dispersivity. The source term placement adjustment was only performed if the contamination site straddled two model grid blocks.

The highest observed contaminant concentrations in the northern shallow perched water are located south, east, and southeast of the tank farm in wells CPP-33-1, MW-2, MW-10-2, MW-20-2, MW-5, and CPP-55-06. This can be seen in the predicted and observed concentration histories presented in Section A-7.3. The model is consistent with this general trend.

The perched water monitoring wells surrounding the tank farm are on the perimeter of the main contaminant flow path to the aquifer and may not sample the highest concentrations resulting from the tank farm leaks and spills. This may explain how simulated aquifer concentrations (Tc-99 in particular) are higher than those obtained in the deep perched water wells surrounding the tank farm, because the perched water wells may not sample the highest perched water concentrations directly under the tank farm.

The Tc-99 simulations indicate the water travel time from the tank farm land surface to the aquifer is approximately 30 years. The water travel time from other areas of the INTEC can be much faster (i.e., the percolation pond travel time was approximately 2 years). During high flow years, the Big Lost River can have a very large impact on contaminant transport rates.

There are insufficient data for conclusive model calibration in the deep vadose zone. Conclusive model calibration requires knowledge of the source strength and release timing in addition to measurements of the concentration history at the locations of calibration. Most often, data collection in the perched water wells began after the peak was predicted to occur. Data collection for the slower-moving contaminants has been taken over periods too short to discern the relative position on the concentration history.

The simulated concentrations were mostly higher than the observed concentrations in the shallow perched water surrounding the tank farm. The higher simulated-than-observed contaminant concentrations suggest that contaminants are not moving horizontally to the extent predicted by the model. This also implies that the model may be underestimating perched water concentrations immediately below the tank farm. However, there are no wells directly below the tank farm to confirm this. For these reasons, the model could underestimate peak aquifer contaminant concentrations.

Although the model has several deficiencies, it adequately represents the bulk movement of tank farm contaminants from land surface to the aquifer and is a significant improvement over the previous modeling studies. The INTEC vadose zone is a complex heterogeneous environment that will always have monitoring results that represent local spatial variabilities and fast pathways that a large-scale equivalent porous media model will not represent.

## **A-7.4 Summary of Vadose Zone Model Assumptions**

The following list contains the primary assumptions used in developing the vadose zone flow and transport models:

- The infiltration rate study presented in Appendix B is adequate for representing precipitation recharge through disturbed and unvegetated INTEC sediments and the recharge from precipitation is steady state.
- The Big Lost River loss rate between the INL Site diversion dam and the Lincoln Boulevard bridge gauging station represents the loss rate near INTEC, and quarterly averages adequately represent transient river recharge.
- Big Lost River recharge prior to 1985 and after 2004 is steady state and is adequately represented by the long-term average between 1965 through 1987.
- The INTEC water balance presented in the OU 3-13 RI/BRA (DOE-ID 1997) is adequate for representing the pre-remedial conditions with the exception of Big Lost River and precipitation recharge.
- The INTEC water balance presented in the INTEC Water System Engineering Study (DOE-ID 2003b) and the Waste Calcining Facility water discharge study (DOE-ID 2004b) are adequate for representing the anthropogenic post-remedial action water sources.

- The surficial sediments and interbeds have spatially varying surfaces and thicknesses that influence water and contaminant movement.
- Six material types (high- and low-permeability alluvium, interbed, and basalt) adequately represent subsurface heterogeneity.
- Flow in the fractured basalt was controlled by the fracture network and could be represented by a high-permeability, low-porosity equivalent porous medium.
- All contaminant sorption processes can be lumped into a single soil/water distribution coefficient ( $K_d$ ) parameter for each COC.
- Perched water elevation is adequate for calibrating the vadose zone flow model.

## **A-8 AQUIFER MODEL CALIBRATION**

The flow and transport models for the aquifer were calibrated independently. The aquifer model boundary conditions and permeability were first adjusted to match the target potentiometric field. Subsequently, the model porosity and dispersivity were adjusted to match the solute arrival histories. Only a subset of the data presented in Section A-4 was used in the model calibration because the complete data set was too voluminous or would not provide useful information for model calibration. The specific observational data used in this calibration process are presented in Section A-8.1 along with a description of any data manipulation needed prior to model calibration. The specific data used in calibrating the aquifer model were taken from the OU 3-13 RI/BRA (DOE-ID 1997) modeling; the *Monitoring Report/Decision Summary for Operable Unit 3-13, Group 5, Snake River Plain Aquifer* report (DOE-ID 2004c); and ongoing remedial investigations at INTEC. These data included aquifer water level measurements taken during spring/summer 2004 and tritium, Tc-99, Sr-90, I-129, and nitrate concentrations observed in aquifer wells. Results of the calibration for flow and transport are presented in Sections A-8.2 and A-8.3, respectively.

### **A-8.1 Specific Calibration Data For the Aquifer Model**

#### **A-8.1.1 Calibration Data for the Flow Model**

The aquifer flow model was calibrated to observed water level elevations obtained during summer 2004. Data were obtained in summer 2004 from all available monitoring wells on the INL Site, including INL Site and USGS wells. Water level measurements taken in the USGS wells can be found in the USGS National Water Information Storage database, and the measurements made in the INL Site wells were obtained from the WAG 10 RI/FS annual report (DOE-ID 2005b). Seventy-eight data points were used in the calibration of this aquifer flow model. The overall large-scale gradient near the INTEC facility is predominantly south/southwest. The relatively flat gradient south and west of INTEC suggests that the aquifer permeability is high in these areas. Figure A-8-1 illustrates the INL Site-wide regional gradient (contour interval = 2 m) obtained from the 2004 measurements

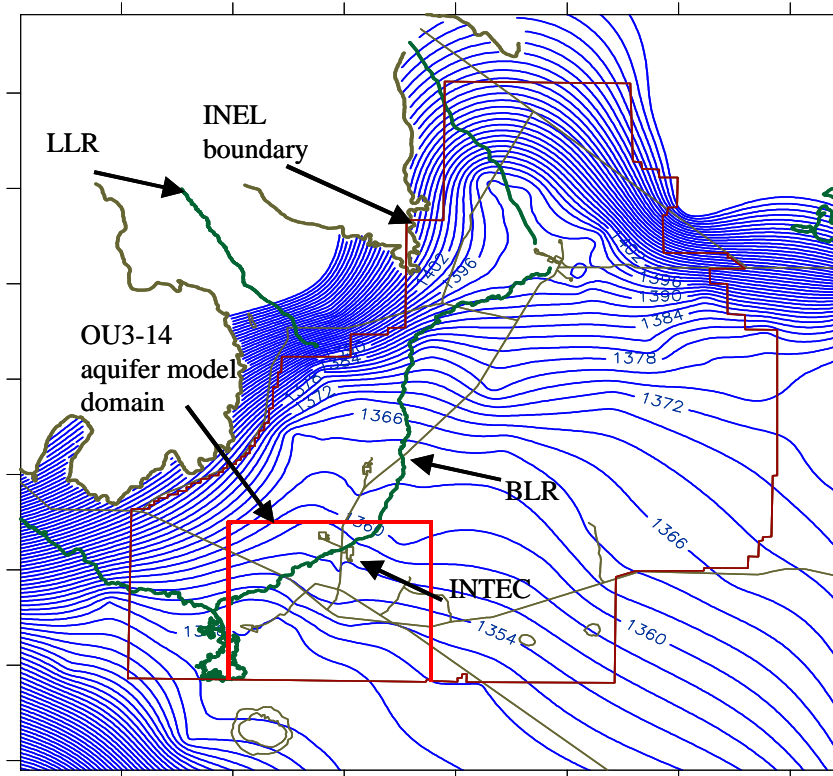


**Figure A-8-1.** WAG-10 regional water levels based on summer 2004 field measurements.

### A-8.1.2 Calibration Data for the Transport Model

Calibration of the aquifer transport model required the magnitude of contaminant sources, the release history of the contaminants, and the concentration history in downgradient wells. The transport model was calibrated to tritium, technetium-99, strontium-90, iodine-129, and nitrate. The contaminant concentration data were obtained from the EDW.<sup>1</sup> The EDW is a database website maintained by the INL and contains well locations, well coordinates, water level, and water quality data. The tritium data were available in 68 wells and was most frequently sampled. The data for nitrate are most sparse, with 40 observation locations. Only wells downgradient and within the INTEC contaminant plumes were used in the model calibration.

Concentration data were first screened based on the validator-assigned data qualifier flags. If the radio analytical result was not statistically positive at the 95% confidence level, which means that the radionuclide is not present and/or the result was below minimum detection concentration in that sample, the contaminant concentration was designated nondetect. Data indicated as having severe analytical and/or quality control issues (R flags) were omitted.

The release mass and history comprising the contaminant source terms were taken from the OU 3-13 RI/BRA or estimated from historical INTEC operational records (see Section A-5.3.2). Table A-8-1 summarizes the source terms incorporated in the aquifer model. The CPP-3 injection well was the source of the

1. Idaho National Laboratory, Bechtel BWXT Idaho, LLC, *Environmental Data Warehouse (EDW)*, <http://icpweb2/edw2/>, Web page updated December 3, 2004, Web page visited December 3, 2004 (Intranet web page).

early releases of contaminants in the aquifer and is the source of contaminants currently appearing in the far downgradient wells near the CFA and also of the contaminants appearing very early in wells nearer INTEC. The aquifer model sources for each simulated contaminant are presented below.

**Table A-8-1** Total source mass or activity used in the vadose zone and aquifer models..

Contaminant	Injection Well Source	Percolation Pond Source	Tank Farm Source
Tritium (in Ci)	20,100	999	9.71
Technetium-99 (in Ci)	11.9	1.13	3.56
Strontium-90 (in Ci)	24.3	0.3	18,100
Iodine-129 (in Ci)	0.86	0.08	0.00126
Nitrate (in kg)	2,830,000	1,310,000	21,200

- Tritium

The main source of tritium was the CPP-03 injection well (20,100 Ci) with minor amounts originating in the former percolation ponds and from the tank farm. Tritium is transported conservatively (non-adsorbing). There were good records of tritium discharges, and it was the focus of early sampling in the aquifer. Early sample collection and reasonably complete disposal history makes it the best target for model calibration. The tritium disposal records included composite sampling of the service waste effluent (Robertson et al. 1974). In these data, tritium discharges prior to 1962 were reported as annual averages. After 1962, the data were reported as a monthly average. Even in this averaged data, there is considerable variation in discharge as shown in Figure A-8-2.

To simplify model input and to increase computational efficiency, the release history of tritium was averaged over various time periods. As shown in Figure A-8-2 for the CPP-3 injection well releases, a smaller averaging period was used when the disposal rate changed rapidly in order to preserve the general character of the data. Throughout the release history, the total amount of tritium was unchanged after applying the averaging algorithm. The period between 1968 and 1972 represents the CPP-3 injection well collapse. During this time, the discharged tritium was accounted for as releases in the vadose zone model.

- Technetium-99

The largest source of Tc-99 may have been from the CPP-03 injection well operation, with smaller amounts originating in the former percolation ponds and the tank farm. A service waste inventory for Tc-99 was not kept and as discussed in Section A-5.3.2, the amount injected at CPP-03 was estimated to be 11.9 Ci. The Tc-99 resulting from the tank farm sources was 3.56 Ci and this Tc-99 is currently entering the aquifer. The flux of vadose zone Tc-99 arriving in the aquifer is illustrated in Figure A-7-15 of Section A-7.3.1. The reported and simulated Tc-99 injection well data are given in Figure A-8-3. As shown by the averaged data incorporated into the numerical model, the discharges of Tc-99 were fairly regular throughout the operation of CPP-03 except for the time period CPP-03 was not receiving waste and during the mid-1980s.

- Strontium-90

Unlike tritium and Tc-99, the primary source of Sr-90 was associated with the tank farm releases. The amount of Sr-90 that was discharged in the CPP-03 injection well was 24.3 Ci, compared to 18,100 Ci released in the tank farm. Observations of Sr-90 in the aquifer are a direct result of the CPP-03 injection. Because of the retardation of Sr-90 in the vadose zone, the Sr-90 released in the tank farm should not reach the aquifer for several more decades. The amount of Sr-90 reaching the aquifer will be greatly attenuated because of radioactive decay and sorption. The disposal history for Sr-90 in the CPP-3 injection well is fairly complete as

illustrated in Figure A-8-4. As with tritium, these releases were smoothed using an averaging process to facilitate incorporation into the numerical model. The Sr-90 aquifer model calibration results are presented in Appendix J.

- Iodine-129

The primary source of I-129 was released via direct injection in CPP-03. It travels as a conservative contaminant and has a relatively long half-life. Total discharges to the CPP-03 injection well were 0.86 Ci compared to 0.00126 Ci originating in the tank farm. This difference illustrates that the I-129 observed in the aquifer was a direct result of the CPP-03 operation. As illustrated in Figure A-8-5, the discharge rate of I-129 in CPP-03 was relatively constant and is nearly identical in form to that of Tc-99.

- Nitrate

Concentrations of nitrate contained in the service waste are relatively constant based on long-term averages. The release rate of nitrate is variable and is a function of the service waste water volumes. Direct injection of nitrate accounts for 2,830,000 kg and is almost matched by the 1,310,000 kg estimated to be discharged via the former percolation ponds. As with I-129 and tritium, nitrate travels as a conservative constituent, which, means the surface releases may also have a significant impact on aquifer concentrations. Figure A-8-6 illustrates the estimated and simulated nitrate disposal history in the CPP-03 injection well.

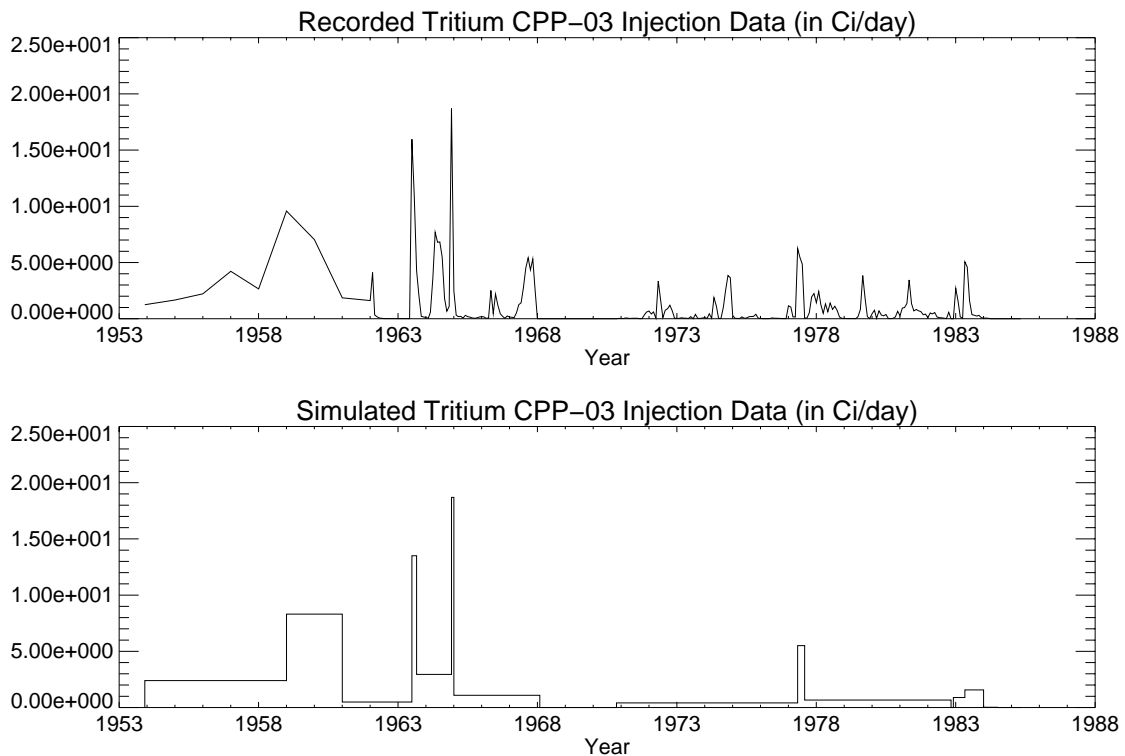


**Figure A-8-2.** Reported and simulated tritium disposal in CPP-03 (Ci/day).

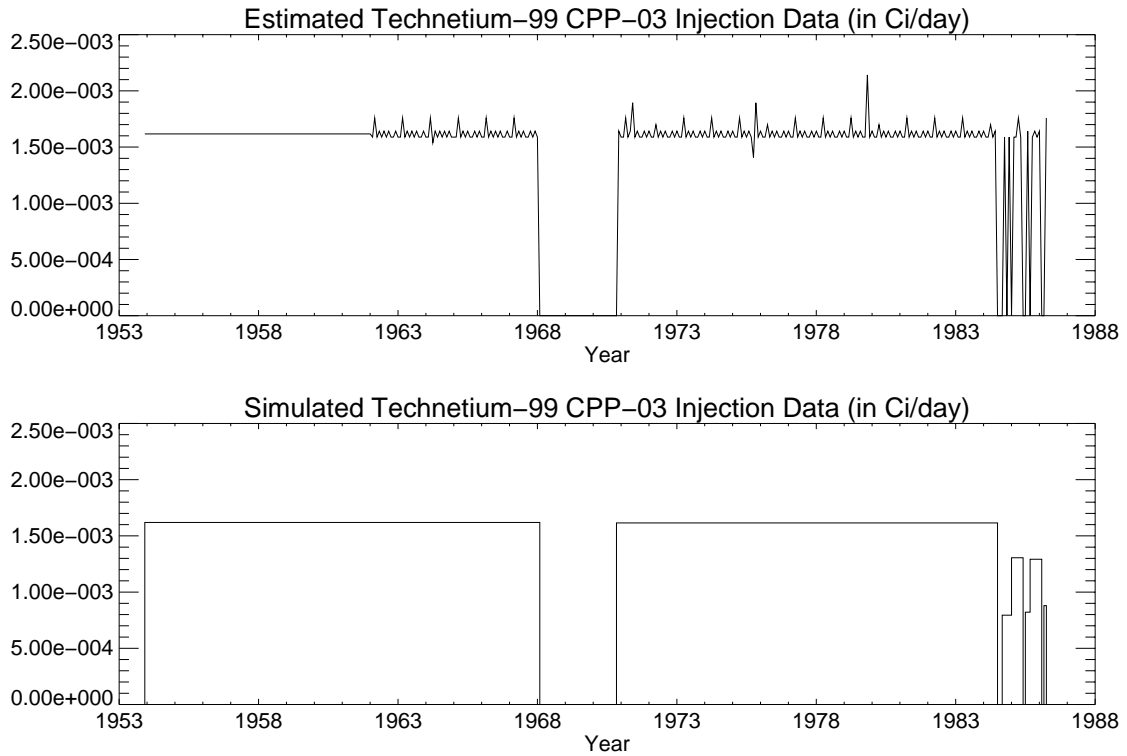


**Figure A-8-3.** Reported and simulated technetium-99 disposal in CPP-03 (Ci/day).

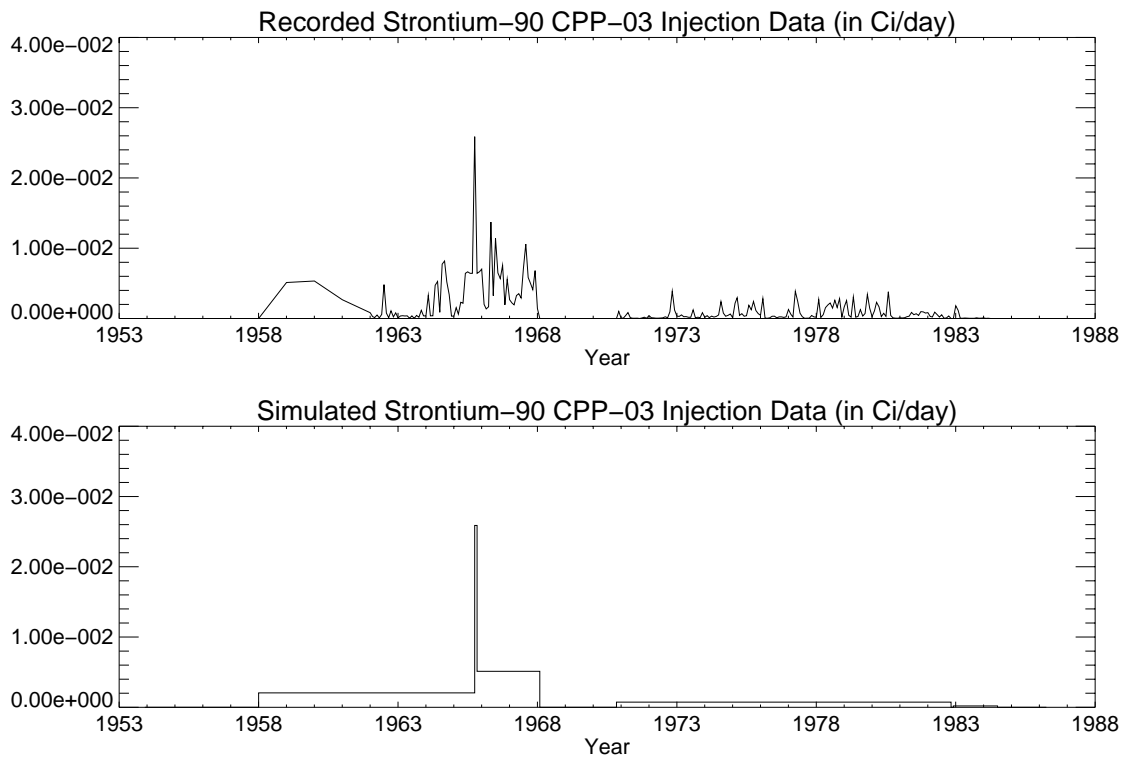


**Figure A-8-4.** Reported and simulated strontium-90 disposal in CPP-03 (Ci/day).

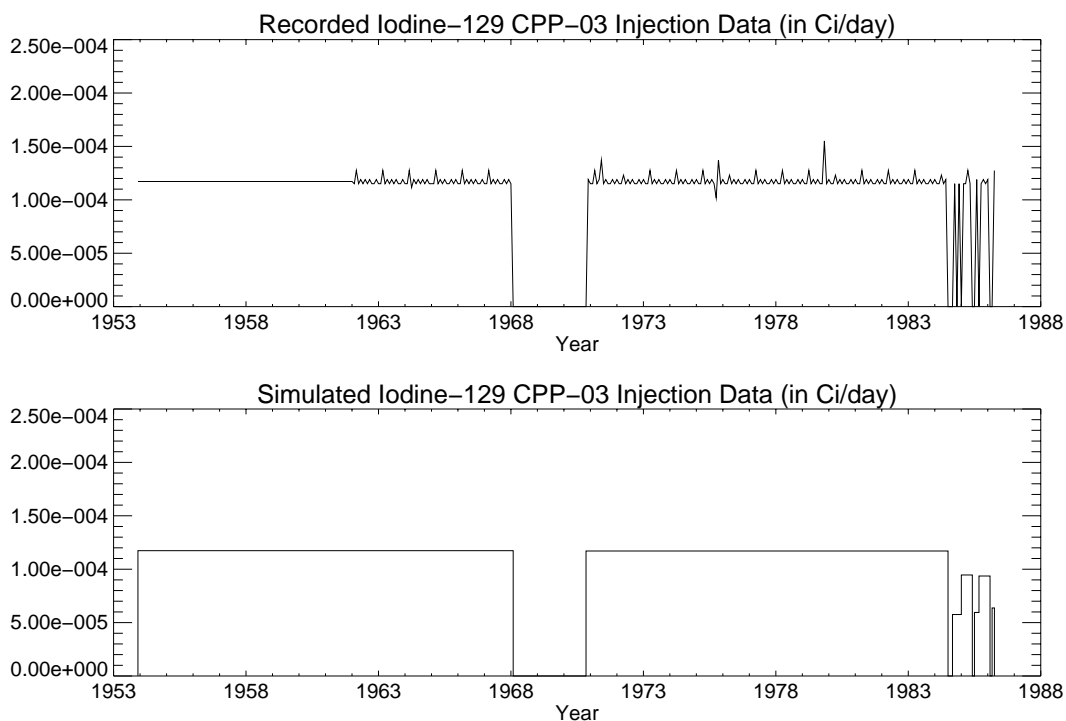


**Figure A-8-5.** Reported and simulated iodine-129 disposal in CPP-03 (Ci/day).

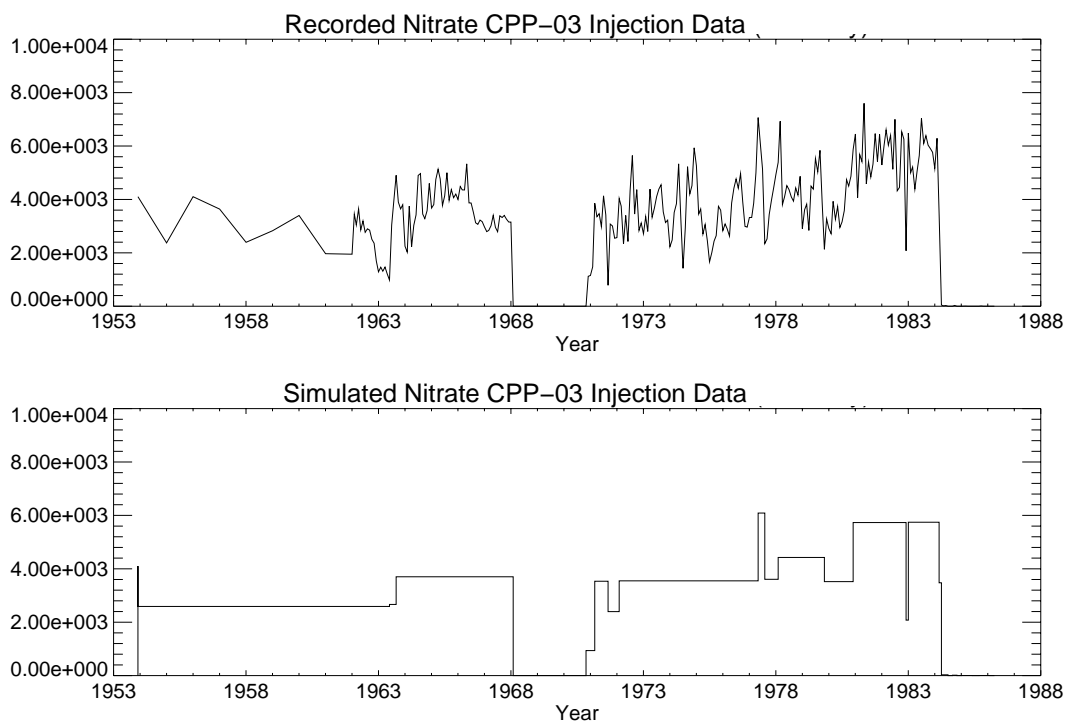


**Figure A-8-6.** Reported and simulated nitrate disposal in CPP-03 (kg/day as N).

## A-8.2 Aquifer Flow Calibration

The aquifer flow model was calibrated to the potentiometric surface based on data from summer 2004. This was achieved by adjusting the model's steady-state Dirichlet (prescribed heads) boundary conditions and performing global adjustment of the aquifer model's permeability in each of the three lithologic layers. The boundary conditions for the aquifer model were first interpolated onto the model grid from the summer 2004 potentiometric field. To obtain a better match, the boundary heads were slightly adjusted in the northwest and along the east side. To match the heads on the interior of the flow domain, the permeability of the H basalt was then increased by a factor of two over the values presented in Section A-5.5.1, and the permeability of the I basalt was decreased by a factor of two. Hydraulic parameters for this stage in calibration are presented in Table A-8-2. The predicted and observed hydraulic heads in the layer corresponding to the top of the model are presented in Figures A-8-7 and A-8-8.

**Table A-8-2** Calibrated aquifer model parameters.

Material Type	Permeability <sup>a</sup> (mD)	Hydraulic Conductivity (ft/day)	Porosity
H basalt	Ranging from 1.0e+3 to 1.7e+6	Ranging from 2.28E+0 to 3.87E+3	0.03
HI interbed	5.0e+2	1.14E+0	0.5
I basalt	4.e+4	1.00E+2	0.03
a. A groundwater temperature of 15 C and the Gottfried viscosity relationship to temperature was used to calculate permeability.			

The large-scale gradient is primarily south through INTEC with a slight westerly component. The flat gradient west of INTEC indicates the presence of a high-permeability zone, which is consistent with the pump test data used to parameterize the initial H basalt permeability. The regional gradient illustrates that the contamination from the INTEC should remain east of the SDA.



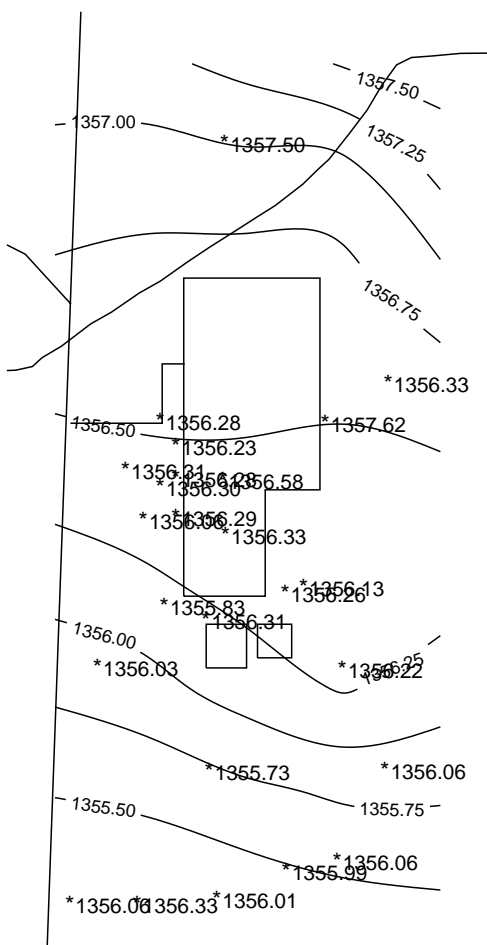


**Figure A-8-8.** Predicted hydraulic head (m) with summer 2004 observations near INTEC (contours represent simulated values and asterisks represent observed values).

Quantitative evaluation of the calibration was based on the RMS error which provides an estimation of the average error throughout the data set (see Section A-6). The model's overall RMS error in hydraulic head was 0.99 m (3.24 ft).

### A-8.3 Aquifer Transport Model Calibration

The primary objective of the aquifer model's transport calibration was to match the timing and concentration of contaminant arrival in wells downgradient of the CPP-3 injection well, percolation ponds, and tank farm. The aquifer model was calibrated to H-3, Tc-99, and Sr-90. Because of limited sample data, model predictions were only compared to observed I-129 and nitrate. Tritium was the primary target because of the fairly certain source term, because its source is associated primarily service waste, and because the service waste stream was regularly monitored. Tritium is also the most frequently monitored contaminant in most aquifer wells. The Sr-90 calibration is presented in Appendix J along with the geochemical model development.

The dispersivity was adjusted to match the observed aquifer plume width and downgradient concentrations. In the area near INTEC, representative of short-distance and short-duration transport, the dispersivity was zero. In the area outside of the vadose zone footprint, where residence- and travel-times were longer, the resultant values were 40 m in the longitudinal direction and 20 m in the transverse. The effective dispersivity is larger than the specified values because of numerical dispersivity, and a 0-m dispersivity near INTEC resulted in sufficient solute spreading to match the observed concentrations. To match contaminant history for the calibrating targets, the permeability was increased by a factor of two over the calibrated flow model values, and a porosity of 3% was used. A summary of the calibrated aquifer model's transport parameters is presented in Table A-8-3.

Matching both the contaminant concentration and velocity required using 3% porosity for the fractured basalt within the aquifer. This is 1/2 of the value used in Appendix F of the OU 3-13 RI/BRA (DOE-ID 1997) aquifer model. The reduction was needed because OU 3-13 model used a constant 76-m thickness and the OU 3-14 model used the aquifer thickness obtained from the temperature profiles (discussed in Sections A-4.1 and A-5.2). The aquifer thickness ranged from 25 to 375 m. The much thicker aquifer required a smaller 3% porosity to match the tritium plume. The 3% porosity was consistent with the final model applied at TAN where a variable-thickness aquifer was also assumed (Martian 1999).

Locations for each of the wells used in the calibration are illustrated in Figures A-8-9 and A-8-10 for wells nearer and further away from INTEC, respectively. Resultant concentration histories for each calibration contaminant are presented in Sections A-7.3.1 through A-7.3.5. The order of presentation in each section corresponds to the distance of the wells to the CPP-3 injection well. In each figure, four data sets are presented. These include: (1) measured concentrations represented by a thin black line with a cross data symbol, (2) simulated data corresponding to the well screen center represented by a thick red line, (3) simulated concentration at the top of the aquifer represented by a thin dashed green line, and (4) simulated concentration at the aquifer bottom represented by a thin blue line. The calibration statistic was calculated for each well by comparing the values between the simulated screen center value to the observed concentration.

**Table A-8-3** Calibrated aquifer model transport parameters.

Contaminant	Interbed $K_d$ (mL/g)	Basalt $K_d$ (mL/g)	Vadose Zone Footprint Dispersivity		Dispersivity External to Vadose Zone Footprint	
			Longitudinal (m)	Transverse (m)	Longitudinal (m)	Transverse (m)
Tc-99	0.	0.	0.	0.	40.	60.
Sr-90	22.	0.035	0.	0.	40.	60.
I-129	0.	0.	0.	0.	40.	60.
H-3	0.	0.	0.	0.	40.	60.
Nitrate	0.	0.	0.	0.	40.	60.

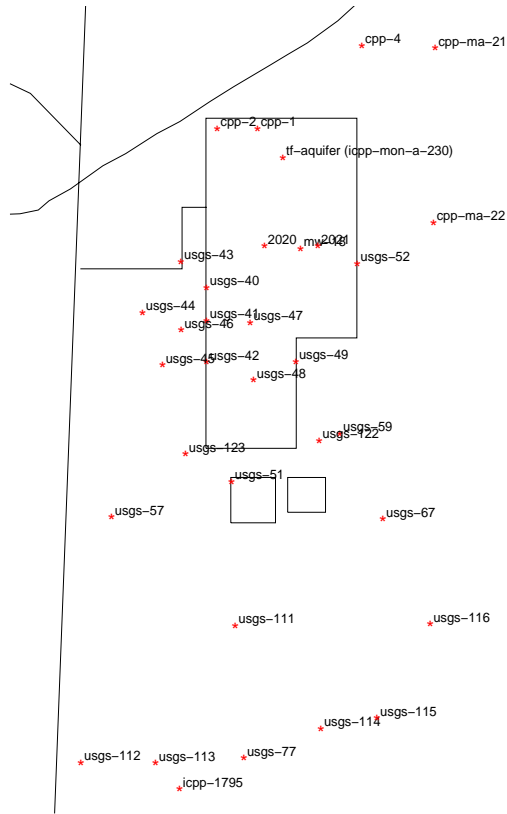


**Figure A-8-9.** Aquifer wells located near INTEC.



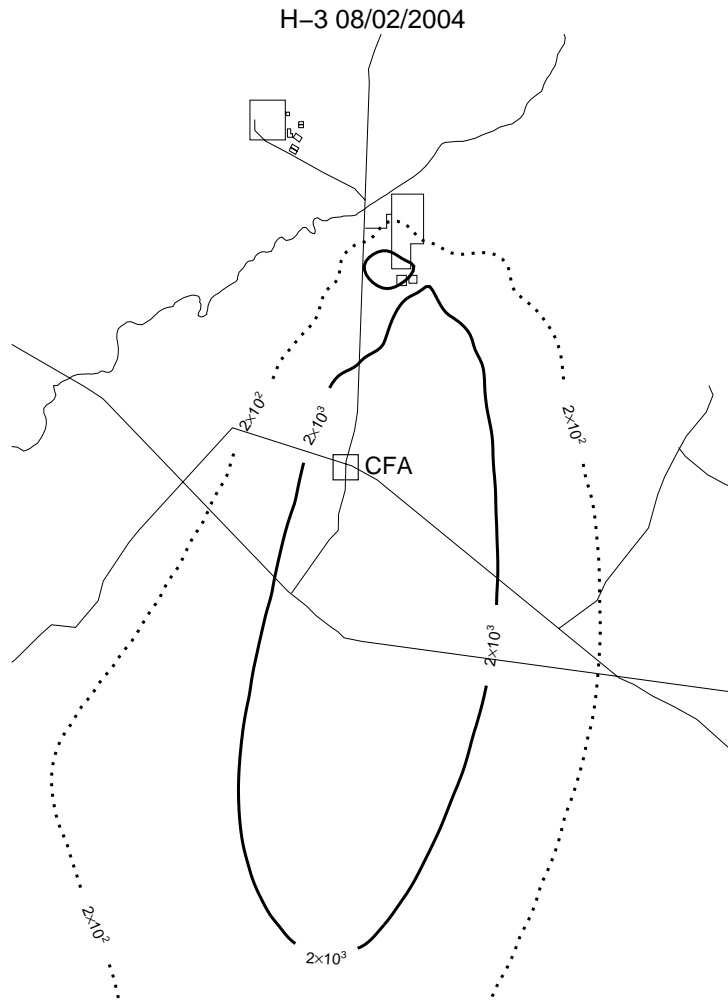


**Figure A-8-11.** Maximum simulated tritium (pCi/L) concentrations in base grid averaged over a 15-m well screen in 2004 (MCL=thick red line, 10\*MCL=thin red line, MCL/10=thin black line, MCL/100=dashed black line).

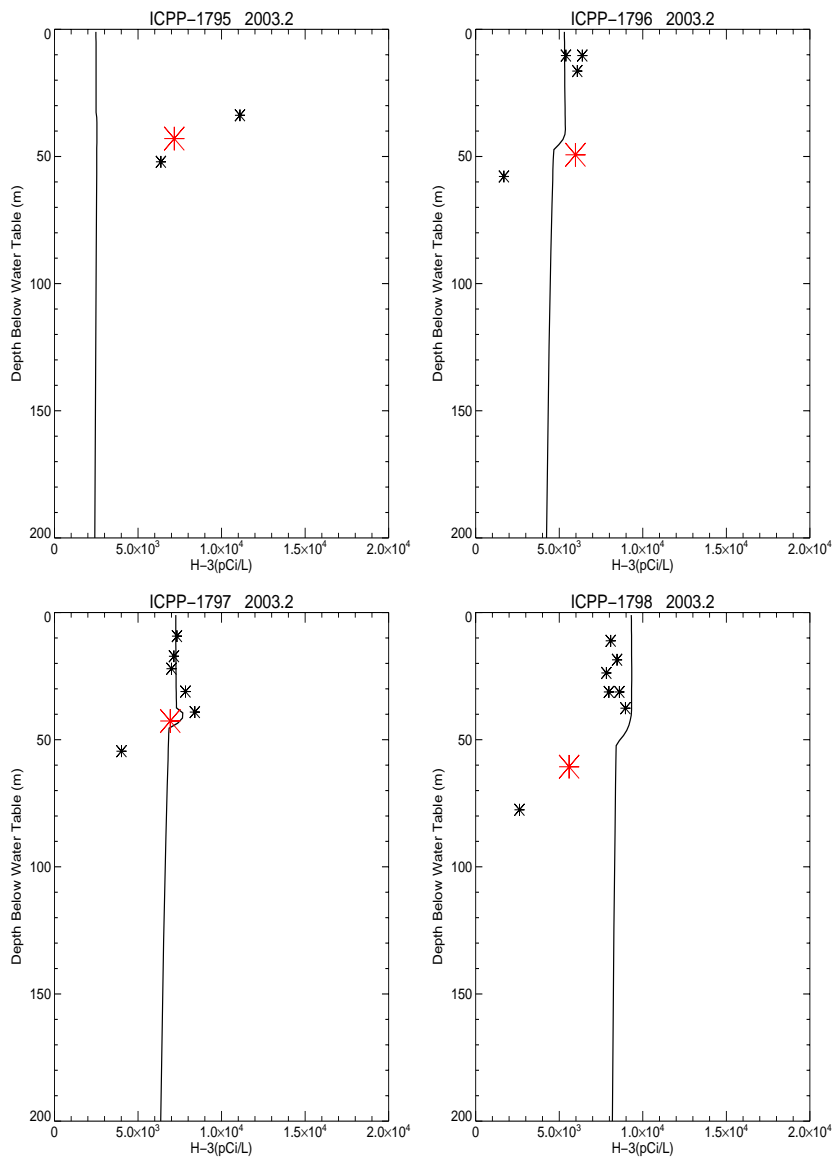


**Figure A-8-12.** Simulated and measured tritium vs. depth at vertical boreholes in 2003 (pCi/L) (simulated data = solid line, small asterisk = data taken in basalt, large red asterisk = data taken in the HI interbed).